Wave-Mean-Flow Interaction

and the

Annular Mode

David J. Lorenz

A dissertation submitted in partial fulfillment of the
requirements for the degree of

Doctor of Philosophy

University of Washington

2003

Program Authorized to Offer Degree: Atmospheric Sciences

ProQuest Information and Learning Company
300 North Zeeb Road
P.O. Box 1346
Ann Arbor, MI 48106-1346

In presenting this dissertation in partial fulfillment of the requirements for the Doctoral degree at the University of Washington, I agree that the Library shall make its copies freely available for inspection. I further agree that extensive copying of the dissertation is allowable only for scholarly purposes, consistent with "fair use" as prescribed in the U.S. Copyright Law. Requests for copying or reproduction of this dissertation may be referred to Bell and Howell Information and Learning, 300 North Zeeb Road, P.O. Box 1346, Ann Arbor, MI 48106-1346, to whom the author has granted "the right to reproduce and sell (a) copies of the manuscript in microform and/or (b) printed copies of the manuscript made from microform."

Signature David J Lowry

Date 8/19/03

University of Washington

Graduate School

This is to certify that I have examined this copy of a doctoral dissertation by

David J. Lorenz

and have found that it is complete and satisfactory in all respects,
and that any and all revisions required by the final
examining committee have been made.

Chair of Supervisory Committee:

Dennis L. Hartmann

Reading Committee:

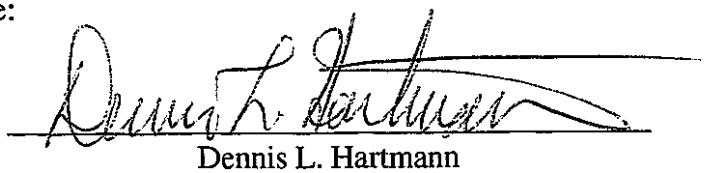

Dennis L. Hartmann

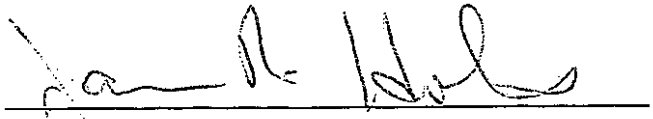

James R. Holton

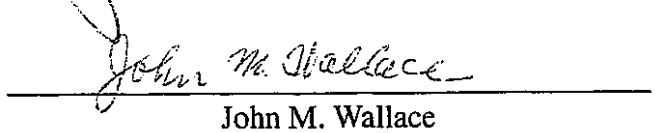

John M. Wallace

Date: 8/20/03

University of Washington

Abstract

Wave-mean-flow interaction

and the

Annular Mode

David J. Lorenz

Chair of Supervisory Committee:

Professor Dennis L. Hartmann
Atmospheric Sciences

The leading EOF of zonal-mean variability (the annular mode) represents the north/south movement of the mid-latitude jet. Analysis of the momentum budget demonstrates that EOF1 dominates over other EOFs because of a positive feedback between the EOF1 zonal-mean wind anomalies and the eddy momentum fluxes. The mechanism of the feedback is as follows: above normal baroclinic wave activity is generated in the region of enhanced westerlies. The propagation of waves from their source latitude is associated with (1) eddy momentum fluxes which enhance the westerly wind anomalies and (2) a mean meridional circulation which helps restore the baroclinicity of the wave source region.

At first sight, this positive feedback mechanism would also appear to work for EOF2 which represents the strengthening/sharpening versus the weakening/broadening of the jet. Indeed, above normal baroclinic wave activity is also generated in the enhanced westerlies for EOF2. This anomalous wave source, however, is offset by the effect of upper level potential vorticity gradients on the propagation of wave activity. A stronger/ sharper (weaker/broader) jet is a stronger (weaker) waveguide which inhibits (enhances)

the meridional propagation of wave activity.

This dissertation has also established that the response of the eddies to the rapid onset of annular mode anomalies is not monotonic. Instead, a transient period of negative eddy forcing is followed, after several days, by a period of long-term reinforcement by the eddies. The results here suggest that a baroclinic mid-latitude jet, that organizes its own wave momentum forcing, is quite sharp. Given a uniform wave activity distribution, a sharp jet will tend to attract wave activity resulting in a negative momentum forcing. The positive response to the changes in the annular mode follows only after baroclinic instability has had time to establish positive wave activity anomalies in the region of westerly anomalies.

Table of Contents

List of Figures

List of Tables

Acknowledgments

This work could not have proceeded without the generous help of others. I would like to thank Dennis Hartmann for his support, guidance and careful critique of this research. I also thank Mike Wallace for helpful discussions, insight and encouragement. Thanks also to Jim Holton for taking the time to read this dissertation. This research could not have been completed without the generous help of Marc Michelsen and Ian Kraucunas with the GCM. Thanks also to Jeff Yin for willingly providing data from his many GCM experiments. I want to thank friends and family for all their support and encouragement, and especially my wife Mary for her enduring patience and love during the past several years.

Chapter 1

Introduction

The variability of the zonal-mean state of the atmosphere has been a topic of research for a long time (Rossby 1939; Namias 1950). Recently, interest in the variability of the zonal-mean has increased by the discovery that the structure of low-frequency variability in both the Northern and Southern Hemispheres is remarkably similar and zonally-symmetric despite the striking differences in the topography and land-sea geometry of the two hemispheres (Gong and Wang 1999; Thompson and Wallace 2000). Recognizing that the general structure of the leading pattern of variability does not depend on a particular geographic region or hemisphere, Thompson and Wallace (2000) called this leading pattern the "annular mode". The annular mode is defined as the leading EOF of geopotential height in the lower troposphere poleward of 20° . It is characterized by equivalent barotropic height anomalies which extend through the depth of the troposphere and even into the stratosphere (see figure 1 in Thompson and Wallace 2000).The importance of this annular mode of low-frequency variability has been further recognized because it so closely resembles the pattern of climate trends observed during the last several decades (Thompson et al. 2000; Hartmann et al. 2000).

An annular mode is the leading mode of variability in many simple quasi-geostrophic and primitive equation models with simple physics and no topography or seasonal cycle (Robinson 1991; James and James 1992; Yu and Hartmann 1993; Robinson 1994; Feldstein and Lee 1996; Lee and Feldstein 1996; Robinson 1996; Akahori and Yoden 1997). In addition, realistic general circulation models with climatological forcing can

simulate the observed structure and amplitude of both the Northern and Southern annular modes of variability (Limpasuvan and Hartmann 1999; Limpasuvan and Hartmann 2000). Because the external forcing for these models that produce a realistic annular mode is independent of time, the variability found in these models is unforced variability associated with dynamic processes internal to the atmosphere.

The zonal-mean zonal wind anomalies associated with the annular mode and the essential role of the eddies in driving this variability has been the subject of much previous work (Karoly 1990; Robinson 1991, 1994, 1996; James and James 1992; Yu and Hartmann 1993; Hartmann 1995; Feldstein and Lee 1996, 1998; Lee and Feldstein 1996; Akahori and Yoden 1997; Hartmann and Lo 1998; Limpasuvan and Hartmann 1999, 2000; Hartmann et al. 2000; Lorenz and Hartmann 2001, 2003: Watterson 2002). Many of these studies also argue that in addition to driving the zonal-mean wind anomalies stochastically, the eddies respond to and reinforce the changes in the zonal-mean flow associated with the annular mode. Recently, Lorenz and Hartmann (2001, 2003) have provided a quantitative estimate of the strength of this positive eddy-zonal-mean flow feedback in observations. They found that the strength of the positive feedback accounts for the greater persistence of the zonal-mean zonal wind associated with the annular mode compared to other zonally-symmetric patterns of variability. Moreover, the positive feedback accounts for all of the excess variance of EOF1 over EOF2 in the Northern Hemisphere (NH) and over 70% of the excess variance of EOF1 over EOF2 at low frequencies in the Southern Hemisphere (SH). Therefore, the positive feedback between the annular mode and the eddies is the most important factor determining the pattern of month-to-month zonal-mean variability in the extratropics.

Robinson (1996) and Lorenz and Hartmann (2001, 2003) hypothesize that the changes in baroclinicity associated with the annular mode are essential for persistent wave momentum fluxes which reinforce the westerly zonal wind anomalies. They show that above normal baroclinic wave activity is generated in the region of enhanced baroclinicity which is collocated with the region of westerly wind anomalies. This anomalous wave generation leads to the anomalous radiation of wave activity at upper levels from the west-

erly wind anomalies. Since meridional propagation of wave activity is associated with westerly momentum fluxes into the wave source region, this propagation of wave activity reinforces the westerly wind anomalies. Furthermore, the tendency of the baroclinic waves to reduce the baroclinicity of the westerlies is countered by the wave induced mean-meridional circulation as long as the waves leave their source region at upper levels (Robinson 2000). Hence, the anomalous baroclinic westerlies are self-maintaining, provided that the waves leave their source region.

While the above theory seems consistent with the observed positive feedback, it does not explain why the positive feedback is strongest for the zonal-mean wind anomalies associated with the annular mode (in most cases the positive feedback is in fact unique to the annular mode). In particular, the theory fails to explain why the eddies do *not* reinforce a similar-scale zonal-mean wind pattern in quadrature with the annular mode. To better understand the problem, it is helpful to understand the relationship between the annular mode and the background time-mean flow: the zonal mean fluctuations associated with the annular mode are best characterized as a north/south shift of the time-mean mid-latitude eddy-driven jet (e.g. Kushner et al. 2000; Lorenz and Hartmann 2001, 2003). The second EOF of the zonal-mean wind is a zonal wind tripole which is the same scale as the annular mode but with the strongest anomaly at the latitude of the mid-latitude jet. The second EOF therefore represents a strengthening and sharpening of the jet in one phase and the weakening and broadening of the jet in the other. The problem therefore becomes: why do the eddies reinforce variations in the mid-latitude jet position but not variations in the jet strength or scale? This question is the focus of the model experiments described in chapters 6 and 7 of this dissertation.

The earlier chapters of this dissertation discuss the results of previous published work we have done relating to the annular mode and the eddies. Chapter 2 describes the data, analysis methods and the numerical models used in this study. In chapter 3, we note the strong similarities between the traditional annular mode definition using low-level geopotential height and the zonal-mean zonal wind definition used in our analysis. In addition, we discuss the time-mean zonal-mean flow and establish that the annular mode

variability is best described by variability in the latitude of the eddy-driven jet. In chapter 4, we look at the zonal-mean momentum budget in detail and determine that the positive feedback between the annular mode and the eddy momentum fluxes is the dominant reason for the excess persistence and variance of the annular mode compared to other zonally-symmetric patterns. In chapter 5, we diagnose the eddy response to the zonal-mean wind anomalies associated with the annular mode using lag-regression analysis of the Eliassen-Palm (EP) flux (Edmon et al. 1980). We also discuss some subtleties relating to the "baroclinic" feedback mechanism (Robinson 2000). As mentioned above, the main goal of chapters 6 and 7 is to determine the reasons why the positive long-term feedback is unique to the leading EOF. In addition to this problem, the initial value experiments employed in chapters 6 and 7 shed light other important dynamics such as the transient eddy response to the zonal wind anomalies. In chapter 6, we also use a simple linear model which includes this transient response to gain further insight into annular mode dynamics. We conclude with a summary of the important results (Chapter 8).

Chapter 2

Methods

In this chapter, we describe the observational data, the statistical methods and the numerical models we use for this study.

2.1 Data

For this study, we used NCEP re-analysis 4 x daily wind, temperature and geopotential height on constant pressure levels (Kalnay et. al. 1996). The data is provided on a 2.5 x 2.5 latitude/longitude grid with 17 vertical levels (1000, 925, 850, 700, 600, 500, 400, 300, 250, 200, 150, 100, 70, 50, 30, 20, 10mb).We used Southern hemisphere data from December 1978 to January 2003 and Northern Hemisphere data from November 1976 to April 2001. We also used NCEP re-analysis spectral-space data for surface pressure and model topography to compute the large-scale mountain torque. The mountain torque is evaluated as in Madden and Speth (1995).

2.2 EOF Analysis

2.2.1 Southern Hemisphere Zonal-mean Zonal Wind

To analyze the variability of the zonal-mean zonal wind in the extratropics, we construct daily anomaly data by removing the mean seasonal cycle, defined as the annual average and the first four Fourier harmonics of the 24 year (1979-2002) daily climatology. We then perform an EOF analysis on the *vertical-average* zonal-mean zonal wind between 80° S and 25° S using the 24 years of daily anomaly data. We average the wind vertically from 1000mb to 100mb because the PC time series of the vertical-average zonal wind anomalies is practically identical to the PC time series of the variability in the latitude/

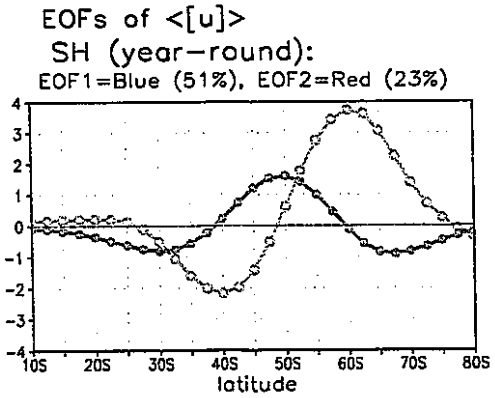

Figure 2.1: EOFs of the vertical- and zonal-mean zonal wind for the Southern Hemisphere shown by regressing the daily vertical- and zonal-mean zonal wind anomalies on the normalized PC index. The units on the *y*-axis are m/s.

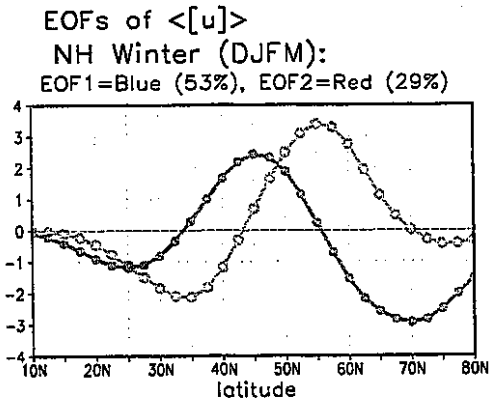

Figure 2.2: Same as 2.1 but for the Northern Hemisphere Winter (Dec.-Mar.).

pressure plane. For the EOF analysis, the zonal-mean wind is properly weighted to account for the decrease of area toward the pole (North et al. 1982a). The first and second EOFs are unique according to the North et al. (1982b) test.

We present the EOFs in m/s and not in standardized form so that the magnitude of the structures can easily be seen. This is done by regressing the daily anomaly data onto the normalized principal component (PC) time series. The first and second EOFs explain 51% and 23% of the daily variance, respectively (Figure 2.1).

2.2.2 Northern Hemisphere Zonal-mean Zonal Wind

The EOF analysis of the Northern Hemisphere is exactly the same as the Southern Hemisphere except that monthly anomalies rather than daily anomalies are used. While

the choice of monthly or daily data does not effect the leading EOF of the Southern Hemisphere, it does have an effect on the leading EOF of the Northern Hemisphere north of 65° N--the center of action at 72.5° N is significantly stronger for daily data than for monthly data. Since the focus of this study is on low frequency variability, the monthly EOF pattern will be used.

The first and second EOFs explain 53% and 29% of the monthly variance, respectively (Figure 2.2). The EOFs are shown using daily anomaly data so that one can compare the amplitude of the structures with the Southern Hemisphere EOFs.

2.2.3 Geopotential height

To analyze the variability of the geopotential height in the extratropics, we perform an EOF analysis of the monthly 1000mb height anomalies from 20° N to 87.5° N. For the EOF analysis, the data fields were weighted by the square root of the cosine of latitude to account for the increase of grid points per area near the pole. This analysis yields the annular mode index defined in Thompson and Wallace (2000).

2.3 Time Series Analysis

To analyze the daily momentum budget for the time series analysis, we find daily anomaly data for the zonal-mean wind, the eddy momentum flux convergence and the large scale mountain torque by removing the mean seasonal cycle. The mean seasonal cycle is defined as the annual average and the first four Fourier harmonics of the daily climatology. We project the vertical average EOF patterns onto the daily anomaly data in order to diagnose the forcing of the vertical- and zonal-mean zonal wind anomalies. This gives a daily time series for zonal wind, eddy momentum flux forcing and mountain torque forcing for each EOF mode.

For the Southern Hemisphere year-round spectral analyses, we divided the input time series into 256 day sections overlapped by 128 days and windowed by a Hanning window. For a time series of length 8766 days this gave at least 68 degrees of freedom for the composite spectrum. For the Northern Hemisphere spectral analyses, we found the spectra for each 121 day winter season (December-March) and windowed by a Hanning window. For 25 winters, this gave at least 50 degrees of freedom for the composite spec-

trum. We also used cross spectrum analysis to find the phase relationship between two time series as a function of frequency. For this analysis, the coherence squared function is a measure of the consistency of the phase and amplitude relationship between the two time series over the sample.

2.4 Definition of synoptic and quasi-stationary eddies

To better understand the dynamics of the zonal wind variability we divide the eddies into three parts: the 'synoptic', 'quasi-stationary' and 'residual' eddies. (For the Southern Hemisphere, there is no advantage in distinguishing between the residual and quasi-stationary eddies. Therefore, we simply combine the residual and quasi-stationary eddies together.) First we divide the eddy components of u, v and T into high frequency, low frequency and quasi-stationary parts: $u' = u'_h + u'_l + u'_s$, $v' = v'_h + v'_l + v'_s$ and $T' = T'_h + T'_l + T'_s$. The high-frequency eddies are found using a 15 day cutoff high-pass Lanczos filter with 41 weights (Hamming 1989) and the 'quasi-stationary' eddies are found using a 40 day cutoff low-pass Gaussian-shaped filter with 45 weights. We use a Gaussian filter for the quasi-stationary eddies because the negative weights of the Lanczos filter give a noticeable artifact in the cross-covariance function (although the same general conclusions are independent of the filter choice). The low-frequency eddies are defined to be the remainder after the high-frequency and quasi-stationary eddies are removed. We define $[u'_h v'_h]$ to be the synoptic eddy momentum flux and $[u'_s v'_s]$ to be the quasi-stationary eddy momentum flux. The remainder $(=[u'_h v'_l] + [u'_l v'_h] + [u'_l v'_l] + [u'_l v'_s] + [u'_s v'_l] + [u'_h v'_s] + [u'_s v'_h])$ is defined to be the residual eddy momentum flux. The same definitions are used for eddy temperature flux by replacing u with T. The additional term in the momentum budget, the mountain torque, is included with the quasi-stationary wave forcing because it is a result of a stationary surface pressure field.

2.5 Numerical Models

2.5.1 Primitive Equation GCM

The GCM used in this study is the dynamical core of NCAR's Community Climate

Model version 3.6. The model resolution is T42 with 28 vertical hybrid sigma/pressure levels. The model is forced by Newtonian heating and Rayleigh friction in exactly the same way as Held and Suarez (1994). The model is dry with no topography or zonally asymmetric heat sources. The biharmonic diffusion coefficient on the vorticity, divergence and temperature is 1.0e16 m^4/s. There is also regular diffusion on vorticity, divergence and temperature in the top three levels of the model to reduce the reflection of upward propagating waves (diffusion coefficient = 2.5e5 m^2/s). We use 30 years of daily wind, temperature and surface pressure data for this study. The data are interpolated to pressure levels for the computation of the EP-fluxes (Edmon et al. 1980).

2.5.2 Two-layer quasi-geostrophic model on β-plane

The dimensionless equations for the 2-layer quasi-geostrophic (QG) model on a β-plane are taken from Lee and Held (1991). The model is spectral and periodic in both x and y. The "baroclinic zone" is localized in y so that there is negligible influence of the periodic y domain on the important dynamics. The model domain is 72 by 72 distance units with a spatial grid resolution of 128 by 128. The value of β is 0.2. The thermal wind is relaxed to a Gaussian jet given by $U_e(y) = 1.0 \cdot \exp(-(y/8)^2)$ with a time scale of 60 time units. Since the model is periodic in y, the domain average U_e is subtracted from the U_e profile and treated as in Panetta (1993). The Ekman damping time scale in the lower layer is 5 time units and the biharmonic diffusion coefficient on the vorticity is 1.0e-3 in nondimensional units. The time stepping is done using the third-order Adams-Bashforth scheme (Durran 1991). The model was run for 32766 time units.

After comparing the time evolution of the zonal-mean eddy momentum fluxes of the QG model with the GCM and observations, we discovered that 1 day in nature more closely resembles 2 nondimensional time units than 1 nondimensional time unit. Hence, we define 1 "day" in the QG model to be 2 time units. (Thus the Newtonian relaxation time-scale is 30 "days" and the lower layer Rayleigh friction time-scale is 2.5 "days".) The parameters were chosen so that the model is in a strongly super-critical regime. In this regime the baroclinic wave packet evolution is irregular and chaotic, as in observations

(see Lee and Held 1993).

Chapter 3

Observed Spatial Structure of Variability

3.1 Definition of the Annular Mode

The annular mode is traditionally defined as the leading EOF of geopotential height in the lower troposphere poleward of 20° (Figure 3.1ac). The annular mode in both hemispheres has a strong zonally symmetric component although significant deviations from zonal symmetry are evident in both hemispheres. In the Southern Hemisphere, annular mode fluctuations are strongest in the Indian Ocean sector and near New Zealand. In the Northern Hemisphere, annular mode fluctuations are strongest in the Atlantic sector with prominent anomalies also present in the Pacific. In both hemispheres, the regions of strongest variability roughly correspond to the regions of strongest baroclinic wave activity and storm tracks. The annular mode is characterized by equivalent barotropic height anomalies which extend through the depth of the troposphere and even into the stratosphere (Thompson and Wallace 2000).

In this study, we base our analysis on the zonal-mean zonal wind so that we can diagnose fluctuations in the annular mode using the zonal-mean momentum budget. Since the leading EOF of the zonal-mean zonal wind is basically the same as the traditional annular mode (e.g. Wallace 2000), our analysis is also relevant for the annular mode in geopotential height. To demonstrate the strong similarity between the zonal-mean wind variability and the traditional annular mode, we compare the height anomalies which accompany EOF1 of the vertical- and zonal-mean zonal wind calculated in chapter 2 with the traditional annular mode anomalies. The position and intensity of nearly every feature

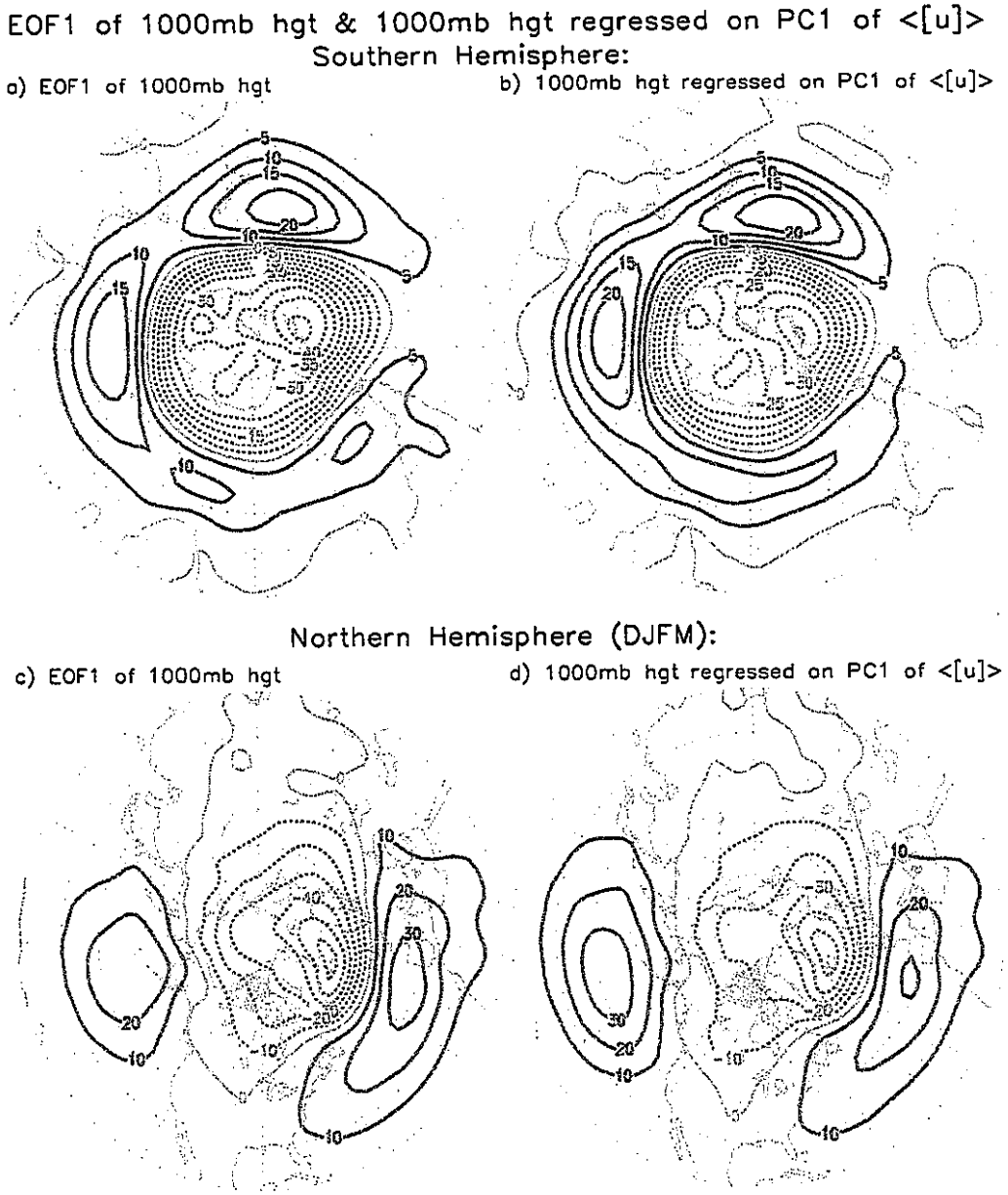

Figure 3.1: 1000mb geopotential height structure associated with leading EOF of monthly mean 1000mb height (plots on the left) and with the leading EOF of vertical- and zonal-mean zonal wind (plots on right). The EOFs are shown by regressing the monthly mean height anomalies on the normalized monthly-mean time series. Units are meters.

of the traditional annular mode is repeated almost precisely using the zonal-mean wind definition (Figure 3.1). The similarities between the anomalies which accompany EOF1 of the vertical- and zonal-mean zonal wind and the traditional annular mode include the wave-like features as well as the zonal-mean portion and therefore justify our use of the

zonal-mean zonal wind in the analysis which follows. But before describing the relationship between the annular mode zonal wind anomalies and the time-mean background flow, we note the slight differences evident in figure 3.1. The biases on the zonal-mean wind definition in the Northern Hemisphere include a slight equatorward shift of the wind anomalies over the northern Pacific Ocean near Alaska and a strengthening of the variability over the Pacific Ocean compared to the Atlantic Ocean. The differences evident in the Southern Hemisphere include a slight poleward shift in the New Zealand center of action and a slight strengthening of the variability over the Indian Ocean using the zonal-mean wind definition compared to the traditional annular mode.

3.2 Relationship between the Annular Mode and the Time-mean Flow

In this section, we calculate the leading EOF of the vertical- and zonal-average zonal wind for each season separately in order to demonstrate (1) the dependence of the annular mode on the position of the mid-latitude jet and (2) the relative insensitivity of the annular mode to the presence or absence of a strong subtropical jet (see also Hartmann and Lo 1998). The annular mode structure is shown by regressing the zonal-mean zonal wind anomalies on the principal component (PC) time series of the leading EOF of vertical- and zonal-average zonal wind.

The time-mean zonal-mean zonal wind in the Southern Hemisphere summer is dominated by the mid-latitude eddy driven jet (Figure 3.2a). The latitude of the eddy driven jet is characterized by surface westerlies which are maintained by the convergence of eddy momentum fluxes at upper levels. The weak subtropical jet in this season is represented by the "shoulder" of westerlies at upper levels on equatorward side of the mid-latitude jet. The latitude of subtropical jet is characterized by the boundary between surface westerlies and surface easterlies which marks the poleward limit of the tropical Hadley cell. The leading EOF of the *vertically* and zonally averaged zonal wind is basically a dipole with the zero wind line at the latitude of the mid-latitude jet (Figure 3.2a). This pattern therefore represents the north/south shift of the mid-latitude jet.

The same relation between EOF1 and the background flow holds for the other seasons, although it is essential that one realizes that the zonal-mean signature of the

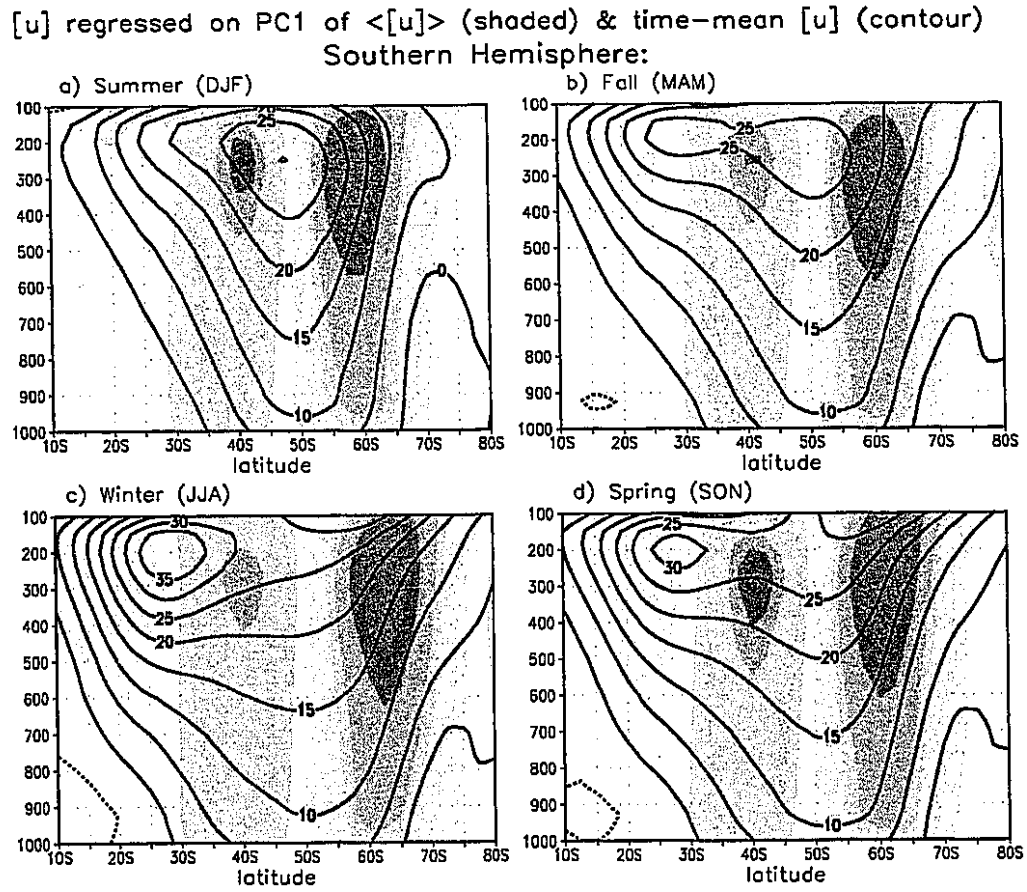

Figure 3.2: Time-mean zonal-mean zonal wind (contours) and EOF1 of the vertical- and zonal-mean zonal wind (shaded) shown by regressing the daily zonal-mean zonal wind anomalies on the normalized PC index. Results are for the Southern Hemisphere during a) Summer, b) Fall, c) Winter, d) Spring.

mid-latitude eddy-driven jet is westerly winds *near the surface*. Because drag on the zonal-mean winds near the surface in the extratropics must balance the eddy momentum flux convergence aloft, the surface winds provide a direct signature of the eddy-driven mid-latitude jet. The winds aloft, on the other hand, are also determined by the meridional temperature gradient which is controlled by a more complex range of processes. Among them is the flow in the tropical Hadley cell which sharpens the meridional temperature gradient at the poleward margin of the Hadley cell giving a dynamically distinct subtropical jet at 30°. Thus, while the strongest winds in the Southern Hemisphere winter occur at 30° S at upper-levels, the mid-latitude jet is located at 50° S where the strongest westerlies reach the surface (Figure 3.2c). Like the summer case, the annular mode is basically a

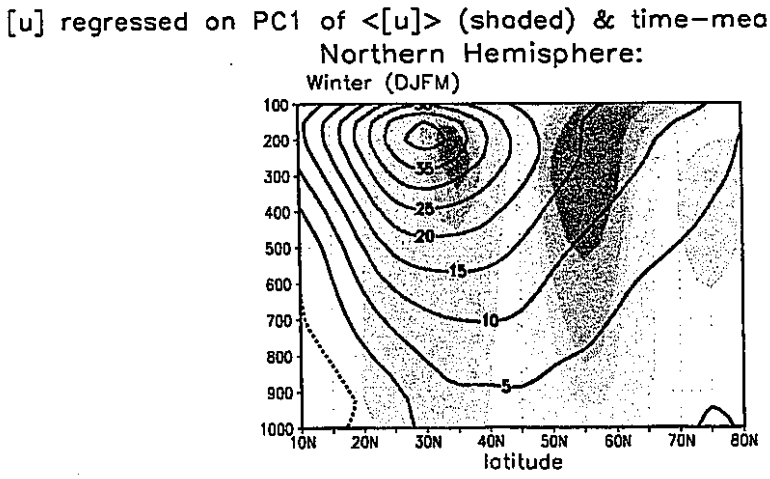

Figure 3.3: Same as 3.2 but for the Northern Hemisphere winter (Dec.-Mar.).

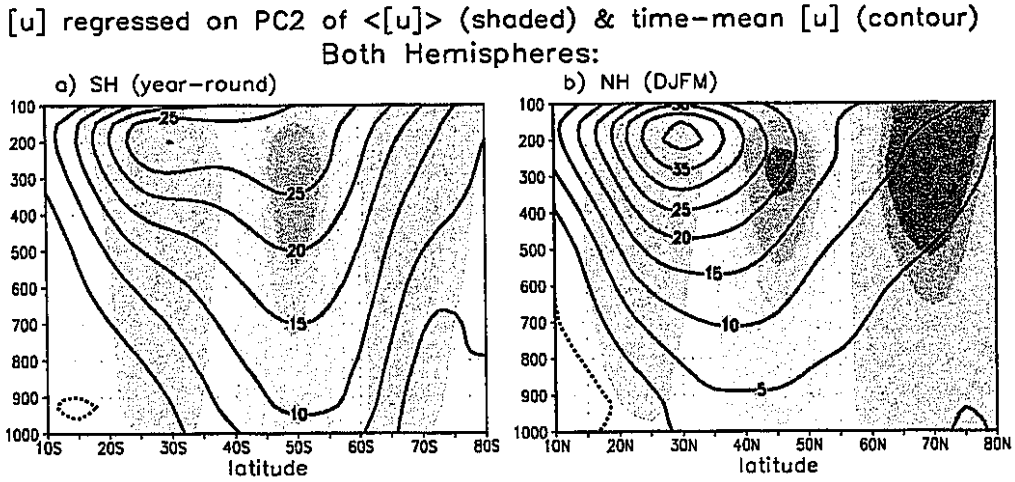

Figure 3.4: Same as 3.2 but for a) EOF2 of Southern Hemisphere (year-round) and b) EOF2 of Northern Hemisphere winter (Dec.-Mar.).

dipole with the zero wind line at the latitude of the mid-latitude jet (Figure 3.2c). The same relationship between the location of the zonal wind dipole associated with the annular mode and the time-mean mid-latitude jet exists for the fall and spring seasons. This pattern therefore represents the north/south shift of the mid-latitude jet.

For Northern Hemisphere winter, the distinction between the subtropical jet and the eddy driven mid-latitude jet is even less obvious than for Southern Hemisphere winter. Nevertheless, it is clear that the strongest surface westerlies are at 42.5° N which also coincides with the zero wind line of the annular mode dipole (Figure 3.3). Therefore, we

conclude that variability of the annular mode is best characterized by variability in the latitude of the eddy-driven jet.

3.3 EOF2

For both hemispheres, the second EOF of the vertical- and zonal-mean zonal wind is a tripole with the strongest anomaly at the latitude of the mid-latitude jet (Figure 3.4). Because EOF2 also has smaller meridional scale than time-mean zonal wind, this pattern represents a strengthening and sharpening of the jet in the positive phase and a weakening and broadening of the jet in the negative phase.

Chapter 4

Diagnosis of the positive Eddy-Zonal-Flow Feedback

In this section we diagnose the zonal-mean momentum budget in order to demonstrate the existence of positive feedback between the eddy momentum fluxes and the zonal-mean wind anomalies associated with the annular mode. In addition, we show that the strength of the positive eddy-zonal-flow feedback accounts for the greater persistence of EOF1 (i.e. the annular mode) compared to other zonally-symmetric patterns of variability. Moreover, the positive feedback accounts for all of the excess variance of the leading EOF in the Northern Hemisphere (NH) and over 70% of the excess variance of the leading EOF at low frequencies in the Southern Hemisphere (SH).

4.1 Definition of Time Series

We diagnose the effect of eddies on the EOF1 and EOF2 patterns using the methods in Lorenz and Hartmann (2001). The essential simplification in the diagnosis is that the direct effect of the eddies on vertical- and zonal-mean zonal wind variability in mid-latitudes is caused by the convergence of the eddy momentum flux alone:

$$\frac{\partial \langle [u] \rangle}{\partial t} = -\frac{1}{\cos^2\phi} \cdot \frac{\partial (\langle [u' \cdot v'] \rangle \cos^2\phi)}{a \cdot \partial\phi} - F, \tag{4.1}$$

where $\langle u \rangle$ is the vertical average of u, $[u]$ is the zonal mean of u, u' is u-$[u]$, ϕ is the latitude, a is the radius of the earth and F is the residual momentum forcing. The eddy induced mean meridional circulation mainly acts to distribute momentum vertically and therefore does not directly effect the vertical average momentum budget (see Hoskins 1983). Equation 4.1 suggests that we can diagnose the effect of the eddies on the $\langle [u] \rangle$

patterns by projecting the vertical and zonal average eddy momentum flux convergence anomalies on the $\langle [u] \rangle$ EOF patterns. This "eddy forcing" time series (=m) gives the effect of the eddies on the $\langle [u] \rangle$ PC time series (=z). For the Northern Hemisphere analysis, the mountain torque is also included in the eddy forcing because of its intimate association with the eddy momentum fluxes by the topographically generated Rossby waves (e.g. Held 1983). Thus the Northern Hemisphere momentum budget is:

$$\frac{\partial \langle [u] \rangle}{\partial t} = -\frac{1}{\cos^2\phi} \cdot \frac{\partial (\langle [u' \cdot v'] \rangle \cos^2\phi)}{a \cdot \partial\phi} - \frac{g}{p_o} \cdot \left[p_s \cdot \frac{\partial h_s}{\partial x} \right] - F ,^{1} \tag{4.2}$$

where g is the acceleration of gravity, p_o is a constant reference surface pressure, p_s is the surface pressure, h_s is the height of the large scale topography and F is the residual momentum forcing. The "eddy forcing" in the Northern Hemisphere is defined in the same way as the Southern Hemisphere except that we now include the projection of the mountain torque anomalies on the EOF patterns in the eddy momentum forcing.

4.2 Cross-spectrum analysis

The relationship between zonal wind time series (=z) and the momentum flux time series (=m) can be seen by plotting the cross spectrum between z and m divided by the z power spectrum for each frequency (Figures 4.1ad 4.2ad). The imaginary part is approximately 2π times the frequency and the real part is a small positive constant. Therefore

$$M(\omega) \cdot Z^*(\omega) = (i\omega + \tau^{-1}) \cdot Z(\omega) \cdot Z^*(\omega), \tag{4.3}$$

where capital letters denote the Fourier transform of the corresponding lower case time series, * denotes the complex conjugate, ω is the angular frequency and τ is a constant. When we divide equation 4.3 by Z^* and take the inverse Fourier transform, we get

$$\frac{dz}{dt} = m - \frac{z}{\tau}. \tag{4.4}$$

This is the same equation we would obtain if we approximated the residual forcing in

1. The true momentum equation should have the mass in both the tendency and eddy flux term and not in the denominator of the mountain torque term, *i.e.* $\langle [u] \rangle$ should be $\langle [p_s u] \rangle$, etc. The changes in momentum, however, are dominated by the wind so that (1) is a good approximation (see Madden and Speth 1995).

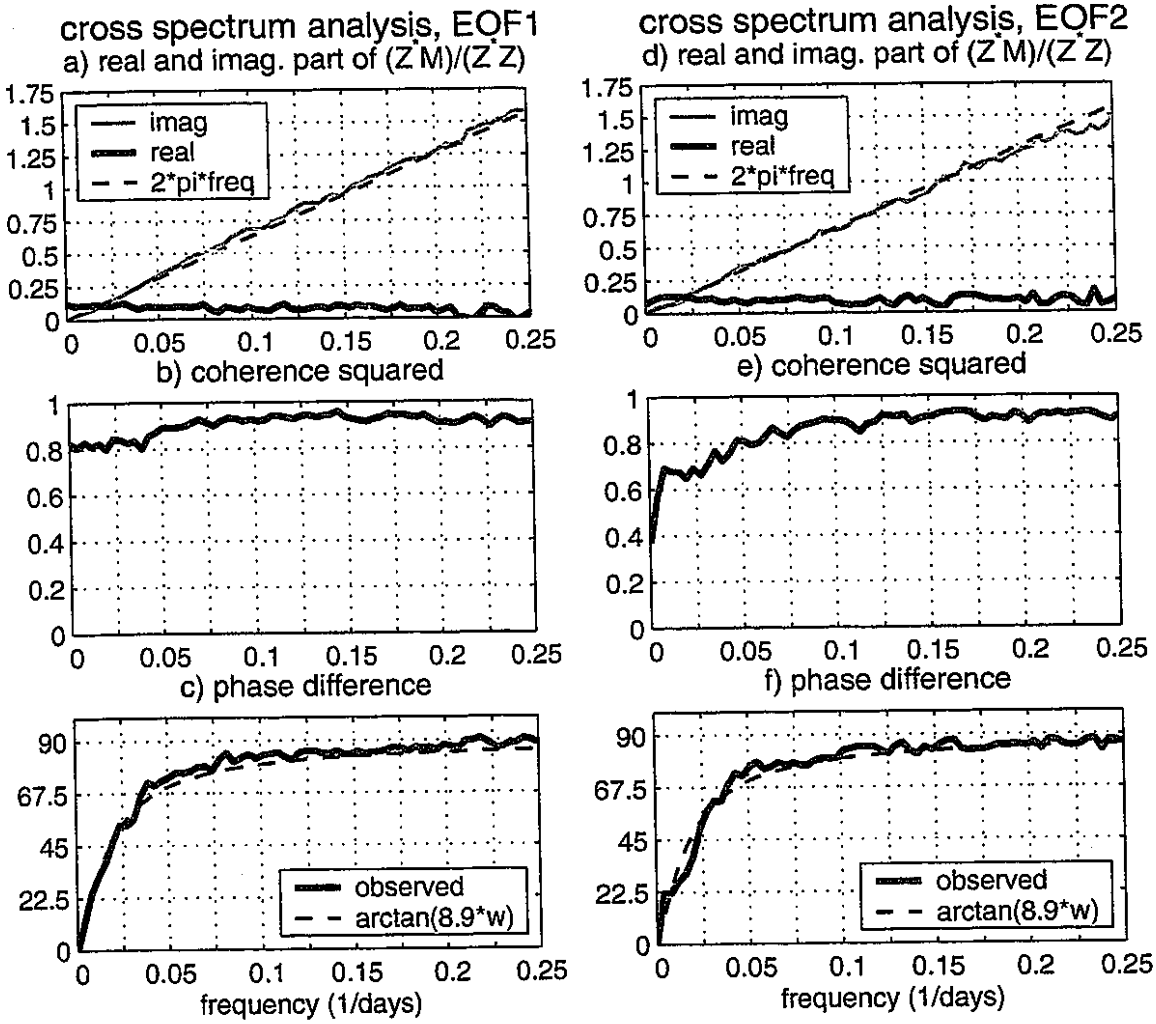

Figure 4.1: Cross spectrum analysis between the PC of the vertical- and zonal-mean zonal wind and its eddy forcing for the Southern Hemisphere. (a) The cross spectrum of PC1 and its eddy forcing divided by the PC1 power spectrum. Both the real and imaginary parts are shown as well as 2π times the frequency (dashed line). (b) Coherence squared function for PC1 and its eddy forcing. (c) Phase difference (in degrees) between PC1 of the zonal wind and its eddy forcing (blue line) and an estimate of the phase difference using equation 4.4 with $\tau = 8.9$ days (dotted line). Positive phase difference means the eddy forcing leads the zonal wind. (d), (e), and (f) are the same as (a), (b), and (c) except for PC2 instead of PC1. The x-axis is frequency in 1/days.

either equation 4.1 or 4.2 as simple Rayleigh damping with a time scale τ. The coherence squared is nearly one for most frequencies which demonstrates that the empirical relationship between z and m is very strong and consistent in the data (Figures 4.1be and 4.2be). Although the imaginary part is not exactly ω, since we only use equation 4.4 to diagnose the importance of feedbacks *relative* to observed, the constant of proportionality can be

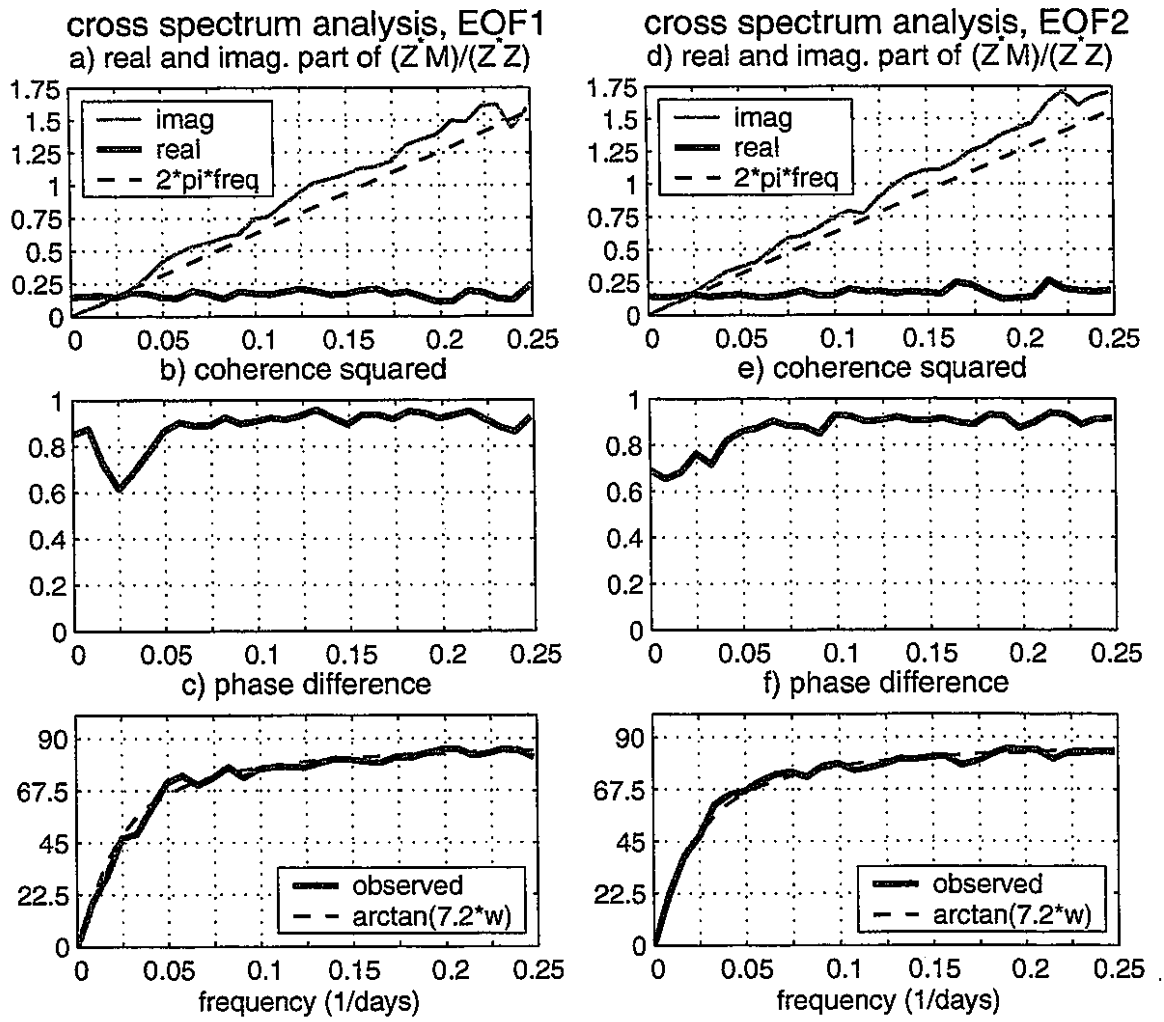

Figure 4.2: Same as 4.1 except for Northern Hemisphere winter (Dec.-Mar.) with the τ for the phase difference plot = 7.2 days.

absorbed into m. Hence, the most important relationship provided by the cross spectrum analysis is the phase between z and m. The phase determines the single relevant parameter τ. The expected phase difference between z and m implied by equation 4.4 is $\text{atan}(\tau\omega)$, where τ is the time constant for the Rayleigh damping (Figures 4.1cf and 4.2cf). The τ measured from this phase difference is 8.9 days for the Southern Hemisphere and 7.2 days for the Northern Hemisphere (see Appendix A). Note that stronger Rayleigh damping in the Northern Hemisphere compared to the Southern Hemisphere is consistent with the greater land surface area in the Northern Hemisphere.

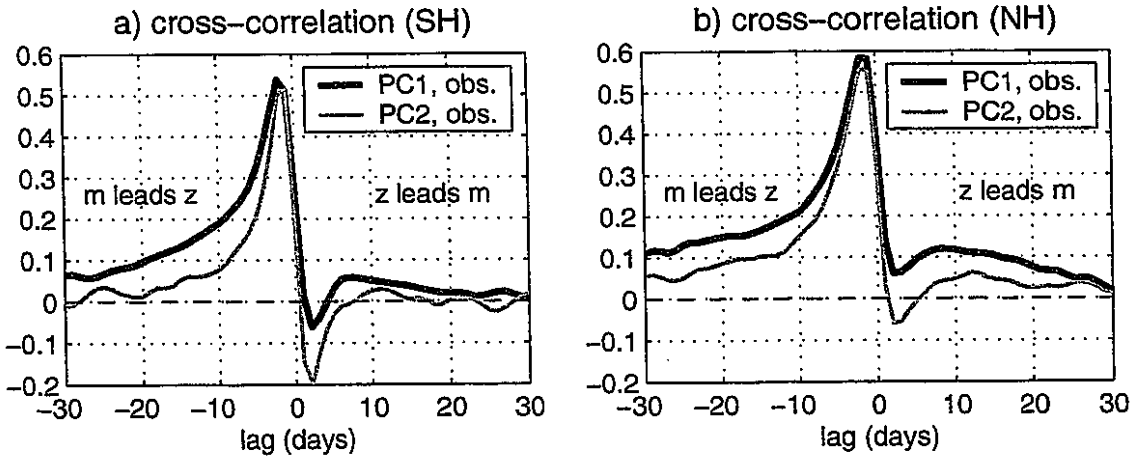

Figure 4.3: Cross-correlation between PC index for the vertical- and zonal-mean zonal wind and its eddy forcing for PC1 (blue) and PC2 (red): a) Souther Hemisphere, b) Northern Hemisphere winter (Dec.-Mar.). Positive lag means the zonal wind leads.

4.3 Effect of the Positive Feedback

To see the positive feedback, we plot the cross-correlation between z and m for different lags (Figure 4.3). Because the eddies force the $\langle [u] \rangle$ anomalies, the strongest correlations are at negative lags. To find evidence for the effect of the $\langle [u] \rangle$ anomalies on the eddy forcing, one must look for significant correlations at large positive lags beyond an eddy lifetime (Lorenz and Hartmann 2001). The assumption implicit in this argument is that without the low frequency variability of $\langle [u] \rangle$, the eddies have no long-term memory. Looking at figure 4.3ab, we see positive correlations at large positive lags for EOF1 (thick blue line) for both the Southern and Northern Hemisphere. Although the positive correlations implying a positive long-term feedback are small, they are consistently positive at all large lags leading to a large integrated zonal wind response (see the quantitative calculations below). The correlations are significant at the 95% level for lags up to 17 days for the Southern Hemisphere and for lags up to 22 days for the Northern Hemisphere (see Appendix B). Moreover, the correlations are reproducible in sub-samples of the data record. For EOF2 in the Southern Hemisphere, the small positive bump at lag +12 days is neither consistent with the correlations at other large positive lags nor reproducible in sub-samples of the data record. Therefore, we conclude that there is no positive feedback for EOF2. For

EOF2 in the Northern Hemisphere, the correlations at large positive lags are significantly different from zero for lags of 8 through 14 days and are reproducible in sub-samples of the data record. In summary, the positive long-term feedback is significant for EOF1 in both hemispheres. The positive feedback is unique to EOF1 in the Southern Hemisphere, while the positive feedback is significantly weaker for EOF2 compared to EOF1 in the Northern Hemisphere.

We repeat analysis of Lorenz and Hartmann (2001, 2003) to quantify the effect of the positive long-term feedback on zonal-mean wind variability. To estimate the effect of the positive feedback, we divide the eddy forcing into two parts: a "random part" which does not depend on the $\langle [u] \rangle$ anomalies ($=\tilde{m}$) and a "feedback part" which is proportional to the $\langle [u] \rangle$ anomalies ($=b \cdot z$, where b is a constant and z is the PC index for $\langle [u] \rangle$):

$$m = \tilde{m} + bz. \tag{4.5}$$

The system is closed by the momentum budget for the case of no feedback:

$$\frac{d\tilde{z}}{dt} = \tilde{m} - \frac{\tilde{z}}{\tau}, \tag{4.6}$$

where $\tilde{z}$ is the $\langle [u] \rangle$ PC when there is no positive feedback. Using equations 4.4, 4.5 and 4.6 we can relate the statistics of $\tilde{z}$ and $\tilde{m}$ to the observed statistics of z and m. In particular we can find the lag-correlation between $\tilde{z}$ and $\tilde{m}$ and adjust the parameter b so that the lag-correlation is zero for large positive lags (*i.e.* greater than a week). This gives the strength of the feedback ($=b$). (See Appendix C for the details of the calculations.)

Figure 4.4 shows various statistics for the zonal wind PC's (z) and their eddy forcing (m) as well as the calculated statistics for EOF1 with the positive feedback either removed (Southern Hemisphere) or reduced to the value for EOF2 (Northern Hemisphere). The long-term feedback basically accounts for the greater persistence of EOF1 compared to EOF2 (Figure 4.4be). The feedback also accounts for a large portion of the $\langle [u] \rangle$ variance in the Southern Hemisphere. In the Northern Hemisphere it appears that the simple model slightly overestimates the effect of the feedback although it is also

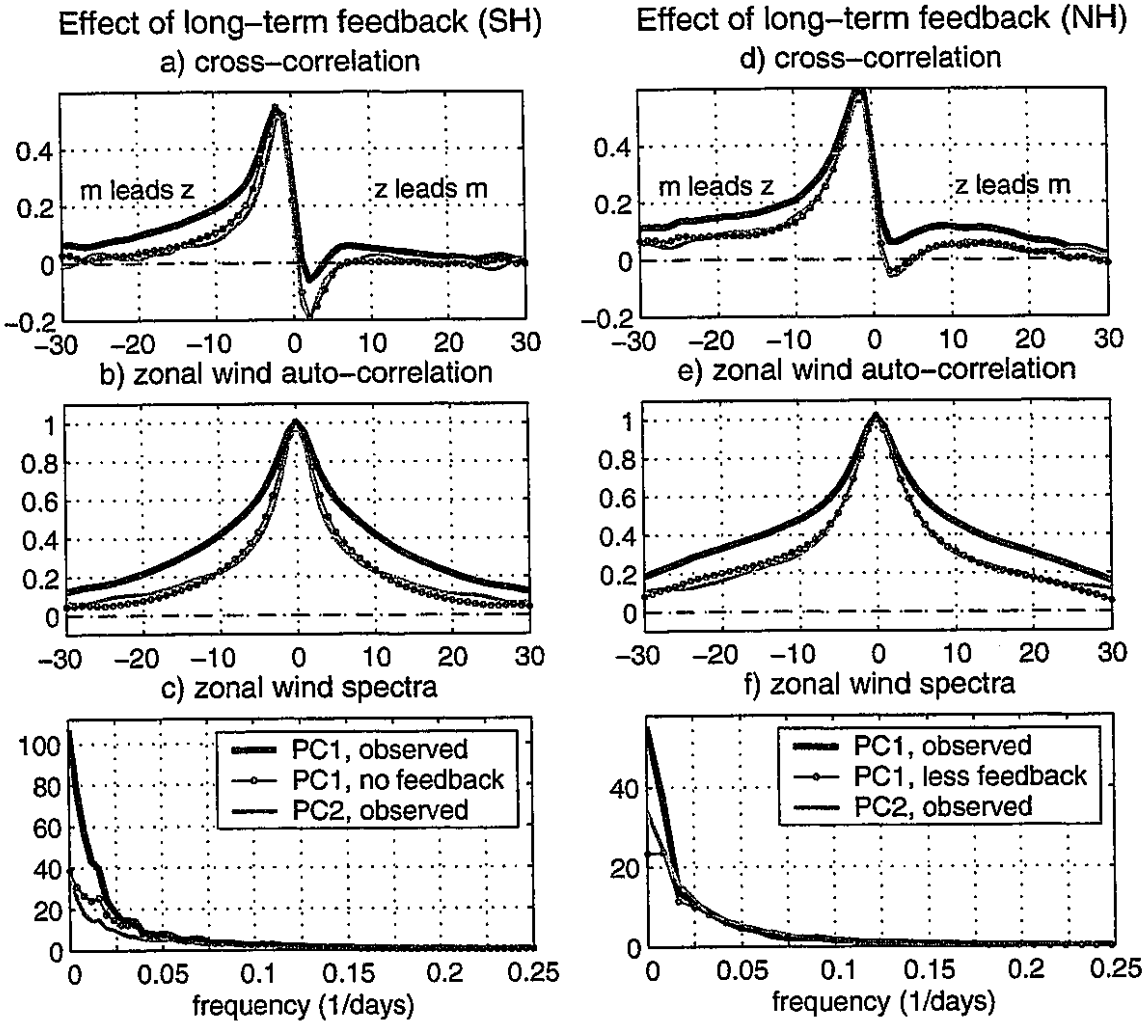

Figure 4.4: The effect of the positive eddy feedback on the variability of PC1: Blue curve=PC1, Red curve=PC2, Black curve with dots=PC1 with feedback reduced to value for PC2: a) Same as 4.3a but with the PC1 feedback removed curve included (black), b) auto-correlation for zonal wind in Southern Hemisphere, c) power spectrum for zonal wind in Southern Hemisphere, d), e), f) are the same as a), b), c) but for Northern Hemisphere winter.

possible that observed EOF2 variability is larger than estimated by the simple model because of subtropical dynamics not related to eddy fluxes.

In summary, the calculations in this section suggest that the positive eddy-zonal flow feedback plays the dominant role in determining the leading pattern of extratropical variability. One can think of "stochastic" eddy forcing variability as exciting both EOF1 and EOF2 equally. The annular mode stands out because the positive feedback makes it the least damped mode.

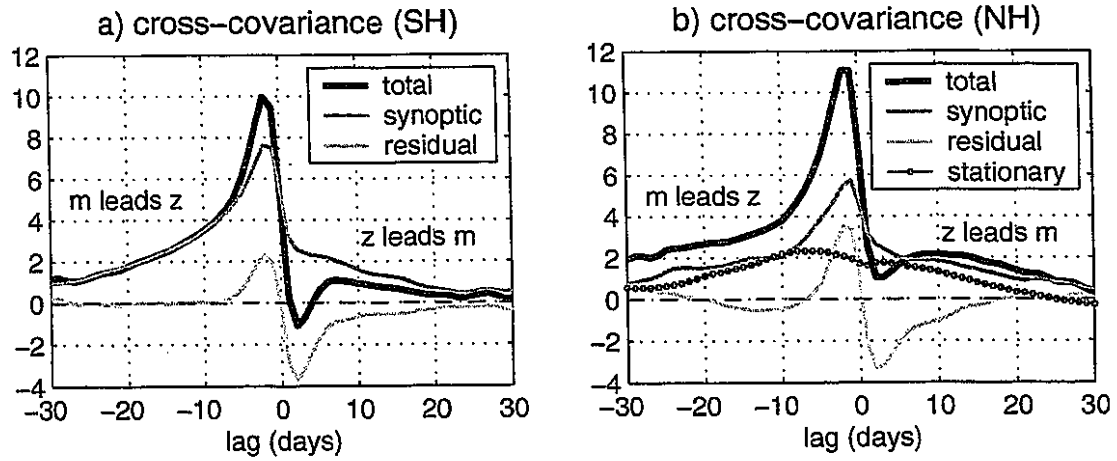

Figure 4.5: The cross covariance between PC1 and its total eddy forcing (blue), PC1 and its synoptic eddy forcing (red), PC1 and its residual eddy forcing (green), and PC1 and its quasi-stationary eddy forcing (black): a) Southern Hemisphere, b) Northern Hemisphere winter. Positive lag means that PC1 leads the eddy forcing.

4.4 Contribution of Synoptic and Quasi-stationary Waves to Positive Feedback

To get a more complete description of the eddy forcing response to the zonal-mean wind anomalies, it is useful to divide the eddies using time filtering (see Chapter 2) into synoptic, quasi-stationary and residual eddies. Thus the eddy forcing consists of three parts: the synoptic eddies, the quasi-stationary eddies and the residual eddies (i.e. everything else). For the Southern Hemisphere no insight is gained by distinguishing the quasi-stationary eddies from the residual eddies, so we simply combine these forcings together. The cross-covariance between PC1 of the zonal wind and these three forcings (Figure 4.5) allows us to compare the contribution to the positive feedback. Looking at the response to the zonal wind anomalies (i.e. positive lags beyond an eddy lifetime) we see that the synoptic eddies reinforce the wind anomalies whereas the residual eddies damp the wind anomalies. In the Northern Hemisphere the quasi-stationary eddies also contribute to the positive feedback but the synoptic eddies still make the leading contribution to the positive feedback. The fact that the synoptic eddies make the leading contribution to the positive feedback in both hemispheres gives us greater confidence that the annular modes are general patterns of extratropical variability which transcend the striking differences in the boundary forcing of each hemisphere.

Chapter 5

Dynamics of Positive Long-term Feedback

The analysis in the previous chapter suggests that the annular modes owe their prominence above other possible patterns of variability because of the reinforcing eddy response to the annular mode wind anomalies. In this chapter, we diagnose the dynamical reasons for this eddy response using time lagged regression analysis of the eddy Eliassen-Palm (EP) fluxes (Edmon et al. 1980). It is *essential* that we look at time-lagged regressions rather than simultaneous or monthly-mean regressions when diagnosing the effect of the zonal-mean wind anomalies on the eddies. The reason for the time lag is to isolate the part of the eddy forcing that is responding to the zonal wind anomalies from the burst of eddy forcing that initially created the zonal wind anomalies (Feldstein and Lee 1996, 1998; Lee and Feldstein 1996; Robinson 1996; Lorenz and Hartmann 2001, 2003). The time lag is very important because the shapes of the patterns and the relative size of the vertical and horizontal EP flux (Edmon et al. 1980) depend on the sign of the time lag. For the following figures, we average the eddy anomalies over time lags from 6 to 20 days (zonal wind leads eddies). The precise time lag is not important as long as it is greater than an eddy lifetime (here taken to be five days).

5.1 Synoptic Eddy Response to EOF1

5.1.1 Southern Hemisphere

The synoptic-eddy response to the EOF1 zonal wind anomalies consists of $[u'v']$ anomalies across the node of EOF1 (50° S) and as well as $[u'v']$ anomalies of the opposite sign in the subtropics (Figure 5.1a). These $[u'v']$ anomalies tend to reinforce the zonal-

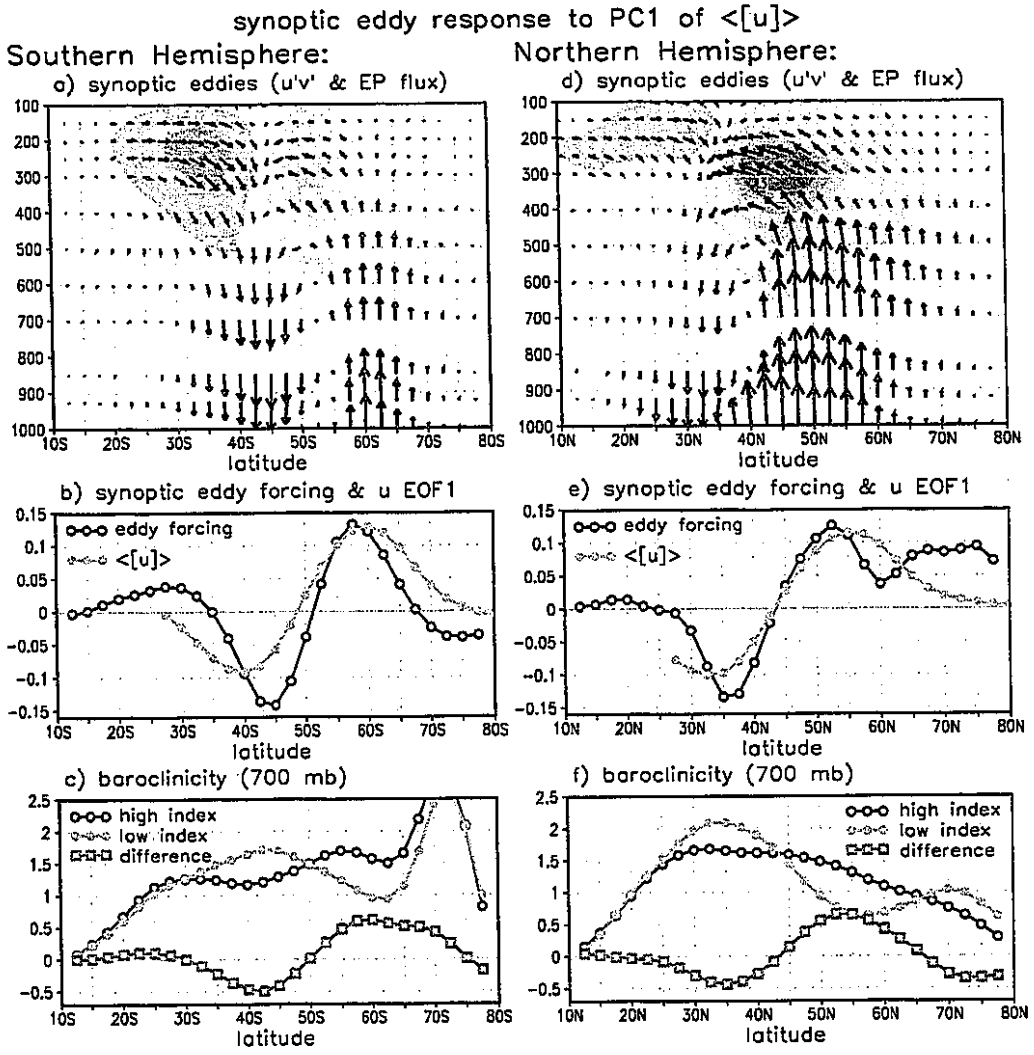

Figure 5.1: Synoptic eddy response to the PC1 wind anomalies. a) Lag regression of [u'v']cos(ϕ) (color) and EP flux (vectors) anomalies by the synoptic eddies on PC1 in Southern Hemisphere. The plot is the averaged over time lags from 6 to 20 days (PC1 of the wind leads eddies). b) Lag regression of the vertical-average synoptic eddy forcing (open circles) on PC1 (units are m/s/day). The curve is averaged over time lags from 6 to 20 days. The EOF1 weighting pattern (solid circles) is included for reference (arbitrary units). c) The composite baroclinicity (see text for definition) during the high and low index as well as the difference (units are 1/day). d), e), f) are the same as a), b), c) but for the Northern Hemisphere winter.

mean wind anomalies associated with EOF1. This is demonstrated by figure 5.1b which shows the vertical-average synoptic eddy momentum flux convergence consistent with figure 5.1a as well as the EOF1 zonal wind pattern. The $[u'v']$ are associated with corresponding changes in the vertical EP flux both north and south of 50° S (Figure 5.1a). These EP flux anomalies imply stronger baroclinic wave generation in the region of stron-

ger westerlies. Looking at the composite 'baroclinicity' ($=(g\theta_y)/(\theta_0 N)$, this is proportional to the Eady (1949) wave growth rate) during the high and low index (Figure 5.1c), we see that the changes in baroclinicity coincide with the zonal wind anomalies and are roughly consistent with the changes in the vertical EP flux. Thus the basic picture is: baroclinic wave generation is strongest (weakest) in the region of positive (negative) wind anomalies which corresponds to the region of above (below) normal baroclinicity. The waves then propagate meridionally from the wave source at upper levels. Because the waves tend to propagate equatorward rather than poleward from their source, the momentum flux anomalies are not symmetric about the latitude of the maximum wind anomalies but are strongest equatorward of the wind anomalies. This bias toward equatorward wave propagation or, equivalently, poleward momentum fluxes results from spherical geometry (Balasubramanian and Garner 1997; Whitaker and Snyder 1993).

5.1.2 Northern Hemisphere

The synoptic-eddy response to the EOF1 zonal wind anomalies consists of strong $[u'v']$ anomalies across the node of EOF1 (42.5° N) and weaker $[u'v']$ anomalies in the subtropics (Figure 5.1d). These $[u'v']$ anomalies tend to reinforce the zonal-mean wind anomalies associated with EOF1 (Figure 5.1e). Like the Southern Hemisphere, the $[u'v']$ across 42.5° N are associated with corresponding changes in the vertical EP flux both north and south of 42.5° N, however, the vertical EP flux anomalies north of 42.5° N are considerably stronger than those south of 42.5° N. These EP flux anomalies imply stronger baroclinic wave generation in the region of stronger westerlies especially in the high index. Looking at the composite 'baroclinicity' during the high and low index (Figure 5.1f), we see that the changes in baroclinicity are roughly consistent with the changes in the vertical EP flux. Moreover, the changes in baroclinicity are stronger north of 42.5° N than south of 42.5° N which is the same sense as the asymmetry in the vertical EP flux, although not as strong. Also note that the weak $[u'v']$ in the Northern Hemisphere subtropics compared to the $[u'v']$ in the Southern Hemisphere subtropics is consistent the rel-

atively weak vertical EP flux in the Northern Hemisphere around 32° N. In general, the same basic pattern and interpretation holds for both hemispheres.

5.1.3 Summary

The main points of this section are that (1) changes in $[u'v']$ are associated with changes in the source of synoptic waves and (2) these changes in the source of synoptic waves are roughly consistent with the changes in the baroclinicity.

5.2 Residual Eddy Response to EOF1

The residual eddy response in the Northern and Southern hemisphere are sufficiently similar that we discuss them together.

The long-term response of the residual eddies to the zonal-wind anomalies is dominated by waves in the 15 to 40 day period range rather than the 'cross-frequency' terms of the residual eddy fluxes. The residual-eddy momentum flux anomalies are strongest near the node of EOF1 and are in a direction that tends to damp the zonal wind anomalies (Figure 5.2). The structure of the residual eddy $[u'v']$ pattern in the mid-latitudes is significantly more barotropic than the synoptic eddies: the amplitude of the fluxes varies by a factor of two between the upper and lower troposphere for the residual eddies, while for the synoptic eddies the amplitude varies by nearly an order of magnitude. The deep vertical structure of the $[u'v']$ anomalies suggests that these waves are predominantly external Rossby waves (Held et al. 1985). External Rossby waves are vertically trapped in the tropospheric 'wave guide' and therefore consist of a superposition equal amounts of upward and downward propagating waves. This simplifies the dynamics in that the relevant index of refraction is $(\beta - u_{yy})/(u - c)$ at a *single* 'equivalent barotropic level' (Held et al. 1985). Composites during the high and low index days (Figure 5.2cf) show that the external Rossby wave index of refraction is basically largest in the region of positive wind anomalies. Thus external Rossby waves tend to propagate poleward across 45°-50° during the high index and equatorward across 45°-50° in the low index. Outside the mid-latitudes the wave anomalies are not barotropic so the simplified index of refraction does not apply.

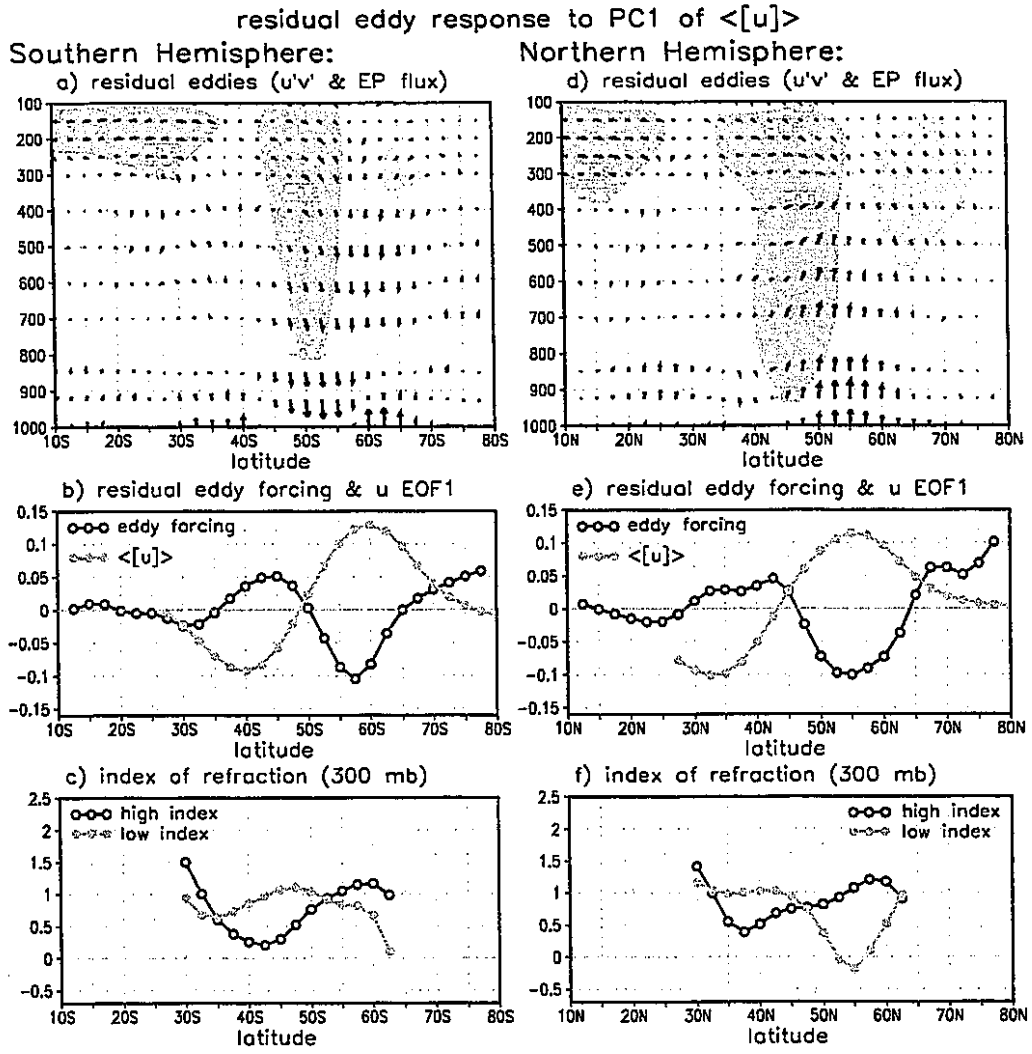

Figure 5.2: Residual eddy response to the PC1 wind anomalies. a), b) same as 5.1 but for the residual eddies c) composite external Rossby wave index of refraction at 300mb during high and low index (plotted only where eddies look like external Rossby waves) . d), e), f) are the same as a), b), c) but for the Northern Hemisphere winter.

In summary, the jet is a wave guide for external Rossby waves (see also Hoskins and Ambrizzi 1993; Yang and Hoskins 1996). Therefore, external Rossby waves tend to propagate into the jet and, since wave momentum transport is opposite to wave propagation, remove momentum from the jet.

Before moving onto quasi-stationary waves, we would like to make a note relating to waveguides and the results in later chapters. While the barotropic external Rossby wave type structure of the low frequency eddy response does not appear to be a general charac-

teristic of annular modes in GCMs, the ideas relating to waveguides developed in this section will turn out to be very important in the theory explaining the relationship between the annular mode and the background flow. In this case, the relevant refractive index will involve the potential vorticity (PV) gradient rather than the 'barotropic version' of the PV gradient ($=\beta - [u]_{yy}$) used here.

5.3 Quasi-stationary Eddy Response to EOF1

In the mid-latitudes of the Southern Hemisphere, the anomalies by the low frequency waves look like external Rossby waves. In the Northern Hemisphere, a portion of these anomalies also look like external Rossby waves (the residual eddies), but the fluxes by the very low frequency (<1/40 days^{-1}) waves have a very different structure: the $[u'v']$ is concentrated at upper levels and the vertical EP flux anomalies are much larger (Figure 5.3a). The reasons for the difference between the Northern and Southern Hemisphere are the strong stationary wave sources in the mid-latitudes of the NH compared to the SH. Near stationary wave sources, the wave field consists of a full spectrum of waves. It is only away from wave sources that the dispersion of excess wave activity and reflections within the tropospheric wave guide set up an external Rossby wave field (Held 1983; Held et. al. 1985). Thus in the NH, waves at very low frequency (e.g. waves that are stationary or nearly stationary) are dominated by waves dispersing from mid-latitude wave sources rather than external Rossby waves. In the NH, it is only in the medium frequency range that external Rossby waves dominate over other waves generated locally (either by stationary sources or by baroclinic instability).

The vertical average forcing by the quasi-stationary waves is very strong especially poleward of 55° N (Figure 5.3b) which agrees with DeWeaver and Nigam (2000a). However, this strong forcing does not project well onto the EOF1 wind anomalies. The positive feedback by the quasi-stationary waves is mixed with a response which tends to move the anomalies poleward (see also Feldstein 1998). Also note that the mountain torque anomalies (due to Greenland) tend to damp the forcing by $[u'v']$ north of 60° N. (The effect of the mountain torque on the $[u'v']$ forcing (open circles) is shown by the open squares.)

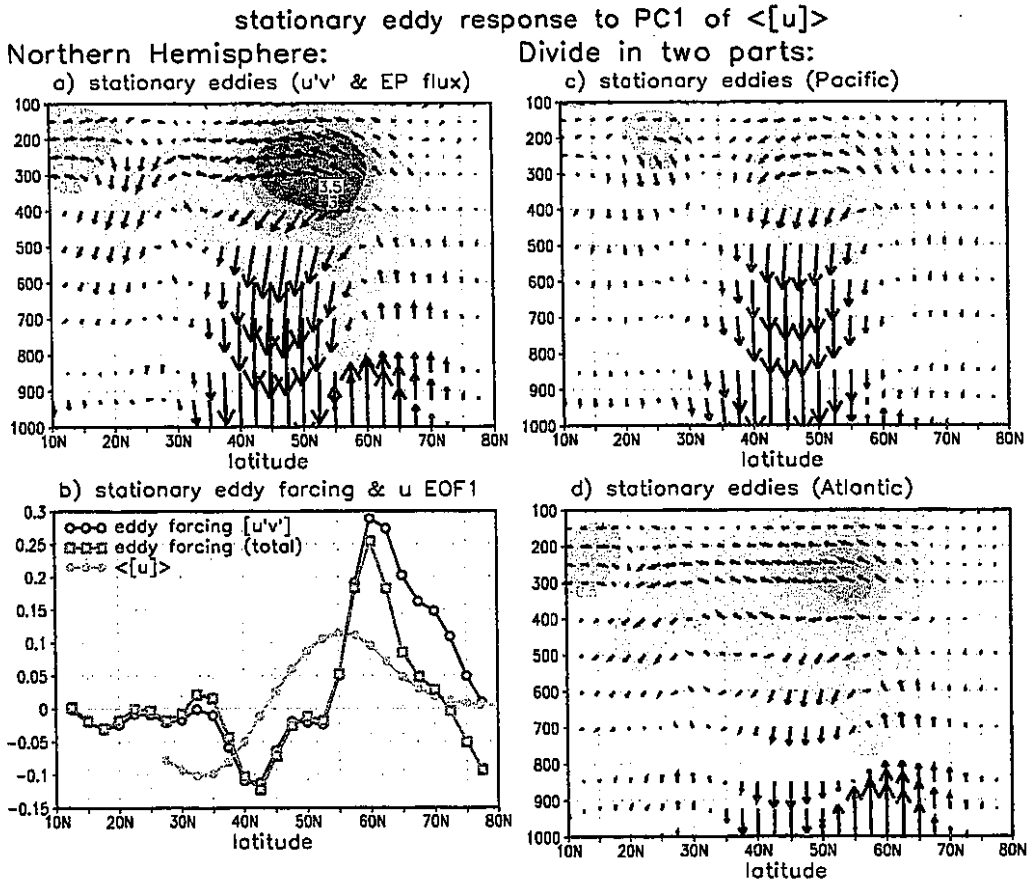

Figure 5.3: Quasi-stationary eddy response to the PC1 wind anomalies. a) b) same as 5.1 but for the quasi-stationary eddies in the Northern Hemisphere winter. The red curve in b) shows the effect of the mountain torque on the usual convergence of meridional momentum flux term. The plots on the right show the response in a) divided up into the contribution from the c) Pacific and the d) Atlantic sector.

Because of the less than optimal projection of quasi-stationary wave forcing onto EOF1 and the stationary eddy mountain torque, the quasi-stationary waves do not dominate the positive feedback associated with EOF1.

At first sight, figure 5.3b suggests the following explanation for the quasi-stationary eddy forcing: the anomalous source of wave activity around 45° N during the low index leads to the anomalous propagation of wave activity away from the source latitude and the observed $[u'v']$ anomalies. Looking more carefully, however, we see evidence that suggests other mechanisms may be more important. First, when we divide the total quasi-stationary wave into contributions from the Atlantic and Pacific sectors (Figure 5.3cd,

90° E and 90° W are the dividing longitudes) we see that the vertical EP flux is concentrated in the Pacific sector while the horizontal EP flux is concentrated in the Atlantic sector. Moreover, the horizontal EP flux anomalies in the upper troposphere in the Atlantic are stronger than the EP flux anomalies below (for example 500mb) so that the horizontal EP flux anomalies appear discontinuous from the wave sources at low levels.[1] Because the majority of the anomalies in the horizontal EP flux seem to be independent of changes in the wave source, it appears that changes in the zonal-mean flow in the middle to upper troposphere are most important (i.e. changes in the refractive index).

To help explain the quasi-stationary wave forcing we use the zonal-mean quasi-geostrophic refractive index (Matsuno 1970) for waves with zero frequency:

$$n^2 = \frac{[q]_\phi}{[u]} - \left(\frac{k}{a\cos\phi}\right)^2 - \left(\frac{f}{2NH}\right)^2, \tag{5.1}$$

where

$$[q]_\phi = \frac{2\Omega}{a}\cos\phi - \frac{1}{a^2}\left(\frac{([u]\cos\phi)_\phi}{\cos\phi}\right)_\phi - \frac{f^2}{\rho_0}\left(\rho_0\frac{[u]_z}{N^2}\right)_z. \tag{5.2}$$

Here, k is the zonal wavenumber, ω is the wave frequency, N is the buoyancy frequency, H is the scale height (8 km), f is the Coriolis parameter, a and Ω are the earth's radius and angular frequency, ρ_0 is the background density, and ϕ is latitude. Waves can propagate in regions of positive refractive index and waves are evanescent in regions of negative refractive index (light shading in Figure 5.4). Also, waves tend to be refracted toward large positive refractive index. Since refractive index for stationary wavenumbers 1 and 2 are very similar, we only show the results for wavenumber 1 below.

In the upper troposphere, the most prominent difference between the high and low phase of PC1 is the large refractive index north of 57.5° N at 500mb-400mb during the low phase (Figure 5.4, see also Limpasuvan and Hartmann 2000). As noted by Limpasuvan and Hartmann (2000), the large quasi-stationary wave forcing poleward of 57.5° N

1. Remember that these EP fluxes are anomalies. The sum of the time mean and the anomalies still implies a lower tropospheric source.

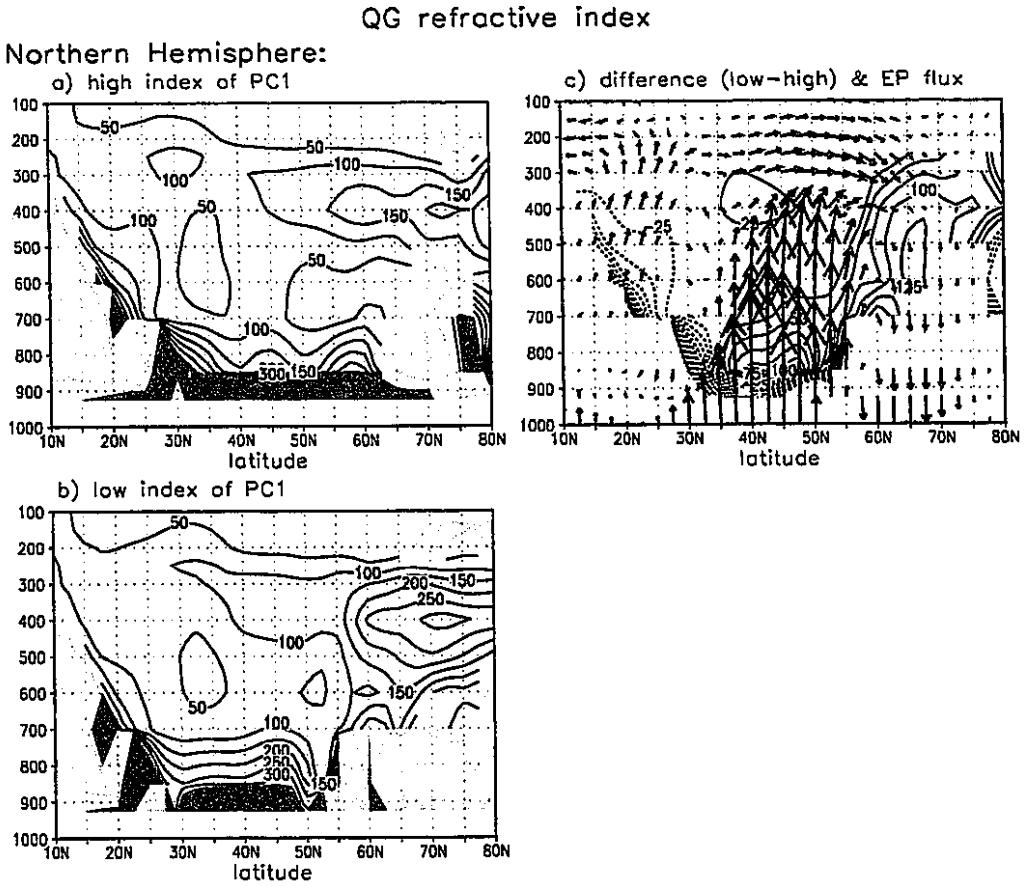

Figure 5.4: Quasi-geostrophic refractive index for stationary wave 1. The values are nondimensionalized by the radius of the earth squared. In (a) and (b) negative values are lightly shaded and values larger than 300 are black. (a) High index. (b) Low index. (c) Low minus high index. The quasi-stationary EP flux anomalies from Figure 5.3a are also shown (with the reverse sign).

bears a striking resemblance to the large difference in refractive index between the high and low phases of PC1. The difference between the low and high phase (Figure 5.4c) shows a large increase as one moves poleward across 57.5° N much like the vertical-average quasi-stationary wave forcing (Figure 5.3b). During the low phase of PC1, this region of increased refractive index tends to attract wave activity leading to an easterly momentum forcing in this region (Limpasuvan and Hartmann 2000). Chen and Robinson (1992) studied the effect of a very similar refractive index profile on quasi-stationary waves in a linear primitive equation model and found similar results. Essentially, a region of high refractive index is a wave sink. In the low phase of PC1, the high latitudes are a more effective sink of wave activity.

5.4 The maintenance of baroclinic westerlies

This chapter has provided dynamical mechanisms whereby $[u]$ anomalies cause reinforcing eddy momentum fluxes. The most important dynamical mechanism seems to involve synoptic waves and the changes in baroclinicity which are collocated with the zonal wind anomalies. The changes in baroclinicity have added another twist to the wave-mean-flow problem. In order to sustain long-term baroclinic westerly anomalies, we must consider not only the dynamics which maintain the surface westerlies (*i.e.* the vertical average momentum budget), but also the dynamics which maintain the baroclinicity against the tendency of the synoptic waves to reduce the baroclinicity. The theory which deals with this problem (Robinson 2000) is outlined below.

While Robinson (2000) considered a continuously stratified quasi-geostrophic fluid, all of the essential points can be demonstrated using a simpler 2-layer quasi-geostrophic model with Newtonian heating for the "temperature" and Rayleigh damping for the low-level wind. The upper-level zonal-mean potential vorticity equation is:

$$\frac{\partial [q_1]}{\partial t} = -\frac{\partial [v_1' q_1']}{\partial y} + \kappa_T \left(\frac{[\psi_1] - [\psi_2]}{2} - \frac{[\psi_e]}{2} \right), \tag{5.3}$$

where q is the quasi-geostrophic potential vorticity, ψ is the streamfunction, κ_T is the Newtonian damping parameter, the subscript e refers to the "radiative equilibrium" profile and the subscripts 1 and 2 refer to the upper and lower layer respectively. Since we are interested in the long-term maintenance of baroclinic westerlies we only consider the steady limit. In the steady limit, the time derivative term is zero. After taking the y derivative and using the fact that $u = -\partial\psi/\partial y$, equation 5.3 becomes:

$$-\frac{\partial^2 [v_1' q_1']}{\partial y^2} = \kappa_T \left(\frac{[u_T]}{2} - \frac{[u_e]}{2} \right), \tag{5.4}$$

where u_T $(=u_1 - u_2)$ refers to the thermal wind. Subtracting the climatological version of the above equation gives:

$$-\frac{\partial^2 [v_1' q_1']_a}{\partial y^2} = \kappa_T \frac{[u_T]_a}{2}, \tag{5.5}$$

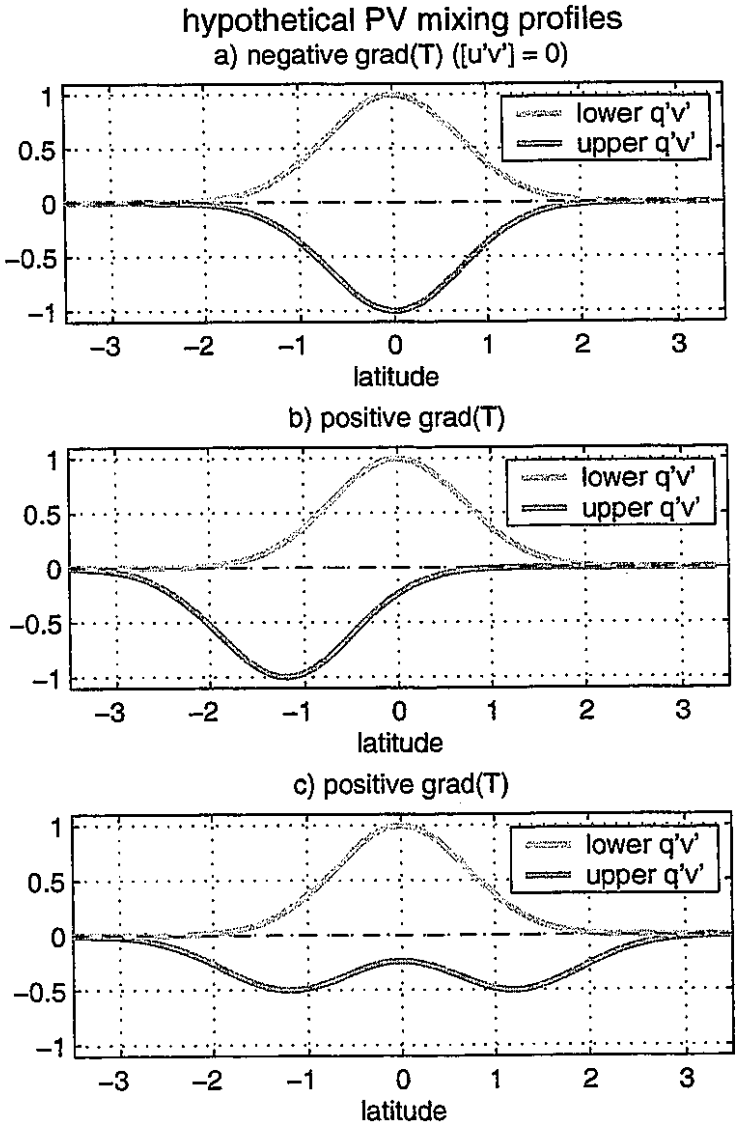

Figure 5.5: Hypothetical PV mixing profiles illustrating scenarios where the steady state temperature gradient forced by [q'v'] either a) does not favor further wave generation at latitude=0 or b) and c) does favor further wave generation at latitude=0 (see text).

where the subscript a denotes anomaly. Equation 5.5 states that the steady state temperature gradient (*i.e.* thermal wind) is determined by the upper-level potential vorticity (PV) flux alone. To gain intuition about our problem, however, we consider the PV flux in both layers.

Suppose there is a localized region of downgradient $[v_1'q_1']$ and $[v_2'q_2']$ due to

baroclinic instability. We want to understand conditions which allow the temperature gradient to be maintained against the mixing of temperature by the waves. 1) If the waves do not propagate meridionally at upper-levels from their source region, then $[v_1'q_1']$ and $[v_2'q_2']$ are the same shape and amplitude but opposite sign (Figure 5.5). Thus $[v_1'q_1']$ has a local minimum at the region of strongest wave generation which means $[v_1'q_1']$ is concave upward. Therefore the temperature gradient is negative in the wave generation region (see equation 5.5) and the baroclinicity is not maintained in this case. 2) If the wave propagate meridionally at upper-levels such that the irreversible mixing ($[v_1'q_1']$) occurs on the flanks of the jet, then the $[v_1'q_1']$ profile is displaced. It is now possible for the $[v_1'q_1']$ profile to be concave downward in the wave generation region. In this case, the temperature gradient is positive and the baroclinicity is maintained despite the action of the baroclinic waves. Figure 5.5 shows two possible scenarios illustrating this case.

In summary, the waves must propagate away from the region of wave generation in order to maintain the anomalous baroclinicity associated with the annular modes. Coincidentally, the vertical-average momentum budget also requires meridional wave propagation in order to maintain the anomalous surface westerlies associated with the annular modes.

Chapter 6

GCM experiments

In this chapter, we describe initial value experiments with a GCM designed to explore the differences between the eddy response to EOF1 and EOF2. In addition, the experiments will (1) confirm that the eddy response to zonal-mean wind anomalies can be diagnosed using lag regressions as in the previous chapters and (2) provide insight into the short-term transient response observed in figure 4.3 at small positive time lags. Before describing the initial value experiments, we confirm that the internal variability of the model is similar to observations.

6.1 Annular mode in Control Run

6.1.1 Time-mean and EOF analysis

The model is a simple, dry GCM forced by zonally uniform Newtonian heating and near-surface Rayleigh damping (see Chapter 2). The time-mean zonal-mean zonal wind for the GCM is most like the Southern Hemisphere summer because the flow is dominated by the mid-latitude eddy driven jet (Figure 6.1, compare with Figure 3.2). The latitude of the eddy driven jet is characterized by surface westerlies which are maintained by the convergence of eddy momentum fluxes at upper levels. The weak subtropical jet in this model is represented by the "shoulder" of westerlies at upper levels on equatorward side of the mid-latitude jet. The latitude of subtropical jet is characterized by the boundary between surface westerlies and surface easterlies which marks the northern limit of the tropical Hadley cell.

The leading EOF of the *vertical* and zonal average zonal wind ($=\langle [u] \rangle$, where <>

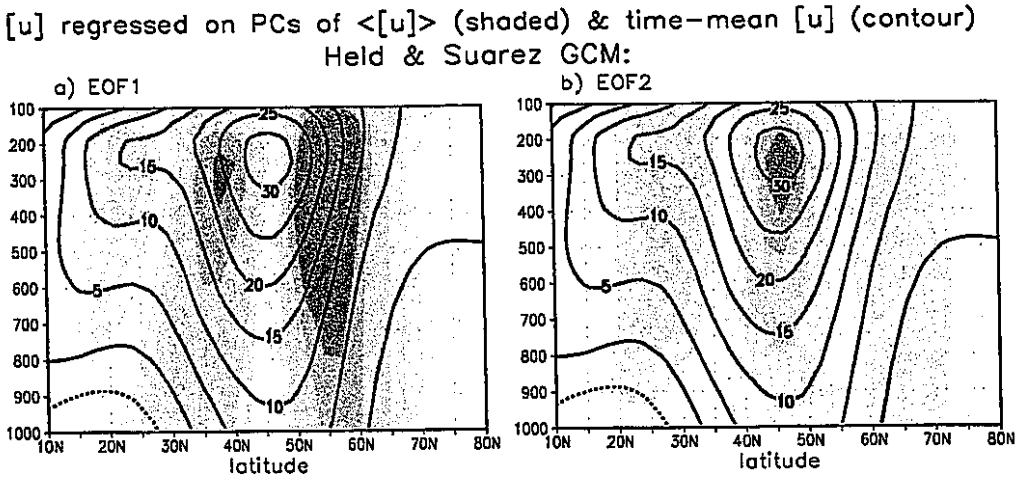

Figure 6.1: Time-mean zonal-mean zonal wind (contours) and the EOFs of the vertical- and zonal-mean zonal wind (shaded) shown by regressing the daily zonal-mean zonal wind anomalies on the normalized PC index. Results are for the GCM for a) EOF1, b) EOF2.

represents a vertical average and [] represents a zonal average) is basically a dipole with the zero wind line at the latitude of the mid-latitude jet (Figure 6.1a). This pattern therefore represents the north/south shift of the mid-latitude jet. The same relation between EOF1 and the background flow holds for observations (Chapter 3). When making the comparison with observations, it is important to note that the latitude of eddy-driven jet is the latitude where the surface westerlies are strongest. There is also a weaker anomaly in subtropics associated with EOF1, which is also present in observations. This feature lags the main EOF dipole in time (see Lorenz and Hartmann 2001) because mid-latitude $[u]$ anomalies cause eddy momentum flux convergence anomalies in the subtropics.

The second EOF of $\langle [u] \rangle$ is a tripole with the strongest anomaly at the latitude of the mid-latitude jet (Figure 6.1b). Because EOF2 also has smaller meridional scale than time-mean $[u]$, this pattern represents the strengthening and sharpening of the jet in the positive phase and the weakening and broadening of the jet in the negative phase. This EOF2 pattern is also observed in nature (Figure 3.4).

6.1.2 Diagnosis of momentum budget

We diagnose the effect of eddies on the EOF patterns using the methods in Chapter 4. A cross-spectrum analysis shows that the vertical- and zonal-mean momentum budget is

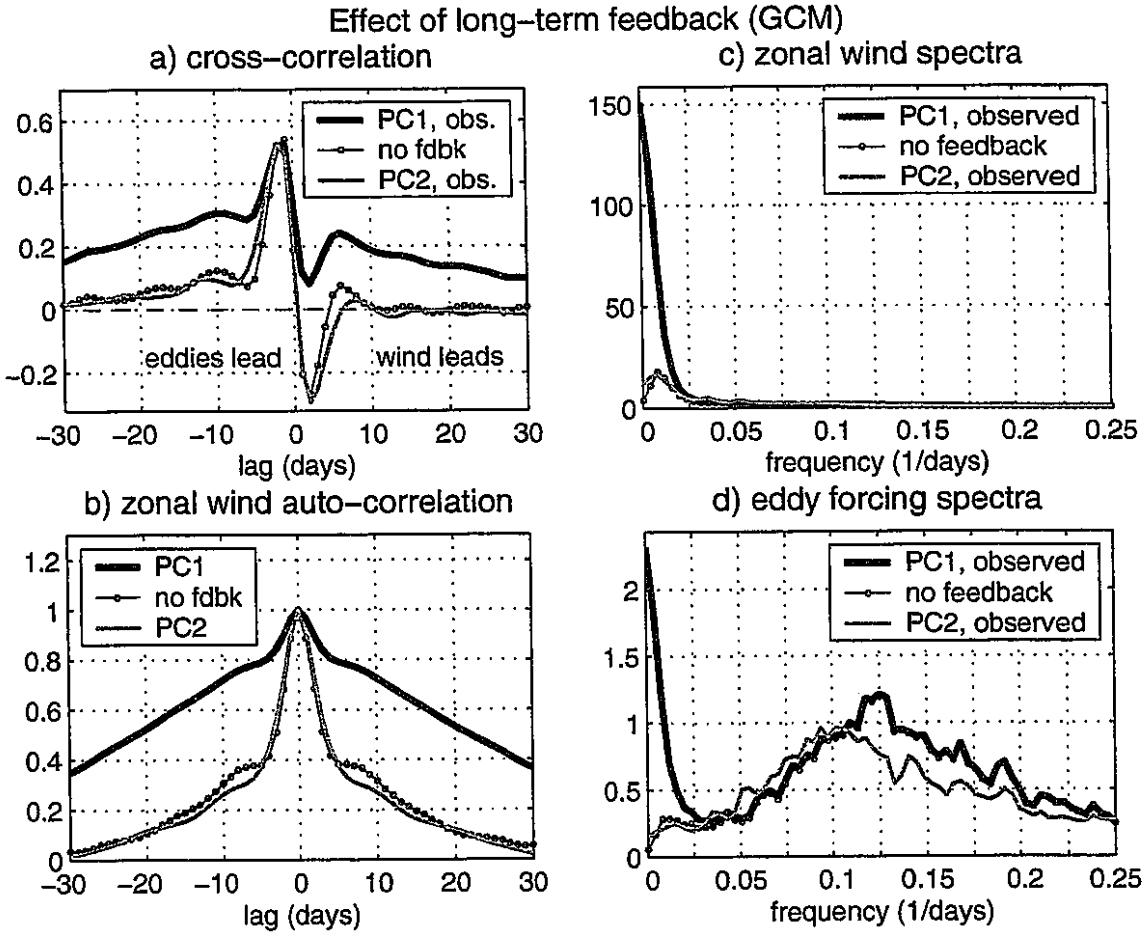

Figure 6.2: The effect of the positive eddy feedback on the variability of PC1: Blue curve=PC1, Red curve=PC2, Black curve with dots=PC1 with feedback removed: a) lag-correlation between zonal wind and its eddy forcing (positive lag means zonal wind leads), b) auto-correlation for the zonal wind, c) power spectrum for zonal wind, d) power spectrum for the eddy forcing.

well approximated by equation 4.4 with $\tau = 11.0$ days. The lag correlation between the zonal-mean zonal wind time series (=z) and the eddy momentum forcing time series (=m) clearly shows that the positive long-term eddy feedback is unique to EOF1 (Figure 6.2a). The effect of the positive feedback on the variability and persistence of the leading EOF is diagnosed using the methods in Chapter 4 (Figure 6.2). The positive feedback accounts for the increased persistence (Figure 6.2b) and variance (Figure 6.2c) of EOF1 compared to EOF2. We also compare the power spectrum of the eddy forcing of EOF1 and the eddy forcing of EOF2 since the signature of the positive feedback can be clearly seen in this case (Figure 6.2d). Note that the EOF2 spectra is basically flat at low frequencies implying

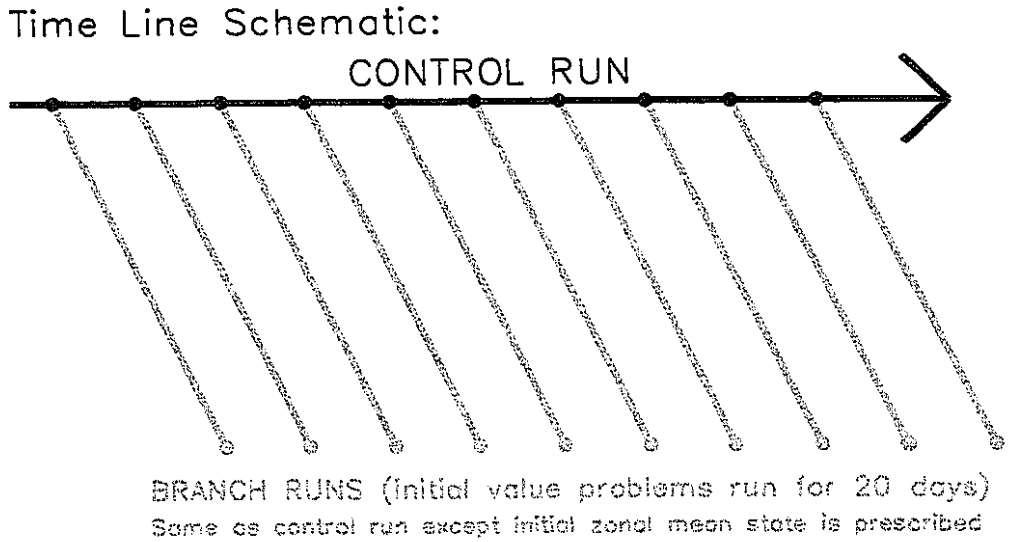

Figure 6.3: Schematic of a branch run experiment. Many initial value problems are integrated with the eddy fields taken from each day of the control run. The initial zonal-mean state, on the other hand, is prescribed and is the same for each branch run.

no long-term memory, while the EOF1 spectrum exhibits a large increase in power at the lowest frequencies because of the feedback. Also, except for the lowest frequencies, the EOF1 and EOF2 spectra have nearly the same power. This implies that the "random forcing" of both EOF1 and EOF2 is the same and that it is the presence of a positive feedback at low frequencies which accounts for the difference between EOF1 and EOF2.

Note also broad maximum in both the EOF1 and EOF2 spectra at frequencies around 0.1 to 0.125 day^{-1}. This maximum is associated with the distinct transient swing in eddy forcing past its final long-term value (see small positive time lags in Figure 6.2a). We will see in next section that this is a transient response of the eddies to zonal wind variability (consistent with results of Robinson (1994)).

6.2 Initial value experiments

6.2.1 Basic Method

To confirm that changes in $[u]$ affect the eddies in the manner diagnosed from the lag regression and the lag correlation analysis in the previous section, we run a very large number of initial value experiments. For each day of a 10 year control experiment we run four 20-day branch runs. The initial eddy fields for these branch runs are the same as the

eddy fields of the corresponding day in the control run. The initial zonal-mean state, on the other hand, is a composite zonal-mean state based on the PC index of either EOF1 or EOF2 of the control run. For each day we run four branch runs based on four zonal-mean states. The initial zonal-mean states for the four experiments are the composite $[u]$, $[v]$, $[T]$ and $[p_{surface}]$ when (1) PC1 of $\langle [u] \rangle$ is positive, (2) PC1 of $\langle [u] \rangle$ is negative, (3) PC2 of $\langle [u] \rangle$ is positive and (4) PC2 of $\langle [u] \rangle$ is negative. A schematic summarizing the setup of one of these experiments is given in Figure 6.3.

To get the mean eddy response to the positive phase of EOF1 we simply average the zonal-mean eddy fluxes for every branch run initialized with the positive phase of EOF1 (= average of 3650 runs). This will give the eddy response to the onset of a positive EOF1 state out to 20 days. We define the response to EOF1 as the response to a positive EOF1 state minus the response to a negative EOF1 state. We do the same thing for EOF2.

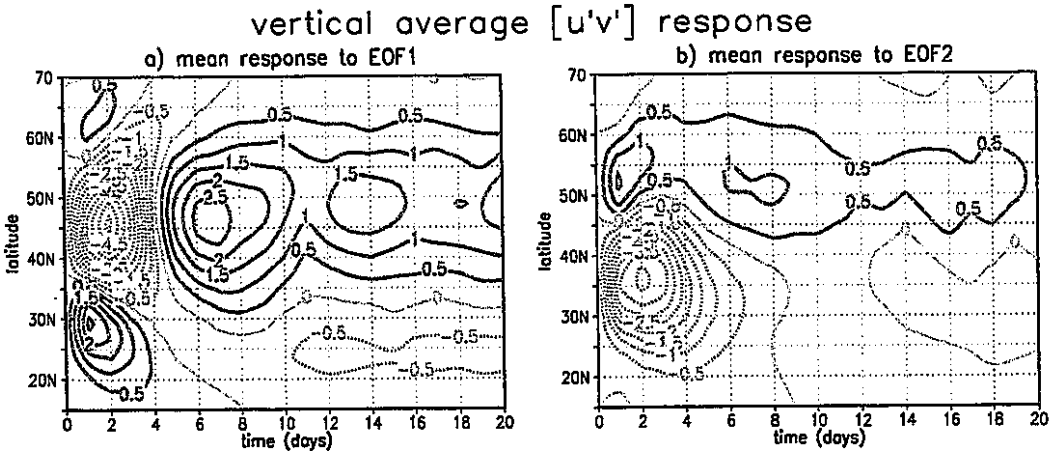

Figure 6.4: The mean response of the vertical average [u'v'] to a) EOF1, b) EOF2. The units are m^2s^2.

6.2.2 Eddy momentum flux response

Figure 6.4 shows the response of the vertical-average eddy momentum flux to EOF1 and EOF2. The long-term response (times greater than about 5 days) is significantly larger for EOF1 compared to EOF2. Moreover, the long-term response to EOF2 does not even project onto EOF2, instead it projects onto EOF1 in the sense to produce a poleward propagation of the $[u]$ anomalies. Such poleward propagation is also seen in the control run and in observations (Feldstein 1998 and Lorenz and Hartmann 2001). Perhaps the

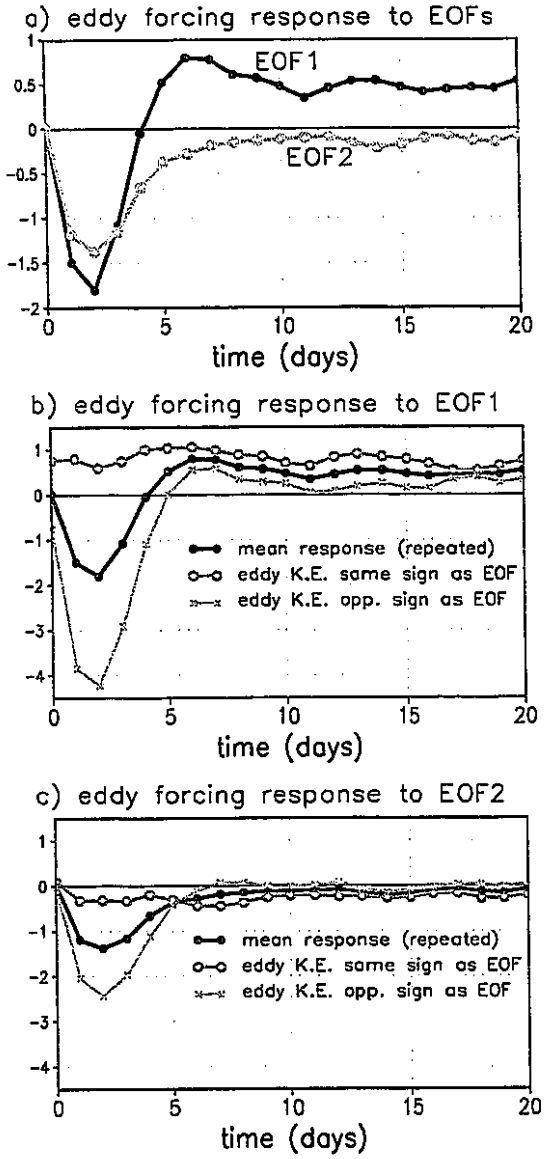

Figure 6.5: Eddy forcing response to the EOFs found by projecting the eddy forcing response on the corresponding EOF pattern. a) Mean response to EOF1 and EOF2. b) Response to EOF1 when initial eddy kinetic energy anomalies are collocated with EOF1 (red) or not collocated with EOF1 (blue). The mean response is repeated (black). c) Same as b) but for EOF2.

more striking result from the initial value runs is the apparent negative eddy forcing of the $[u]$ anomalies on short time scales (times less than 5 days). To see this effect better, we project the vertical average eddy momentum flux convergence (*i.e.* the eddy forcing) on the initial EOF anomaly pattern. Thus, the sign of the response gives the sign of the eddy feedback onto the prescribed anomaly (Figure 6.5). We can clearly see two parts of the

eddy forcing response to the prescribed $[u]$ anomalies: 1) a negative transient response which is present for both EOF1 and EOF2 and 2) a long-term response which is positive for EOF1 and zero or perhaps slightly negative for EOF2. The general shape of these curves is much like the cross-correlation curves between the $\langle [u] \rangle$ PCs and their corresponding eddy forcing (Figure 6.2a).

The above results have implications on the interpretation given in Lorenz and Hartmann (2001). They suggested that the transient response to $[u]$ onset observed here was instead a result of "intrinsic eddy variability" independent of *changes* in the zonal-mean $[u]$. Using Southern Hemisphere observations, Lorenz and Hartmann (2001) could not distinguish between a short time scale response to $[u]$ or intrinsic eddy variability because the time scale of transient response is similar to the time scale of eddies. In contrast to the interpretation in Lorenz and Hartmann (2001), results here imply that the negative swing in eddy forcing past the long-term value (see small positive time lags in Figure 6.2a) does not depend directly on the eddy forcing impulse proceeding it. Instead the negative forcing is a response to the changes in the mean flow. The difference in sign between the long-term and transient response for EOF1 that we observe here is consistent with the experiments of Robinson (1994) on the response of the eddy forcing to imposed EOF1 $[u]$ variability. He found that when the frequency of the imposed $[u]$ variability is low (high) the eddies reinforce (damp) the $[u]$ variability.

We get further insight into the transient eddy response to EOFs when we divide the mean response into two parts based on the location of eddy kinetic energy at the start of initial value problem (Figure 6.5b). For this analysis we create an index of eddy kinetic energy by projecting the eddy kinetic energy anomalies onto the $\langle [u] \rangle$ EOFs. We then divide the mean eddy response in two parts based on the sign of this index. When there is anomalously strong (weak) eddy kinetic energy in the region of positive $\langle [u] \rangle$ anomalies, then the transient response is very weak (strong). Thus, it appears that the positive $\langle [u] \rangle$ anomalies attract wave activity. As the wave activity propagates from the negative to the positive $\langle [u] \rangle$ anomalies, the associated wave momentum flux weakens the $\langle [u] \rangle$ anom-

alies. This weakening of the $\langle [u] \rangle$ anomalies occurs only when the wave activity is located outside of the region of positive $\langle [u] \rangle$ anomalies. When we divide the total eddy forcing into the contribution of the long and the short waves, we find that the long waves account for the transient eddy response (not shown).[1] This is consistent with index of refraction arguments described later which suggest that the jet is a (leaky) waveguide for the long waves.

6.2.3 Eddy temperature flux response

The initial value experiments also help determine the eddy temperature flux response to the $[u]$ anomalies. These experiments are particularly useful for determining the response to EOF2 wind anomalies because the important dynamics for EOF2 occur over relatively short time scales. Therefore it is not possible to separate the eddy response to EOF2 from "intrinsic eddy variability" based on lag regression diagnostics from a control run alone. With the initial value experiments, however, we can clearly see that the response of the vertical EP flux (similar to eddy temperature flux) to the $[u]$ anomalies is similar for *both* EOF1 and EOF2. Figure 6.6 shows the imposed wind anomaly and the average EP flux response 1 to 8 days afterward. For both EOF1 and EOF2, the vertical EP flux is enhanced at the latitudes of anomalous westerlies and vice versa. Moreover the magnitude of the response is about the same for both EOF1 and EOF2 (the EOF1 results are scaled so that the imposed $[u]$ anomalies are the same size). The similarities in the vertical EP flux response for EOF1 and EOF2 is in sharp contrast to the very different momentum flux response. This suggests that the baroclinic wave source (*i.e.* vertical EP flux) does not explain the *difference* between EOF1 and EOF2. While the changes in the wave source might enhance the persistence of EOF1 in the manner out forth by Robinson (1996, 2000) and Lorenz and Hartmann (2001, 2003), these results suggest that changes in the wave source are *not* the fundamental reason for the *difference* between EOF1 and EOF2.

---

1. This result is for the lag regressions based on the control run but presumably also holds for the branch runs. We did not partition the eddy response into long and short waves for the branch runs.

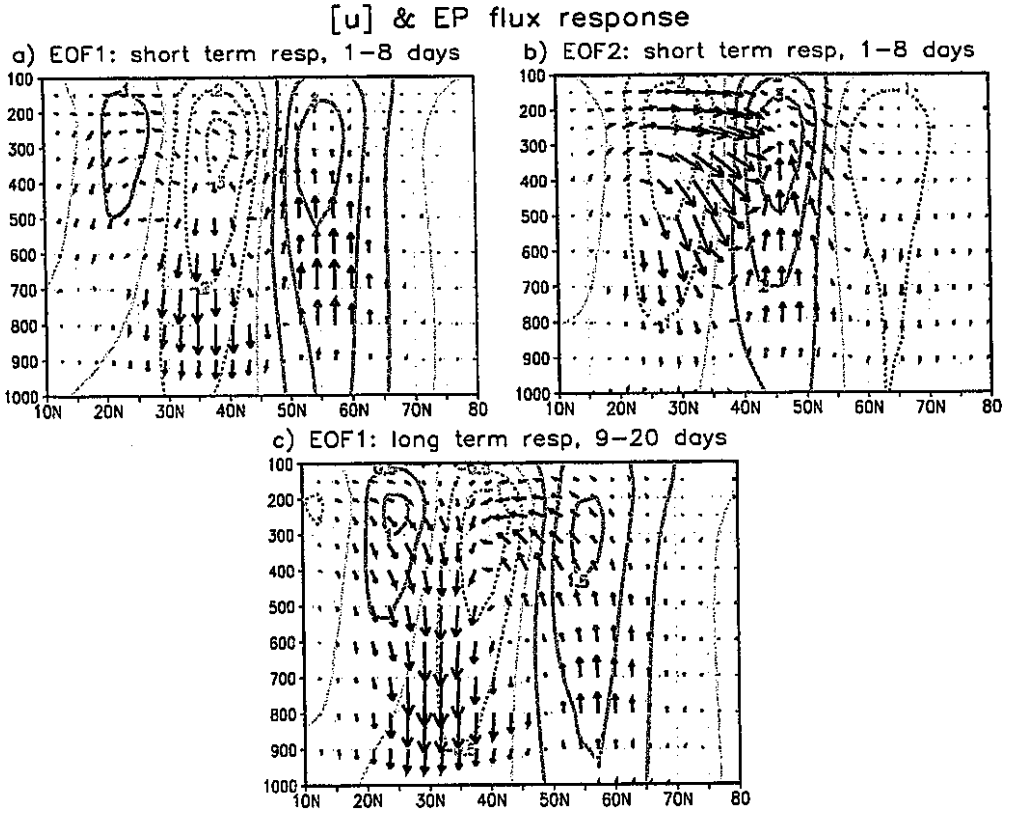

Figure 6.6: Mean EP flux response (vector) to the EOFs (countour). a) short-term response to EOF1 (time average from 1 to 8 days), b) short-term response to EOF2 (time average from 1 to 8 days), c) long-term response to EOF1 (time average from 9 to 20 days). In c) the zonal wind anomalies are plotted for time = 8 days.

Results in this section were repeated for a 2-layer quasi-geostrophic model on a β-plane which also showed a positive long-term feedback for EOF1 but not for EOF2. Similar results regarding the eddy response to the $[u]$ anomalies also hold in that model. In particular, the response of the eddy temperature flux to EOF1 and EOF2 is the same while the response of the eddy momentum flux is very different. Thus we will use the simpler 2-layer quasi-geostrophic model to design experiments to determine the essential difference between EOF1 and EOF2 variability in the next Chapter. In the next section, we introduce a possible mechanism to explain the difference using index of refraction diagnostics.

6.3 Index of Refraction diagnostics

The fact that the eddy temperature flux response is similar for EOF1 and EOF2 suggests that the important difference between EOF1 and EOF2 affects the eddies later in

their life-cycle. To help explain the reasons why it is more difficult (easier) for wave activity to leave its source region when EOF2 is positive (negative) we look at the index of refraction for different phases of EOF2 (Matsuno 1970):

$$n^2 = \frac{[q]_\phi}{[u]-(a\omega\cos\phi)/k} - \left(\frac{k}{a\cos\phi}\right)^2 - \left(\frac{f}{2NH}\right)^2, \tag{6.1}$$

where

$$[q]_\phi = \frac{2\Omega}{a}\cos\phi - \frac{1}{a^2}\left(\frac{([u]\cos\phi)_\phi}{\cos\phi}\right)_\phi - \frac{f^2}{\rho_0}\left(\rho_0\frac{[u]_z}{N^2}\right)_z \tag{6.2}$$

is the zonal-mean (quasi-geostrophic) potential vorticity gradient. Here, k is the zonal wavenumber, ω is the wave frequency, N is the buoyancy frequency, H is the scale height (8 km), f is the Coriolis parameter, a and Ω are the earth's radius and angular frequency, ρ_0 is the background density, and ϕ is latitude. The wave frequency (ω) can be written in terms of the wave phase speed (c) so that equation 6.1 becomes:

$$n^2 = \frac{[q]_\phi}{[u]-c\cos\phi/\cos\phi_0} - \left(\frac{k}{a\cos\phi}\right)^2 - \left(\frac{f}{2NH}\right)^2, \tag{6.3}$$

where ϕ_0 is a constant reference latitude here taken to be the latitude of the time-mean jet (=45°). Waves can propagate in regions of positive refractive index and waves are evanescent in regions of negative refractive index. Also, waves tend to propagate toward high values of the refractive index which implies a wave flux of momentum out of the regions of high values of refractive index.

To determine representative values for c and k, we look at the phase speed/zonal wavenumber spectrum of the eddy kinetic energy and eddy momentum flux convergence at 250mb at the latitude of the jet center (e.g. Randel and Held 1991). The eddy kinetic energy is clearly dominated by waves of phase speed 3.5 m/s and zonal wavenumber 5 (Figure 6.7). The convergence of eddy momentum flux is also largest for wavenumber 5, although the contribution by other waves with larger phase speed and zonal wavenumber has increased relative to wavenumber 5 for this field compared to the eddy kinetic energy.

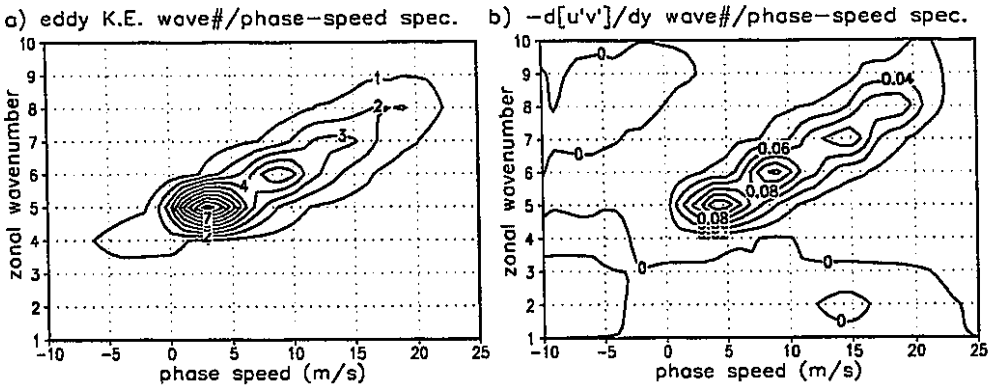

Figure 6.7: Zonal wavenumber versus phase speed spectra for the GCM at 43 degrees latitude, 250mb. a) eddy kinetic energy. b) convergence of eddy momentum flux.

Presumably, this is related to the fact that it is easier for waves with smaller scale and therefore larger c to propagate out of the jet (see discussion in Chapter 7 section 3 below).[1] Because wavenumber 5 dominates the eddy kinetic energy in the jet, we use $c = 3.5$ m/s and $k = 5$ in equation 6.3.

The refractive index of the time-mean flow gives a general sense of the appearance of the refractive index in this particular model (Figure 6.8a). Regions of negative refractive index (where the waves are evanescent) are lightly shaded and the regions of very large refractive index (near critical layers) are darkly shaded. Because the wave momentum fluxes are dominated by fluxes in the upper troposphere, we concentrate on the value of the refractive index in the upper troposphere. Also, because we are interested in the meridional propagation of wave activity, we average the refractive index from 500mb to 250mb so that the meridional profile of the refractive index can more easily be seen.[2]

The refractive index profile based on composites during different phases of EOF1 and EOF2 are shown in Figure 6.8bc. The EOF2 composites are the average of days when the PC time series exceeds 0.5 standard deviations from the mean. The threshold for the EOF1 composites is adjusted so that the amplitude of the anomalies in the upper troposphere is the same as that for the EOF2 composites. Looking at the EOF2 composites, we

1. The phase speed (c) is measured relative to the ground not relative to the background flow. Thus smaller scale waves have larger c.
2. Note that we average over pressure levels where the refractive index is relatively well behaved.

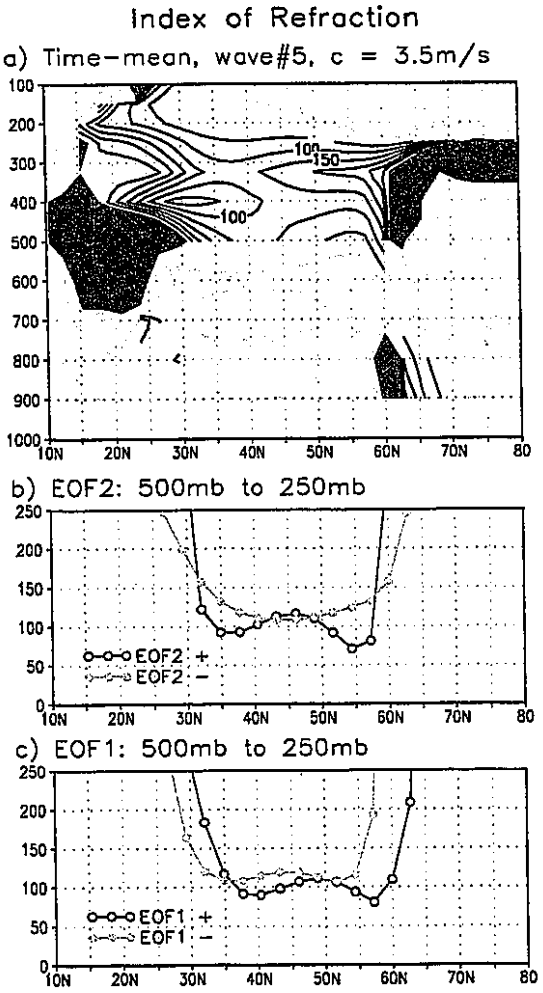

Figure 6.8: a) Quasi-geostrophic refractive index for the time-mean flow in the GCM (zonal wavenumber = 5, phase speed = 3.5 m/s at 45 degrees. The values are nondimensionalized by the radius of the earth squared. Negative values are lightly shaded and values larger than 300 are black. b) Same as a) except the refractive index is averaged from 500mb to 250mb for the positive and negative composite of EOF2. c) Same as b) but for EOF1.

see that the weak/broad jet (*i.e.* negative phase of EOF2) has a refractive index profile which is concave upward at the jet center while the strong/sharp jet (*i.e.* positive phase of EOF2) has a refractive index profile which is concave downward at the jet center. Thus waves generated in the jet will have a greater tendency to leave the jet when the jet is weak and broad than when it is strong and sharp (because waves tend to propagate toward higher refractive index). Thus, the effect of EOF2 on the refractive index is of the correct sense to counter the effect of the anomalous wave source on the wave momentum fluxes:

when PC2 is positive (negative) more (less) baroclinic wave activity is generated in the jet. This wave generation would tend to reinforce EOF2 except that the waves are less (more) likely to propagate out of the jet at upper levels when PC2 is positive (negative).

The EOF1 composites show the north/south shift of a refractive index profile which is not as concave downward as the positive EOF2 composite. The EOF1 composites are significantly more concave downward than the time-mean index of refraction profile which has been excessively smoothed by time averaging over all possible zonal-mean states. One can think of EOF1 variability as representing meridional shifts of a typical index of refraction profile which shows features of a zonal-mean waveguide. EOF2 variability, on the other hand, represents the strengthening and weakening of this waveguide-like structure.

In summary, when PC2 is positive (negative) more (less) baroclinic wave activity is generated in the jet. This wave generation would tend to reinforce EOF2 except that the waves are less (more) likely to propagate out of the jet at upper levels when PC2 is positive (negative).

In this section, we use the refractive index as a rough guide into the behavior of the waves. In particular, the refractive index provides a sense of the relative importance of the potential vorticity (PV) gradient versus the zonal wind in determining the meridional propagation of wave activity. In the next chapter, we will describe experiments which give a more rigorous demonstration of the strong sensitivity of the eddies to the upper-level zonal-mean PV gradient.

6.4 Simple linear model of the annular mode and the eddies

In this section we present a simple linear stochastic model which provides important insight into the dynamics of the annular mode. In particular, the model explains all the features of the auto- and cross-correlation statistics including the peculiar transient response of the eddy forcing to the $[u]$ anomalies (section 6.2.2). The model also provides greater understanding of the direct effect of the $[u]$ anomalies on the upper-level wave activity and the importance of the wave generation anomalies in the maintenance of the annular mode anomalies.

The model is based on the zonal-mean momentum budget (see equation 4.4):

$$\frac{dz}{dt} = m - \frac{z}{\tau} \tag{6.4}$$

and the upper-level "wave activity" budget which is approximated here by the upper-level enstrophy budget:

$$\frac{1}{2}\frac{\partial[q'^2]}{\partial t} = -[v'q']\frac{\partial[q]}{\partial y} - \frac{1}{2}\frac{\partial[v'q'^2]}{\partial y} - [dissipation]. \tag{6.5}$$

We then divide the potential vorticity flux into two parts:

$$\frac{1}{2}\frac{\partial[q'^2]}{\partial t} = -[v'\varsigma']\frac{\partial[q]}{\partial y} + [BaroclinicSource]\frac{\partial[q]}{\partial y} - \frac{1}{2}\frac{\partial[v'q'^2]}{\partial y} - [dissipation]. \tag{6.6}$$

Equation 6.6 is approximated by:

$$\frac{da}{dt} = -m + b - \frac{a}{\tau_a}, \tag{6.7}$$

where a is a measure of the wave activity (for example a could be $[q'^2]/(2\partial[q]_{clim}/\partial y)$), m is the eddy momentum flux convergence ($=[v'\varsigma']$), b is the baroclinic source and the remaining two terms are together approximated by a relaxation to climatology. The system given by equations 6.4 and 6.7 is closed by assuming a simple form for the momentum forcing (m) and the baroclinic source (b):

$$m = r_m - c_1 z + c_2 a, \tag{6.8}$$

$$b = r_b + c_3 z, \tag{6.9}$$

where r_m and r_b represent noise forcing which is nearly white in time, and c_1, c_2 and c_3 are *positive* "feedback" constants. It is important to note that z, a, m and b are time series representing anomalies which have been projected on zonal wind anomaly patterns. Thus equations 6.4, 6.7, 6.8 and 6.9 describe the evolution of anomalies collocated with zonal wind anomalies. In addition, the simple model is intended to provide qualitative insight into the dynamics, not a quantitative estimate of the strength of various feedbacks. Indeed, we know that equation 6.7 is significantly less accurate than equation 6.4, which is in fact a very good approximation to the observed momentum budget (see Chapter 4).

The exact parameters for the simple model are given in appendix D. Figure 6.9 shows the auto- and cross-correlation statistics for the zonal-mean wind (z), the eddy forcing (m), and the "wave activity" (a) for the simple stochastic model. The corresponding statistics for the annular mode in the GCM are shown on the left. Since we are aiming for qualitative correspondence, we simply use eddy kinetic energy as our measure of "wave activity".

The most important advantage of this particular second order model over the first order model given by equations 4.4 and 4.5 is that we now can reproduce the negative transient feature in the eddy forcing auto-correlation (Figure 6.9b compare with 6.9a) without having to explicitly incorporate this structure into the random noise forcing. This feature is also reproduced in the z and m lag-correlation (Figure 6.9d compare with 6.9c). The zonal wind (z) and "wave activity" (a) associated with the annular mode are basically positively correlated, however, there is a peculiar dip in correlation at zero lag (Figure 6.9e). This feature is also reproduced in the simple model (Figure 6.9f). In addition, the general structure of the "wave activity" (a) and eddy forcing (m) lag-correlation is also reproduced.

We now interpret the simple model: the transient feature in the z and m lag-correlation (Figure 6.9d) exists because a burst of positive (negative) eddy momentum forcing (m) is accompanied by a divergence (convergence) of wave activity flux. The decrease (increase) of wave activity (a) in turn decreases (increases) the eddy forcing (m) (equation 6.8). In addition, the burst of positive (negative) eddy forcing (m) drives a zonal wind anomaly (z) whose direct effect is to decrease (increase) the eddy forcing (m) (equation 6.8). While hints of the transient feature occur without including the latter effect of z on m, the initial value experiments clearly indicate that the direct effect of z on m weakens the z anomaly. In addition, the general form of the feedbacks in the simple model correctly explains the fact that the transient feedback disappears when the sign of the "wave activity" index (a) is the same as the initial zonal wind anomaly (z) (see section 6.2.2).

The eventual positive long-term feedback arises because the baroclinic source (b) supplies wave activity to the region of positive zonal wind anomalies. This source of wave

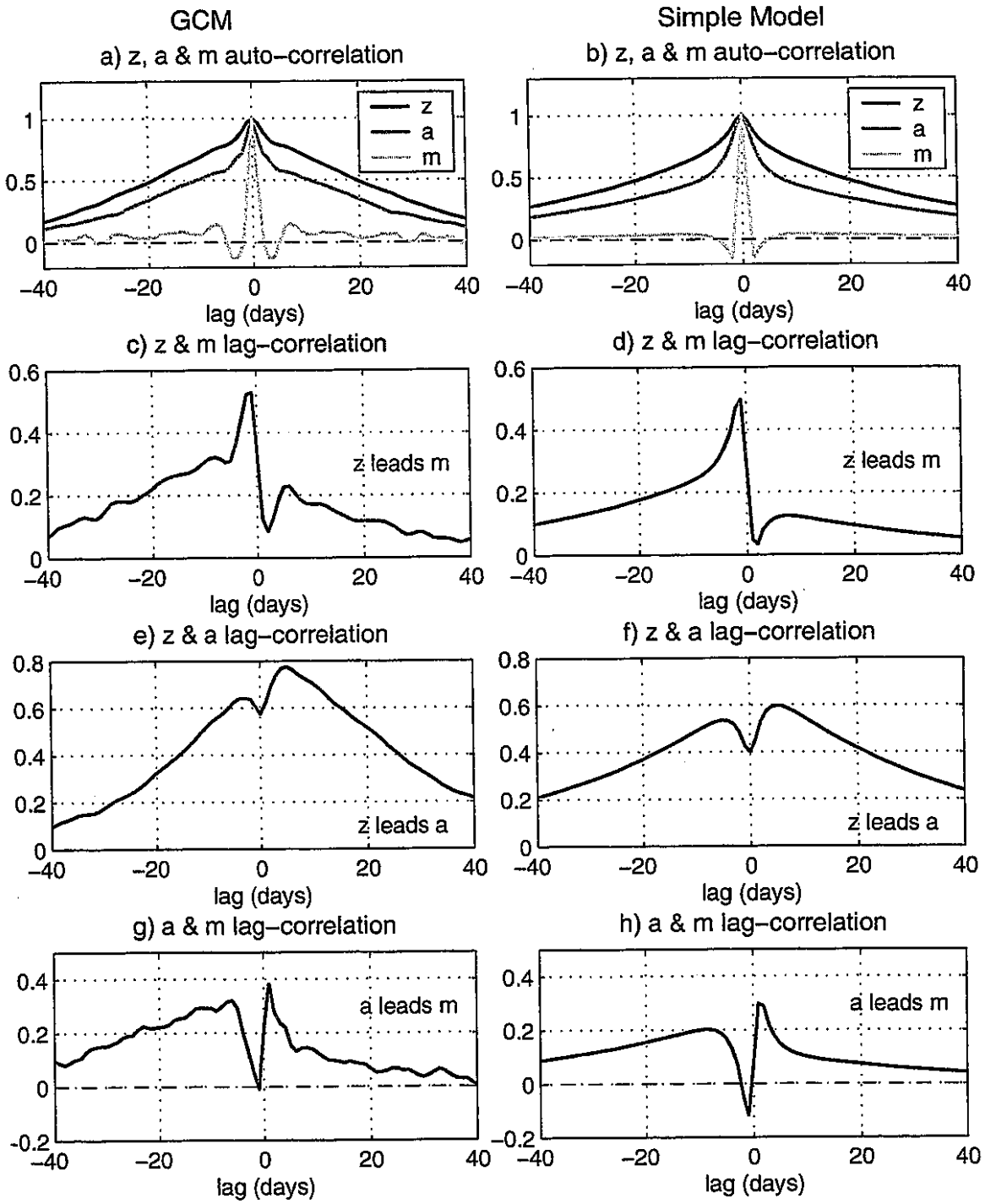

Figure 6.9: Statistics for zonal-mean wind (z), wave activity (a) and eddy forcing (m) for the GCM (left) and the simple stocastic model (right).

activity eventually overrides the direct effect of the zonal wind on the eddy forcing, which is negative.

To model EOF2 we can change the "feedback" parameters to reduce the long-term positive feedback in the z and m lag-correlation. The results of the previous section and of Chapter 7 (see below) suggest that one should do this by increasing the strength of the direct negative feedback on z on m (*i.e.* one should increase c_1). Modeling EOF2 in this way is consistent with the idea mentioned previously that the changes in the baroclinic source are necessary but not sufficient for a positive long-term feedback. Thus the *difference* between EOF1 and EOF2 does not depend on the strength of baroclinic source term (*i.e.* c_3) but on the strength of the negative feedback term c_1, which represents the effect of the zonal-mean waveguide on the meridional propagation of wave activity.

Chapter 7

Quasi-geostrophic model

The results of Chapter 6 suggest that changes in the source of wave activity consistent with a positive feedback are not unique to the leading EOF. Thus the difference between the eddy momentum flux response to EOF1 and EOF2 must be attributable to other factors. We will explore the difference in the eddy response further using a 2-layer quasi-geostrophic model on a β-plane (QG model). The relative simplicity of the QG model will allow us to perform initial value experiments which allow greater understanding of the dynamics. First we will confirm that the internal variability of the QG model is similar to observations and the GCM.

7.1 Zonal-mean variability

7.1.1 Internal variability of the Control Run

The details about the forcing and setup of the QG model are given in Chapter 2. Briefly, the 2-layer QG β-plane model is forced by heating which relaxes the thermal wind to a Gaussian wind profile and by mechanical Rayleigh damping which relaxes the lower layer wind to zero. The eddies that grow on this unstable wind profile concentrate the zonal-mean flow into an eddy driven jet at the center of the baroclinic zone (Figure 7.1a). The $[u]$ anomalies associated with the leading EOFs of the vertical-average $[u]$ are shown in Figures 7.1b and 7.1c. Like the GCM, EOF1 represents changes in the jet latitude and EOF2 represents a strengthening/sharpening of the jet in its positive phase and a weakening/broadening of the jet in its negative phase. Figure 7.2a shows the lag correlation between the $\langle [u] \rangle$ PC and its eddy forcing (*i.e.* $-d\langle [u'v'] \rangle / dy$ projected onto the EOF

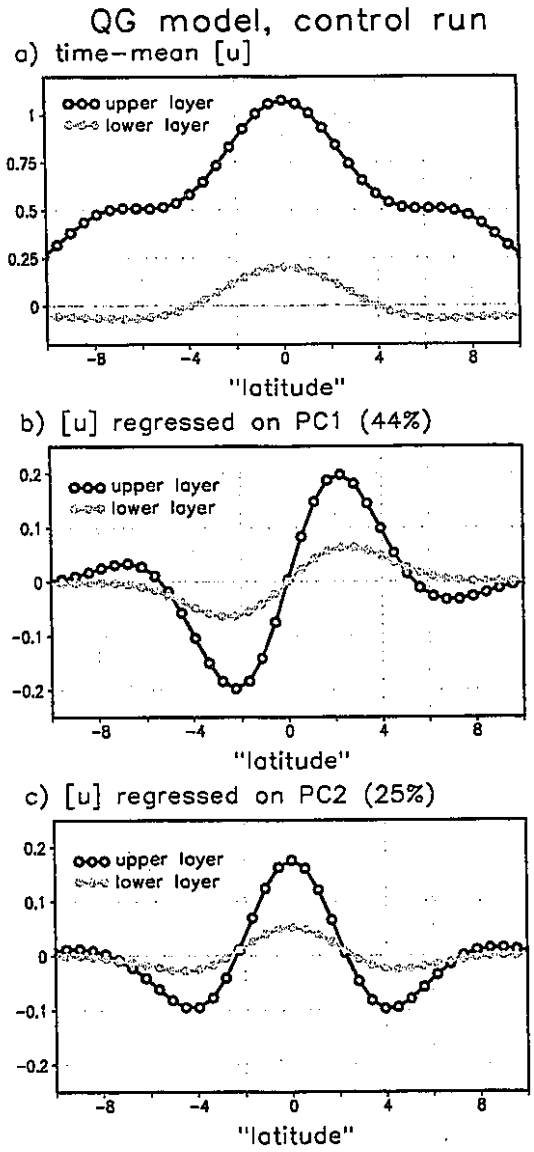

Figure 7.1: a) Time- and zonal-mean zonal wind for the upper and lower layer of the QG model. b) EOF1 of the vertical- and zonal-mean zonal wind shown by regressing the daily zonal-mean zonal wind anomalies on the normalized PC index. c) Same as b) but for EOF2.

pattern). Like the GCM, the long-term response to the EOF1 anomalies is positive and the long-term response to EOF2 anomalies is zero (look at large positive lags). This is directly related to the difference in the persistence of PC1 and PC2 (Figure 7.2b). For time lags greater than 10 days, the auto-correlation for PC1 slowly decays to zero while the auto-correlation for PC2 rapidly decays away.

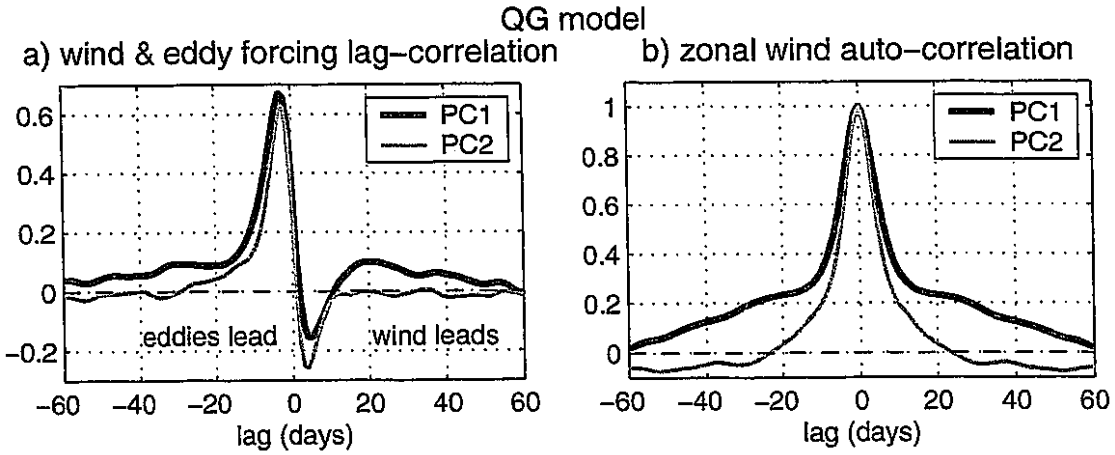

Figure 7.2: a) Lag-correlation between the zonal-mean zonal wind and its eddy forcing for PC1 (blue) and PC2 (red), b) same as a) but for the zonal-mean zonal wind auto-correlation.

7.1.2 Standard initial value branch runs

We also performed initial value experiments just like the GCM experiments in chapter 6 on the QG model except that we run the branch runs out to 30 "days" instead of 20 days. Figure 7.4 shows the mean eddy response to an imposed $[u]$ anomaly determined from the initial value problems. The eddy response is calculated in the same way as in section 6.2.1. For comparison, we also show the lag regression of the eddy fluxes on the PC time series in the control run for positive lags (Figure 7.3). According to the discussion in Chapter 4, the lag regression should also provide a good representation of the eddy response to the $[u]$ anomalies.

Comparing figures 7.3 and 7.4, we see that in general the plots are very similar in both the location and amplitude of the eddy fluxes. For the lag regression plot of the eddy momentum flux, it is important to remember that at very small lags (*i.e.* time lags of 0 to 1 days) the eddy momentum fluxes must be supporting the wind anomalies because the wind anomalies are created by eddy momentum fluxes at negative lags and the eddy momentum fluxes apparently have a small decorrelation time of a few days. Like the GCM, we see that for both EOF1 and EOF2, there is a transient response when the eddy momentum fluxes damp the wind anomalies (Figure 7.3be and 7.4be). After this transient period, the eddy momentum flux response is quite different for EOF1 and EOF2: the eddies reinforce the EOF1 wind anomalies (Figure 7.3b and 7.4b) but the eddies provide

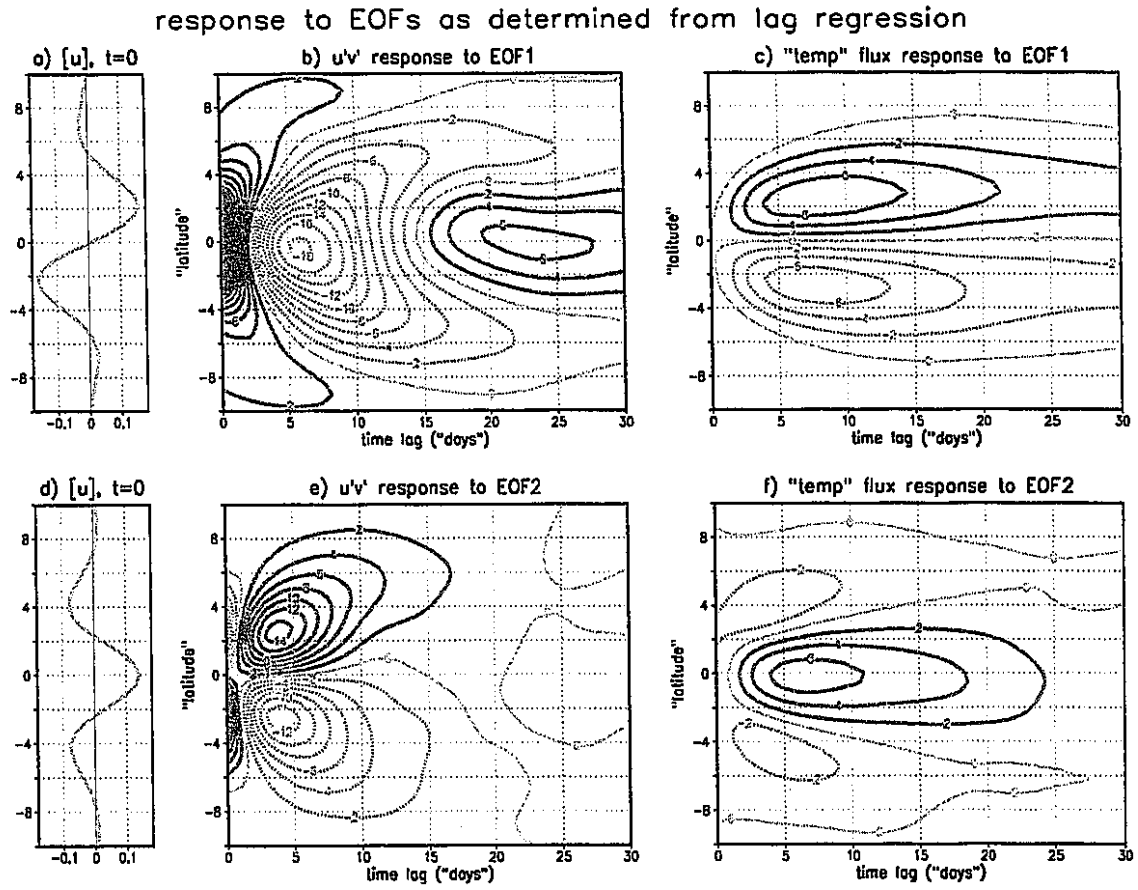

Figure 7.3: a) upper-level [u] regressed on PC1 (vertical axis is latitude), b) lag regression of upper level [u'v'] on PC1 (PC1 leads [u'v']), c) lag regression of [T'v'] on PC1 (PC1 leads [T'v']), d), e), f) are the same as a), b), c) but for PC2. The units are (nondimensional units)*1000.

little forcing to the EOF2 wind anomalies (Figure 7.3e and 7.4e). As in the GCM experiments, the presence (absence) of a strong transient response depends on whether anomalous wave activity exists in the region of easterly (westerly) wind anomalies (not shown).

The eddy temperature flux response shows increased (decreased) baroclinic wave generation in anomalous westerlies (easterlies) soon after the onset of the $[u]$ anomalies (Figure 7.3cf and 7.4cf). Note that the initial amplitude of the temperature flux response is about the same for both EOF1 and EOF2, but that the EOF2 temperature flux response is less persistent than the EOF1 response presumably because the $[u]$ anomalies are also less persistent (see Figure 7.2b). The response of baroclinic wave generation to the $[u]$ anomalies suggests reinforcing eddy momentum fluxes later in the baroclinic life-cycle for both

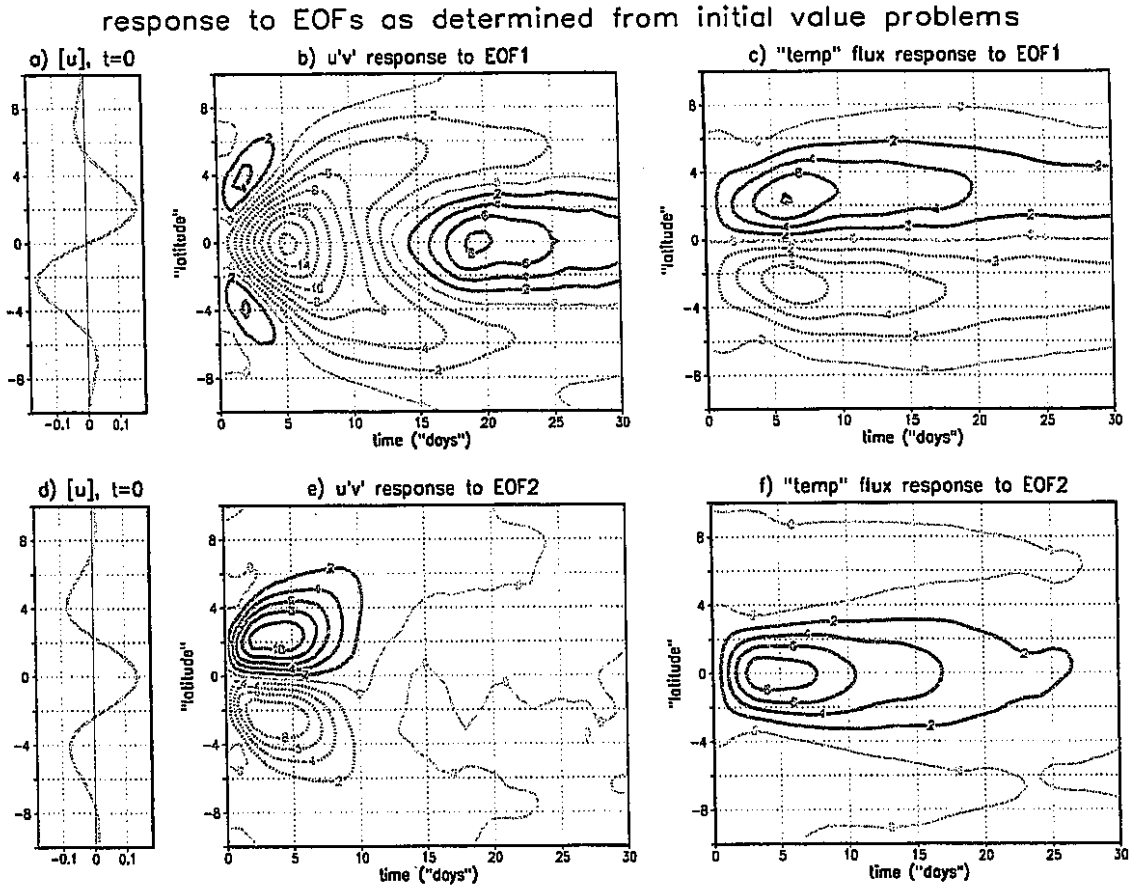

Figure 7.4: Mean response to EOFs as determined from initial value experiments. a) Initial upper level [u] anomaly for EOF1. b) Mean upper-level [u'v'] response to EOF1. c) Mean [T'v'] response to EOF1, d), e), f) are the same as a), b), c) but for EOF2. The units are (nondimensional units)*1000.

EOF1 and EOF2. As mentioned before, however, the reinforcing momentum fluxes are only present for EOF1.

We have also run initial value experiments to test the linearity of the eddy response to the amplitude of the imposed $[u]$ anomalies. In these experiments, we initialized the zonal-mean flow with EOF1 and EOF2 anomalies of exactly one half the amplitude of the EOF1 and EOF2 anomalies in the original experiments. The response of the eddy fluxes in these new experiments is practically identical to one half response in the original experiments at all latitudes and time lags. Thus the eddy response appears to be linear in $[u]$ amplitude.

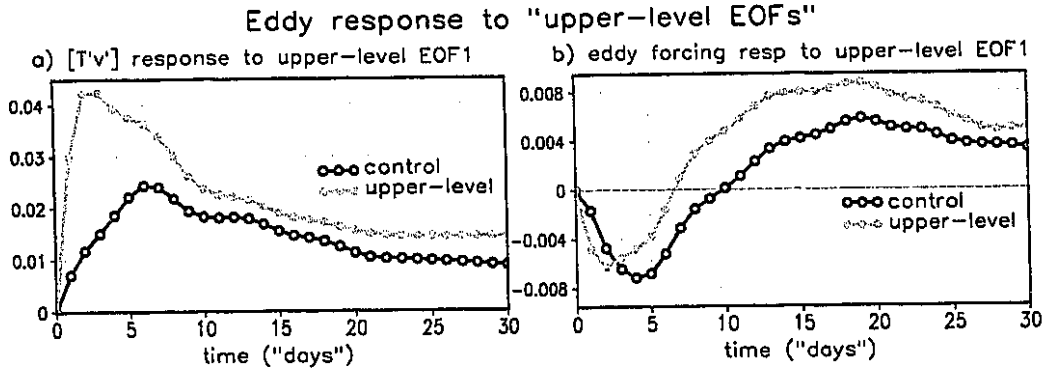

Figure 7.5: Mean response to upper-level EOF1 anomalies and to standard EOF1 anomalies as determined from initial value problems. Response is found by projecting the [T'v'] and eddy forcing anomalies on the EOF1 patterns. a) [T'v'] response, b) eddy forcing response.

7.2 Effect of changes in zonal-mean baroclinicity

7.2.1 Upper-level initial value branch runs

Since the eddy temperature flux responses to EOF1 and EOF2 wind anomalies are similar (in relation to the $[u]$ anomalies) yet the eddy momentum flux response is so different, it is not obvious that the anomalous eddy temperature fluxes are essential for the positive zonal-flow-eddy feedback for EOF1. To test the importance of the changes in the baroclinic wave source on the positive feedback we perform the following initial value experiment: for every day of the control run we run a branch run with composite EOF zonal-mean zonal wind at the upper level just as before. At the lower level, on the other hand, we initialize the zonal-mean wind with the climatology. Thus, we initialize the zonal-mean $[u]$ in the same way as before at the upper levels but now the change in baroclinicity is larger. We diagnose the eddy response to the EOF anomalies by projecting the eddy "temperature" flux and the eddy momentum forcing on the EOF pattern. Consistent with the larger baroclinicity change, we see a larger change in baroclinic wave generation (Figure 7.5a). Moreover, the stronger baroclinic generation leads to stronger momentum fluxes out of the region of wave generation (Figure 7.5b). In fact, even the upper-level EOF2 anomalies give rise to supporting eddy momentum fluxes although they are still much smaller than EOF1 (not shown). Thus, it appears that the strength of the eddy temperature flux response is directly related to the long-term eddy momentum flux response.

It is important to note that the prescribed vertical structure with zero $[u]$ anomalies

in the lower-layer is very short lived. The $[u]$ anomalies return to a more typical vertical structure within a few days. Hence the difference between eddy temperature flux response in the "upper-level EOF" case and the control is most pronounced at short time scales. This pronounced difference at short time scales seems somewhat at odds with the difference in eddy forcing response, which is largest around 10 days. The upper-level eddy kinetic energy anomaly, however, seems to persist longer than the eddy temperature flux and thus helps account for the pronounced eddy forcing response at longer time scales.

7.2.2 Branch run with low-level baroclinicity fixed to climatology

To help confirm that changes in baroclinic wave generation are essential for the positive feedback we perform an alternative experiment: we run branch runs from the control run with the zonal-mean flow prescribed to evolve in exactly the same way as the control except for one difference: the eddies do not feel the low-level zonal-mean potential vorticity gradient ($d[q]/dy$) of the control run, instead the eddies feel the climatological low-level $d[q]/dy$. Thus the eddy evolution equation for the upper-level q' becomes:

$$\frac{\partial q'}{\partial t} = -[u]_{control}\frac{\partial q'}{\partial x} - v'\frac{\partial [q]_{control}}{\partial y} + \ldots \tag{7.1}$$

and the eddy evolution equation for the lower-level q' becomes:

$$\frac{\partial q'}{\partial t} = -[u]_{control}\frac{\partial q'}{\partial x} - v'\frac{\partial [q]_{climatology}}{\partial y} + \ldots \tag{7.2}$$

where the three dots denote the usual wave-wave interaction, forcing and dissipation terms. Since the sign reversal of $d[q]/dy$ is essential for baroclinic instability, this is like fixing the low-level baroclinicity to climatology.[1] The eddies are free to evolve on this prescribed zonal-mean flow.

We then compare the normal lag regression between the $\langle [u] \rangle$ PC and the eddy fluxes in the control run to the lag regression computed using the eddy fluxes in the branch runs. The lag regression based on the branch runs for a time lag of +10 days is computed

1. The sign reversal of the low level $d[q]/dy$ depends on the strength of the thermal wind: $\partial [q]/\partial y = \beta - u_{yy} - ([u]_{upper} - [u]_{lower})/2$. Hence, we refer to $d[q]/dy$ as the low-level baroclinicity.

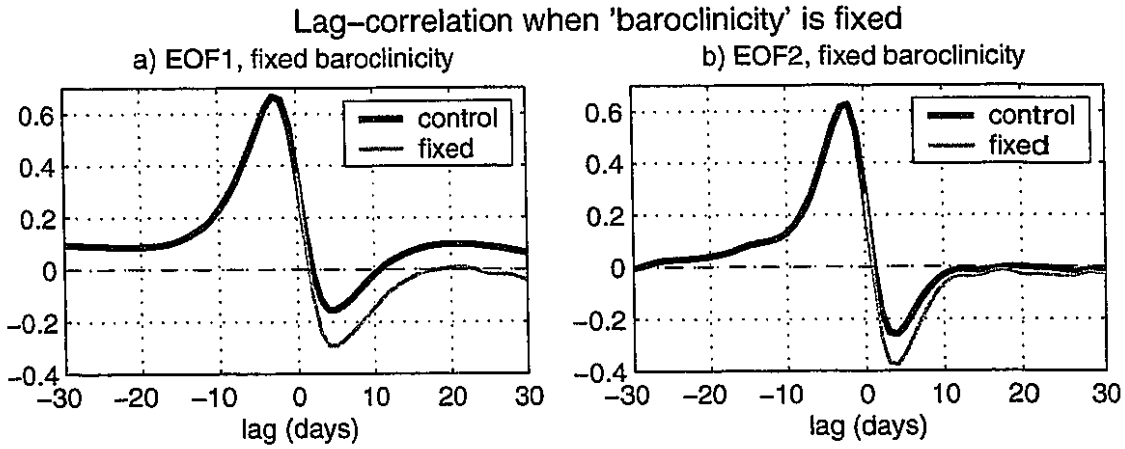

Figure 7.6: a) The lag-correlation between PC1 and its eddy forcing for the control run (blue) and the lag correlation between PC1 at the start of branch run and the eddy forcing with baroclinicity fixed to climatology (red). b) Same as a) but for PC2.

as follows: we regress the value of the PC index at the start-up day with the eddy fluxes 10 days into the corresponding branch run. (Note that this only gives the lag regression at positive lags.) When we look at the eddy temperature fluxes in the lag regression based on the branch runs we see that the response is much smaller compared to the control (not shown). The effect of this smaller baroclinic wave generation is clearly seen when we compare the lag-correlation of between the $\langle [u] \rangle$ PC and its eddy forcing (Figure 7.6). When the low-level baroclinicity is set to climatology, the eddy forcing for EOF1 is more negative for all time lags and the long-term positive feedback for EOF1 is gone. Similar results hold for EOF2 except that (1) the difference between the branch run and the control run is smaller compared to EOF1 for large lags (presumably because PC2 is much less persistent than PC1) and (2) the long-term response is actually very slightly negative. Since the upper-level $[u]$ and $[q]$ are evolving in exactly the same way as the control run, the difference between the control and the branch runs is entirely due to the low-level zonal-mean "baroclinicity". Thus, the changes in the low-level zonal-mean "baroclinicity" are essential for the positive long-term zonal flow-eddy feedback for EOF1.[1]

1. We have confirmed that the average eddy statistics have changed very little after 30 days in these branch runs. This is not true if similar experiments are performed but with the upper-level zonal-mean fields fixed.

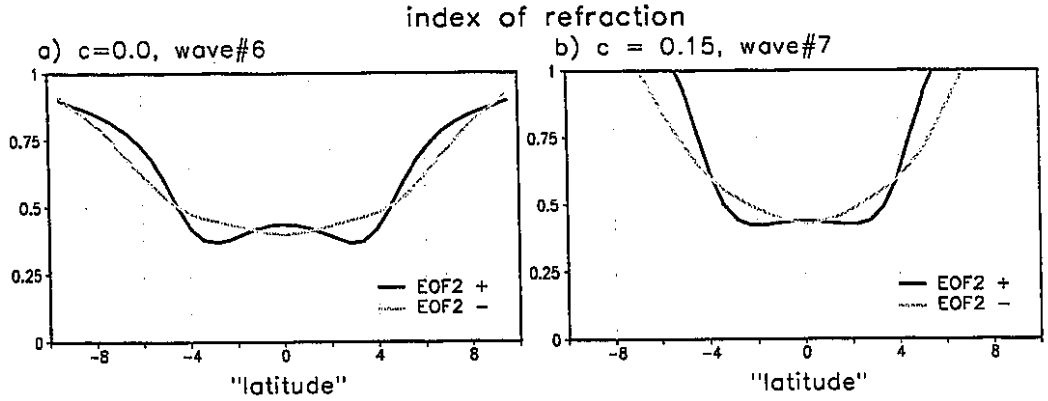

Figure 7.7: Upper-level refractive index for the positive (black) and negative (green) composites of EOF2. a) zonal wavenumber 6, phase speed = 0.0. b) zonal wavenumber 7, phase speed = 0.15.

7.3 Index of Refraction diagnostics

In this section, we repeat the index refraction diagnostics of the GCM to show that the QG model exhibits similar behavior. In addition, we will discuss the factors which determine the shape of the refractive index.

The index of refraction is

$$\frac{\partial [q]/\partial y}{[u]-c} - k^2, \tag{7.3}$$

where $d[q]/dy$ is the upper-level potential vorticity (PV) gradient, $[u]$ is the upper-level zonal-mean zonal wind, c is the phase speed of the waves and k is the zonal wavenumber of the waves. Waves tend to propagate toward high values of the refractive index which implies a wave flux of momentum out of the regions of high values of refractive index. Figure 7.7 shows the refractive index for both phases of EOF2 for several representative values of phase speed (c). The zonal wavenumber (k) does not *directly* effect the shape of the refractive index profile but simply shifts the profile up or down. We use the phase speed/zonal wavenumber spectrum of the upper-level momentum flux (e.g. Randel and Held 1991) at the jet center to determine representative values of the zonal wavenumber for each phase speed (not shown).

For each of the representative wave phase speeds shown (Figure 7.7), we see that the weak/broad jet (*i.e.* negative phase of EOF2) has a refractive index profile which is concave upward at the jet center while the strong/sharp jet (*i.e.* positive phase of EOF2)

has a refractive index profile which is concave downward at the jet center. Thus waves generated in the jet will have a greater tendency to leave the jet when the jet is weak and broad than when it is strong and sharp (because waves tend to propagate toward higher refractive index). Thus, the effect of EOF2 on the refractive index is of the correct sense to counter the effect of the anomalous wave source on the wave momentum fluxes. In summary, when PC2 is positive (negative) more (less) baroclinic wave activity is generated in the jet. This wave generation would tend to reinforce EOF2 except that the waves are less (more) likely to propagate out of the jet at upper levels when PC2 is positive (negative). We will show experiments which demonstrate the sensitivity of the wave momentum fluxes to the upper-level flow in a later section. First, we will discuss the factors that determine the shape of the refractive index.

For a westerly jet, the maximum upper-level zonal-mean PV gradient ($d[q]/dy$) and zonal-mean zonal wind ($[u]$) are collocated at the jet center. Since $d[q]/dy$ and $[u]$ are on opposite sides of the division in the refractive index (equation 7.3), they have opposite effects on the propagation of wave activity. Since $d[q]/dy$ is in the numerator, a stronger $d[q]/dy$ maximum means a stronger refractive index at the jet center relative to the jet flanks which *discourages* wave propagation out of jet (unless $[u]$ in denominator compensates). Since $[u]$ is in the denominator, a stronger $[u]$ maximum means a weaker refractive index at the jet center relative to the jet flanks which *encourages* waves to propagate out of jet.

When c is larger (*i.e.* closer in magnitude to $[u]$) then fractional change of $[u]$-c between jet center and the flanks is larger which means effect of $[u]$-c term is larger compared to effect of $d[q]/dy$ for these waves. Thus shorter waves (large c) tend to "feel" the $[u]$ more than the $d[q]/dy$ and thus tend to propagate out of the jet (*i.e.* shorter waves show greater tendency to tilt with the zonal wind shear). As the wave scale increases (and c therefore decreases) the $d[q]/dy$ term starts to play a more important role in the shape of the refractive index. For these larger waves, the jet can behave like a (somewhat leaky) waveguide which traps waves in the jet.

Also the scale of the jet helps determine the importance of $d[q]/dy$ relative to $[u]$.

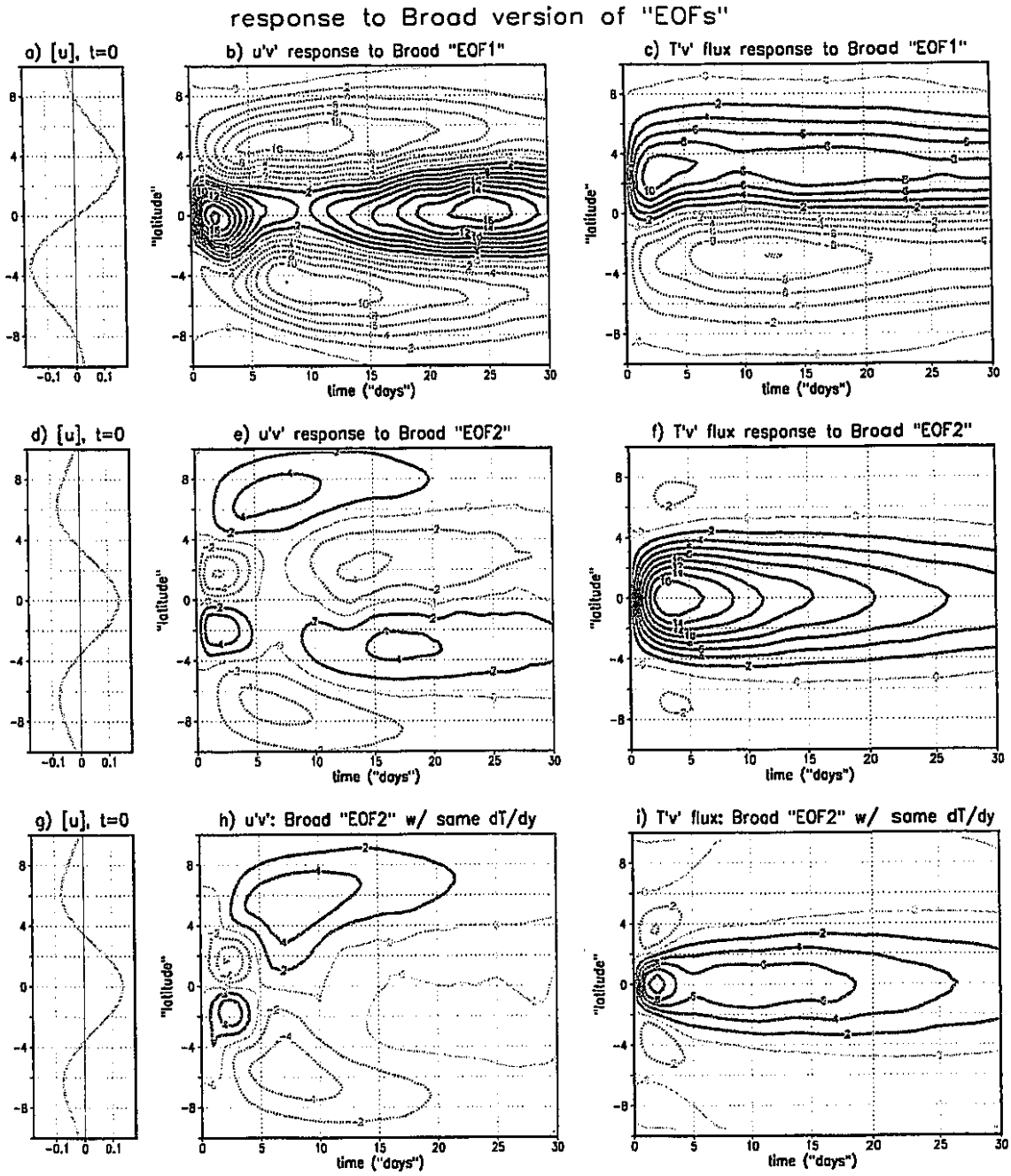

Figure 7.8: Same as 7.4 but for "Broad EOF1" (top row), "Broad EOF2" (middle row), and "Hybrid EOF2" (bottom row).

Since $d[q]/dy$ tends to enhance the smaller meridional scales compared to $[u]$, the importance of $d[q]/dy$ relative to the $[u]$ increases as jet scale decreases. In other words, a sharper jet behaves more like a waveguide than a broader jet.

It is important to note that the usefulness of the refractive index is limited to providing a qualitative sense of importance of the PV gradient relative to the zonal wind in determining the propagation of wave activity. In the next section, we describe more convincing numerical experiments which suggest that the strength of the PV front at the jet center limits the positive eddy feedback for EOF2.

7.4 Effect of mean flow on upper-level wave propagation

7.4.1 Broad anomaly initial value problems

The discussion in the previous section suggests that zonal wind anomalies with broader meridional scale than the observed EOFs might favor stronger momentum flux convergence into the westerly anomalies. To test this idea, we repeat the initial value experiments in section 3b but we initialize the branch runs with broader zonal wind anomalies. The meridional scale of the anomalies is increased by a factor of 1.5 relative to the observed EOFs. The "broad EOFs" have the same relationship to the time-mean $[u]$ as the observed EOFs: EOF1 is a dipole with the node centered at the jet maximum and EOF2 is a tripole with the middle anomaly centered at the jet maximum.

In contrast to the eddy forcing response to the observed EOFs, the transient eddy forcing response to the broad $[u]$ anomalies reinforces the zonal wind anomalies (Figure 7.8be). The refractive index profile of the "broad EOF2" clearly shows that the difference between the positive and negative phase near the jet center is much reduced (compare Figure 7.9 with Figure 7.7) although the refractive index does not predict that the transient response is now positive. Thus the refractive index correctly predicts that the waves will show a greater tendency to tilt with the zonal wind shear for the "broad EOFs" compared to the observed EOFs, although it does not predict the precise scale of the zonal wind pattern where the transient response changes sign.

The long-term eddy forcing response to the broad $[u]$ anomalies is significantly larger compared to the observed EOFs (compare Figure 7.8 with Figure 7.4). In particular, the eddy response to the "broad EOF2" reinforces the initial $[u]$ anomalies on long time scales (Figure 7.8e). Unfortunately, the interpretation of this long-term eddy forcing response in terms of upper-level wave propagation is clouded by the fact that the

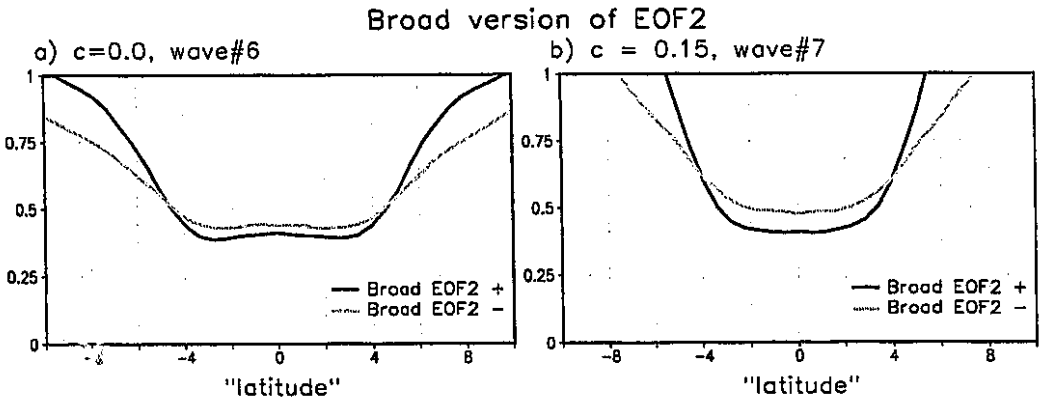

Figure 7.9: Same as 7.7 but for "Broad EOF2".

baroclinic wave generation response is significantly larger for the broad $[u]$ anomalies compared to the observed $[u]$ anomalies.[1] Thus it is not clear whether the strong eddy forcing response to the broad $[u]$ anomalies is due to (1) a refractive index which is favorable for upper-level wave propagation or to (2) strong baroclinic wave generation anomalies (Figure 7.8cf). In order to test the role of the baroclinic wave source, we repeat the initial value experiments with the same "broad EOF2" $[u]$ at the upper-level but with the low-level $[u]$ initialized such that the meridional temperature gradient is the same as the observed EOF2. We denote this initial $[u]$ profile as the "hybrid EOF2". Note that the transient $[u'v']$ response to the "hybrid EOF2" is very similar to the transient response to the original "broad EOF2" (compare Figure 7.8h with 7.8e at small times). On the other hand, the strength of the eddy temperature flux response to the "hybrid EOF2" is much closer to the observed EOF2 than to the "broad EOF2" (compare Figure 7.8i with Figure 7.4f and Figure 7.8f). Similarly, the long-term $[u'v']$ response is much like the observed EOF2. Thus, the transient $[u'v']$ response seems to be insensitive to the baroclinicity of the zonal-mean flow, while the long-term $[u'v']$ response depends crucially on the changes in baroclinicity.

Because the long term $[u'v']$ response is weak for both the observed EOF2 and the

1. The large baroclinic wave generation response for the broad $[u]$ anomalies is consistent with linear baroclinic instability theory. For a given zonal wavenumber, the fastest growing normal modes have the largest meridional scale (e.g. Pedlosky 1987).

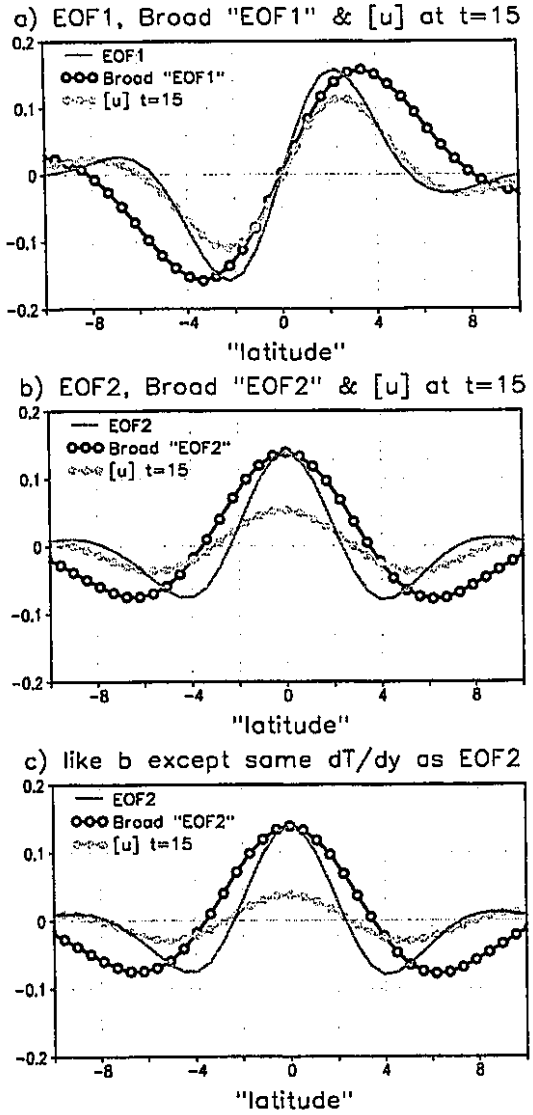

Figure 7.10: a) Upper-level zonal wind for EOF1 (magenta), "Broad EOF1" (black) and "Broad EOF1" after 15 days of integration in branch run (green). b) Same as a) but for EOF2 and "Broad EOF2". c) Same as a) but for EOF2 and "hybrid EOF2".

"hybrid EOF2", one might be tempted to conclude that the upper-level refractive index has relatively little impact on the long-term response. In particular, one might conclude that broad $[u]$ anomalies do not encourage wave propagation out of anomalous westerlies. When we look at the evolution of the upper-level $[u]$, however, we see that 15 days after initializing $[u]$ with a broad anomaly the eddies have concentrated the anomaly to a meridional scale similar to the observed EOFs (Figure 7.10). Note that in addition to the usual

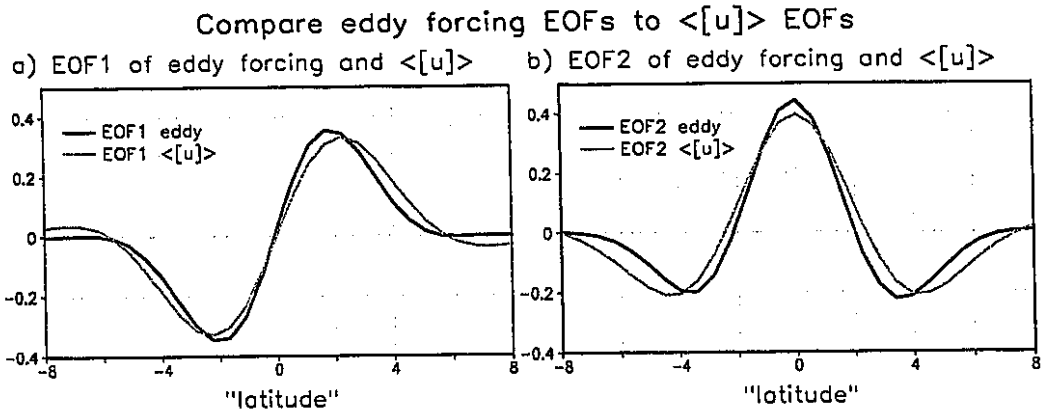

Figure 7.11: The EOFs of the eddy forcing (black) and the vertical- and zonal-mean zonal wind (magenta). a) EOF1, b) EOF2.

decrease in the magnitude of the $[u]$ anomaly, the scale of the $[u]$ anomalies (as measured by the distance between zero crossings) has decreased. This is especially true for the "broad EOF1" and "hybrid EOF2" patterns (Figure 7.10ac). Because the eddies have concentrated the scale of the "hybrid EOF2" by the time the long-term response has begun, it is not clear what effect the scale of $[u]$ anomalies have on the long-term response. In the next subsection, we design an experiment that more clearly demonstrates the important role of the upper-level refractive index on the long-term response.

The above results suggest that the natural scale of the eddy momentum forcing is significantly smaller than the broad $[u]$ anomalies and that this may explain why the "broad EOFs" are not observed despite the fact that the magnitude of the eddy forcing response is larger than that for the observed EOFs. In fact, an EOF analysis of the eddy forcing variability suggests that the scale of the eddy forcing is actually slightly smaller than the $\langle [u] \rangle$ variability which it forces (Figure 7.11).[1] Thus, it appears that the eddies try to concentrate the zonal-mean flow until zonal flow-eddy feedbacks become strong enough to limit this concentration. These feedbacks which limit the scale of the jet are presumably related to the feedbacks which prevent the wave generation anomalies associated

1. It is important to note that the EOFs of $\langle [u] \rangle$ and its forcing are not necessarily the same. Since $\langle [u] \rangle$ is an integrator of its forcing, $\langle [u] \rangle$ highlights the low frequency variability of the forcing. Also note that the scale of the eddy flux convergence is not necessarily related to the scale of the eddies.

with EOF2 from reinforcing EOF2 variability.

7.4.2 Initial value experiments with weak smoothing of upper-level PV

To explore the effects of the $[u]$ anomalies on the long-term eddy response we need experiments that are not simply initial value problems because the transient eddy response modifies the initial $[u]$ anomalies. The design of such an experiment is hampered by the fact that the model evolution is particularly sensitive to the upper-level zonal-mean flow. For example, if we simply fix the upper-level zonal-mean flow then the mean eddy statistics change drastically over the course of a branch run. This is not true if we fix the low-level $d[q]/dy$ as in section 4b. Thus in order to test the effect of the upper-level zonal-mean state on the eddies, we need to alter the upper-level zonal-mean in a more subtle way. We want to avoid making large changes to the mean eddy statistics so that our conclusions are also relevant to the internal variability of the control run. In summary, we must do something more intrusive than letting the model simply evolve freely from prescribed zonal-mean initial conditions, but less intrusive than strongly relaxing or locking the zonal-mean flow to a particular state.

A way to alter the zonal-mean state in the model is suggested by the index of refraction diagnostics. During the positive phase of EOF2 the jet behaves like a waveguide because the upper-level $d[q]/dy$ profile is too sharp compared to the $[u]$-c profile. This sharp $d[q]/dy$ inhibits the meridional propagation of wave activity and offsets the anomalously strong wave generation during the positive phase of EOF2. To test this idea, we apply a weak smoother in the y-direction to the upper-level $d[q]/dy$ when calculating the evolution of the eddies. Thus the usual eddy evolution equation for the upper-level q':

$$\frac{\partial q'}{\partial t} = -[u]\frac{\partial q'}{\partial x} - v'\frac{\partial [q]}{\partial y} - \frac{\partial (u'q')}{\partial x} - \frac{\partial ((v'q') - [v'q'])}{\partial y} + \ldots, \tag{7.4}$$

where the three dots denote the usual forcing and dissipation terms, becomes:

$$\frac{\partial q'}{\partial t} = -[u]\frac{\partial q'}{\partial x} - v'\frac{\partial [q]_{smooth}}{\partial y} - \frac{\partial (u'q')}{\partial x} - \frac{\partial ((v'q') - [v'q'])}{\partial y} + \ldots. \tag{7.5}$$

We apply the smoothing at every time step of a branch experiment.The equation for the zonal-mean q is unchanged. The experiments are initialized with either the positive phase

Table 7.1: Smoothed [q] experiments

Experiment	initial zonal-mean state	# of smoothing applications
1	+ EOF1	1
2	+ EOF1	2
3	+ EOF2	1
4	+ EOF2	2

of EOF1 or the positive phase of EOF2. To smooth the $d[q]/dy$ we apply a 1-2-1 grid point smoother either once or twice (*i.e.* $q_{smooth}(y) = (q(y+\delta) + 2 \cdot q(y) + q(y-\delta))/4$ for one application of the smoother, where δ is the grid spacing). We run four initial value branch run experiments (Table 7.1). Two applications of the smoothing of $d[q]/dy$ makes the positive EOF2 index of refraction profile slightly less concave downward at the jet center (Figure 7.12). The change in the refractive index seems quite small yet this change

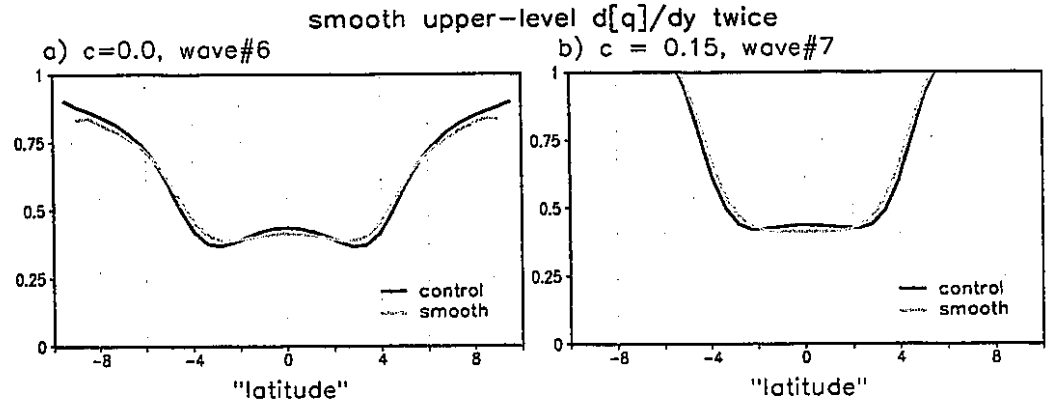

Figure 7.12: Upper-level refractive index for the positive composite of EOF2 (black) and the positive composite of EOF2 after [q] has been smoothed twice by the 1-2-1 grid point smoother (green). a) zonal wavenumber 6, phase speed = 0.0. b) zonal wavenumber 7, phase speed = 0.15.

has a strong effect on the $[u'v']$ response. The effect of the $d[q]/dy$ smoothing on the eddies is diagnosed by projecting the anomalous eddy fields on the initial [u] anomalies.[1] Figure 7.13 compares the eddy forcing and eddy temperature flux response to the EOFs

1. The anomalous eddy fields are anomalies from the climatology of the control run.

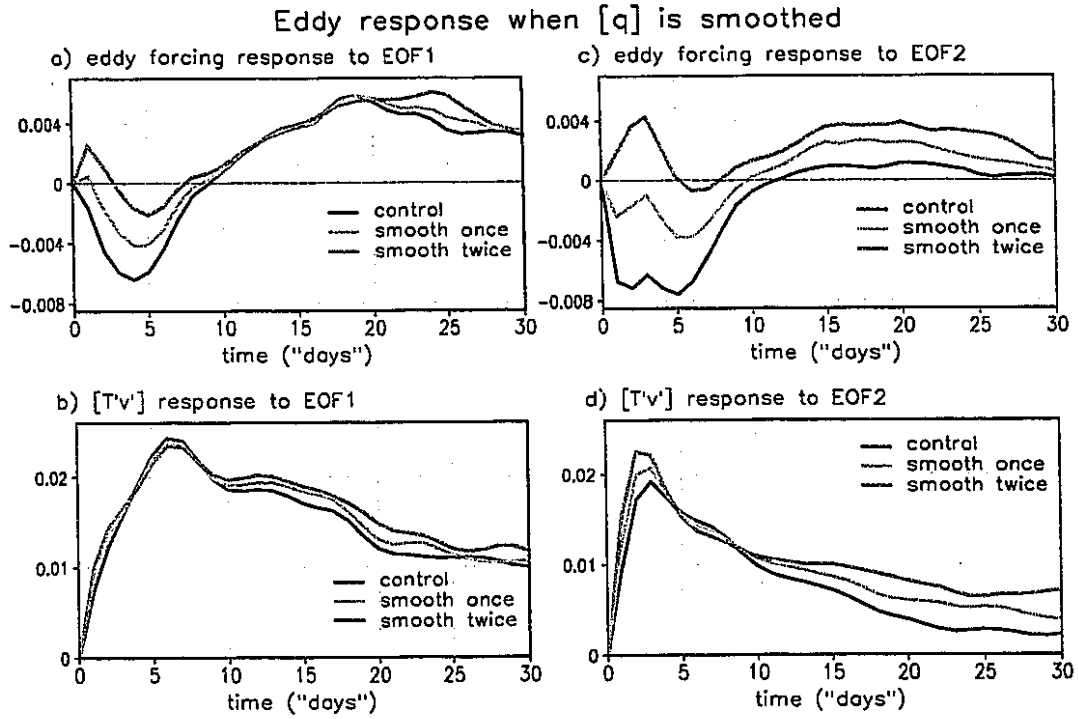

Figure 7.13: Mean response to EOF anomalies as determined from initial value problems for the standard case (black) and for the case where $[q]$ is smoothed once (blue) or twice (red). The response is found by projecting the [T'v'] and eddy forcing anomalies on the EOF patterns. a) eddy forcing response to EOF1, b) [T'v'] response to EOF1, c) eddy forcing response to EOF2, d) [T'v'] response to EOF2.

for the standard branch run experiments (section 7.1.2, here designated as the "control") and the branch runs with weak smoothing of the upper-level $d[q]/dy$. The smoothing of $d[q]/dy$ weakens and even reverses the transient eddy forcing response for both EOF1 and EOF2 (Figure 7.13ac). This is consistent with the "broad EOF" and "hybrid EOF" experiments which show that the sign of the transient response reverses for broad anomalies regardless of their position relative to the time mean jet. For the long-term response, on the other hand, the smoothing of $d[q]/dy$ has a much stronger effect on EOF2 compared to EOF1. The dependence of the long-term EOF2 response to the weak smoothing of $[q]$ demonstrates the sensitive dependence of wave momentum fluxes to the sharpness of the upper-level PV front. In addition, the reinforcing eddy momentum fluxes increase the persistence of the EOF2 anomalies which in turn increases the persistence of the eddy temperature fluxes (Figure 7.13d).

In summary, the smoothing of upper-level $[q]$ has allowed the anomalous wave

generation anomalies associated with EOF2 to give rise supporting momentum fluxes. With the smoothed $[q]$, the strength of the EOF2 eddy forcing anomalies relative to the temperature flux is now more in line with EOF1.

7.4.3 Effect of smoothing on other zonal-mean fields

We also ran branch runs with smoothing applied to the zonal-mean $[q]$ at the lower level and with smoothing applied to the zonal-mean $[u]$ at either the upper or lower level. We found that the model is most sensitive to the smoothing of the upper-level $[q]$ followed by upper-level $[u]$, lower-level $[u]$ and finally by lower-level $[q]$. The model response to smoothing the upper-level $[u]$ has implications on another possible mechanism which might limit the eddy momentum forcing response to EOF2. We describe this mechanism as it relates to the positive phase of EOF2: when the jet is strong and sharp, a wave's critical level on the flanks of the jet moves meridionally toward the jet center. If the movement of the critical level causes the region of wave breaking to overlap meridionally with the region of wave generation, then the wave momentum forcing will decrease, resulting in a negative feedback. The effect of this negative feedback is enhanced if the wave's phase speed increases for a stronger, sharper jet because the latitude of the wave's critical level becomes even closer to the jet center (and the region of wave generation).

The critical-level mechanism described in the previous paragraph implies that the smoothing of the upper-level $[u]$ will allow wave activity to propagate farther from its source, increasing the strength of the jet. The observed response is in fact the opposite: the smoothing of $[u]$ weakens and broadens the jet. The sign of this result is consistent with the mechanism described in the previous section which relates to the index of refraction (see also the discussion in 7.3). Thus it appears that dynamics relating to the ability of wave activity to leave the sharp PV front at the jet center are more important than critical level dynamics in determining the eddy response to the internal modes of variability.

After 15 "days", the amplitude of the smoothed upper-level $[u]$ response is about 45% of the smoothed upper-level $[q]$ response and is the opposite sign. The amplitude of the smoothed lower-level $[u]$ response is about 14% of the smoothed upper-level $[q]$ response and is the opposite sign. The smoothing of the lower-level $[q]$ has a small effect

on the model after 15 "days" (3%).

Chapter 8

Conclusions

This dissertation has shown that one zonally symmetric pattern of variability stands out above other patterns because of a positive feedback between the zonal-mean anomalies and the eddy momentum fluxes. This leading pattern of variability is the annular mode. In other words, one can think of "stochastic" eddy momentum fluxes as driving a range of zonally symmetric patterns equally. The annular mode stands out because the eddies reinforce the annular mode, making it the least damped mode of variability.

The annular mode represents north/south shifts in the mid-latitude jet. The shifts in the mid-latitude jet are maintained primarily by the synoptic-scale baroclinic waves by the following mechanism: above normal baroclinic wave activity is generated in the region of enhanced baroclinicity which is collocated with the region of westerly wind anomalies. This anomalous wave generation leads to the anomalous radiation of wave activity at upper levels from the westerly wind anomalies. Since meridional propagation of wave activity is associated with westerly momentum fluxes into the wave source region, this propagation of wave activity reinforces the westerly wind anomalies. Furthermore, the tendency of the baroclinic waves to reduce the baroclinicity of the westerlies is countered by the wave induced mean-meridional circulation as long as some of the wave activity leaves its source region at upper levels (Robinson 2000). In other words, the anomalous baroclinic westerlies are self-maintaining provided that the waves propagate meridionally out of their source region.

At first sight, this positive feedback mechanism would also appear to work for

EOF2 of zonal-mean variability, which represents a strengthening/sharpening versus a weakening/broadening of the jet. Indeed, anomalously strong baroclinic wave activity is also generated in the enhanced westerlies for EOF2. This anomalous wave source, however, is offset by the effect of upper level PV gradients on the propagation of wave activity. A stronger/sharper (weaker/broader) jet is a stronger (weaker) waveguide which inhibits (enhances) the meridional propagation of wave activity. Thus the difference between EOF1 and EOF2 arises because EOF2 is in phase with the jet and thus represents changes in the strength of the waveguide. EOF1, on the other hand, simply describes a meridional shift in the waveguide and presumably can be maintained by the eddies, provided the baroclinic zone is sufficiently wide.

This dissertation has also established that the response of the eddies to the rapid onset of annular mode anomalies is *not* monotonic. Instead, a transient period of *negative* eddy forcing is followed, after several days, by a period of long-term reinforcement by the eddies. The results here suggest that a baroclinic mid-latitude jet, that organizes its own wave momentum forcing, is quite sharp. Given a uniform wave activity distribution, a sharp jet will tend to attract wave activity resulting in a negative momentum forcing. The positive response to the changes in the annular mode follows only after baroclinic instability has had time to establish positive wave activity anomalies in the region of westerly anomalies.

The results in this dissertation relate to a fundamental problem in geophysical fluid dynamics regarding the meridional scale of eddy-driven jets. The focus of this dissertation, however, differs from previous studies (*e.g.* Held and Larichev 1996) in at least two important respects. In this study, no attempt is made to predict the jet scale *a priori*, instead we are concerned with the dynamical processes which limit the jet scale once the flow has settled into a statistically steady state. In addition, because of momentum constraints, we are less interested in changes in jet scale alone than with changes in both the jet strength and scale together. Our results suggest that the eddy momentum fluxes strengthen and concentrate the flow until the strength of the upper-level PV front limits the meridional propagation of the eddies (and therefore the eddy momentum fluxes). The processes

which maintain the above balance act on relatively fast time scales compared to the processes which determine the jet position. Also, the index of refraction diagnostics suggest that the longer waves will tend to limit the degree of flow concentration before the shorter waves.

Bibliography

Akahori, K., and S. Yoden, 1997: Zonal flow vacillation and bimodality of baroclinic eddy life cycles in a simple global circulation model. *J. Atmos. Sci.*, **54,** 2349-2361.

Balasubramanian, G., and S. T. Garner, 1997: The role of momentum fluxes in shaping the life cycle of a baroclinic wave. *J. Atmos. Sci.*, **54,** 510-533.

Chen, P., and W. A. Robinson, 1992: Propagation of planetary waves between the troposphere and stratosphere. *J Atmos. Sci.*, **49**, 2533-2545.

DeWeaver, E., and S. Nigam, 2000a: Do stationary waves drive the zonal-mean jet anomalies of the northern winter? *J. Climate*, **13**, 2160-2176.

DeWeaver, E., and S. Nigam, 2000b: Zonal-eddy dynamics of the North Atlantic oscillation. *J. Climate*, **13**, 3893-3914.

Durran, D. R., 1991: The third-order Adams-Bashforth method: an attractive alternative to leapfrog time differencing. *Mon. Wea. Rev.*, **119**, 702-720.

Eady, E. T., 1949: Long waves and cyclone waves. *Tellus*, **1,** 35-52.

Edmon, H. J., B. J. Hoskins and M. E. McIntyre, 1980: Eliassen-Palm cross sections for the troposphere. *J. Atmos. Sci.*, **37, 38,** 2600-2616, 1115.

Feldstein, S. B., and S. Lee, 1996: Mechanisms of zonal index variability in an aquaplanet GCM. *J. Atmos. Sci.*, **52,** 3541-3555.

Feldstein, S. B., 1998: An observational study of the intraseasonal poleward propagation of zonal mean flow anomalies. *J. Atmos. Sci.*, **55**, 2516-2529.

Feldstein, S. B., and S. Lee, 1998: Is the atmospheric zonal index driven by an eddy feedback? *J. Atmos. Sci.*, **55,** 3077-3086.

Gong, D., and S. Wang, 1999: Definition of Antarctic Oscillation index. *Geophys. Res. Lett.*, **26,** 459-462.

Hamming, R. W., 1989: *Digital Filters*. Prentice Hall, 284pp.

Hartmann, D. L., 1995: A PV view of zonal flow vacillation. *J. Atmos. Sci.*, **52,** 2561-2676.

Hartmann, D. L., and F. Lo, 1998: Wave-driven zonal flow vacillation in the Southern Hemisphere. *J. Atmos. Sci.*, **55,** 1303-1315.

Hartmann, D. L., J. M. Wallace, V. Limpasuvan, D. W. J. Thompson and J. R. Holton, 2000: Can ozone depletion and global warming interact to produce rapid climate change? *Proc. Nat. Acad. Sci.*, **97,** 1412-1417.

Held, I. M., 1983: Stationary and quasi-stationary eddies in the extratropical troposphere: theory. *Large Scale Dynamical Processes in the Atmosphere*, R. P. Pearce and B. J. Hoskins, Eds., Academic Press, 127-168.

Held, I. M., R. L. Panetta, and R. T. Pierrehumbert, 1985: Stationary external Rossby waves in vertical shear. *J. Atmos. Sci.*, **42**, 865-883.

Held, I. M., and M. J. Suarez, 1994: A proposal for the intercomparison of the dynamical cores of atmospheric general circulation models. *Bull. Amer. Meteor. Soc.*, **75**, 1825-1830.

Held, I. M., and V. D. Larichev, 1996: A scaling theory for horizontally homogeneous, baroclinically unstable flow on a beta plane. *J Atmos. Sci.*, **53**, 946-952.

Hoskins, B. J., 1983: Theory of transient eddies. *Large-Scale Dynamical Processes in the Atmosphere.*, B. J. Hoskins and R. P. Pearce, Eds., Academic Press, 397 pp.

Hoskins, B. J., and T. Ambrizzi, 1993: Rossby wave propagation on a realistic longitudinally varying flow. *J Atmos. Sci.*, **50**, 1661-1671.

James, I. N., and P. M. James, 1992: Spatial structure of ultra-low frequency variability of the flow in a simple atmospheric circulation model. *Quart J. Roy. Meteor. Soc.*, **118,** 1211-1233.

Kalnay, M. E., and co-authors, 1996: The NCEP/NCAR Reanalysis Project. *Bull. Amer. Meteor. Soc.*, **77,** 437-471.

Karoly, D. J., 1990: The role of transient eddies in the low-frequency zonal variations in the Southern Hemisphere circulation. *Tellus*, **42A,** 41-50.

Kushner, P. J., I. M. Held, and T. L. Delworth, 2001: Southern Hemisphere atmospheric circulation response to global warming. *J. Climate.*, **14**, 2238-2249.

Lee, S., and S. B. Feldstein, 1996: Mechanisms of zonal index evolution in a two-layer model. *J. Atmos. Sci.*, **53**, 2232-2246.

Lee, S., and I. M. Held, 1991: Subcritical instability and hysteresis in a two-layer model. *J. Atmos. Sci.*, **48**, 1071-1077.

Lee, S., and I. M. Held, 1993: Baroclinic wave packets in models and observations. *J. Atmos. Sci.*, **50**, 1413-1428.

Limpasuvan, V., and D. L. Hartmann, 1999: Eddies and the annular modes of climate variability. *Geophysical Research Letters*, **26,** 3133-3136.

Limpasuvan, V., and D. L. Hartmann, 2000: Wave-maintained annular modes of climate variability. *J. Climate*, **13,** 4414-4429.

Lorenz, D. J., and D. L. Hartmann, 2001: Eddy-zonal flow feedback in the Southern Hemisphere. *J. Atmos. Sci.*, **58**, 3312-3327.

Lorenz, D. J., and D. L. Hartmann, 2003: Eddy-zonal flow feedback in the Northern Hemisphere winter. *J. Climate*, **16**, 1212-1227.

Madden, R. A., and P. Speth, 1995: Estimates of atmospheric angular momentum, friction, mountain torques during 1987-1988. *J. Atmos. Sci.*, **52**, 3681-3694.

Matsuno, T., 1970: Vertical propagation of stationary planetary waves in the winter Northern Hemisphere. *J. Atmos. Sci.*, **27**, 871-883.

Namias, J., 1950: The index cycle and its role in the general circulation. *J. Meteor.*, **7,** 130-139.

North, G. R., F. J. Moeng, T. L. Bell, and R. F. Cahalan, 1982a: The latitude dependence of the variance of zonally averaged quantities. *Mon. Wea. Rev.*, **110**, 319-326.

North, G. R., T. L. Bell, R. F. Cahalan, and F. J. Moeng, 1982b: Sampling errors in the estimation of empirical orthogonal functions. *Mon. Wea. Rev.*, **110,** 699-706.

Panetta, R. L., 1993: Zonal jets in wide baroclinically unstable regions: persistence and

scale selection. *J. Atmos. Sci.*, **50,** 2073-2106.

Pedlosky, J. 1987: *Geophysical Fluid Dynamics*. Springer-Verlag, 710 pp.

Randel, W. J., and I. M. Held, 1991: Phase speed spectra of transient eddy fluxes and critical layer absorption. *J. Atmos. Sci.*, **48**, 688-697.

Robinson, W. A., 1991: The dynamics of the zonal index in a simple model of the atmosphere. *Tellus*, **43A,** 295-305.

Robinson, W. A., 1994: Eddy feedbacks on the zonal index and eddy-zonal flow interactions induced by zonal flow transience. *J. Atmos. Sci.*, **51,** 2553-2562.

Robinson, W. A., 1996: Does eddy feedback sustain variability in the zonal index? *J. Atmos. Sci.*, **53,** 3556-3569.

Robinson, W. A., 2000: A baroclinic mechanism for the eddy feedback on the zonal index. *J. Atmos. Sci.*, **57,** 415-422.

Rossby, C.-G., 1939: Relation between variations in the intensity of the zonal circulation of the atmosphere and the displacements of the semi-permanent centers of action. *J. Mar. Res.*, **2,** 38-55.

Thompson, D. W. J., and J. M. Wallace, 2000: Annular modes in the extratropical circulation. Part I: Month-to-month variability. *J. Climate*, **13,** 1000-1016.

Thompson, D. W. J., J. M. Wallace and G. C. Hergerl, 2000: Annular modes in the extratropical circulation. Part II: Trends. *J. Climate*, **13,** 1018-1036.

von Storch, H., F. W. Zwiers, 1999: *Statistical Analysis in Climate Research*. Cambridge University Press, 494pp.

Wallace, J. M., 2000: North Atlantic oscillation / annular mode: two paradigms - one phenomenon. *Quart J. Roy. Meteor. Soc.*, **126**, 791-805.

Whitaker, J. S., and C. Snyder, 1993: The effects of spherical geometry on the evolution of baroclinic waves. *J. Atmos. Sci.*, **50,** 597-612.

Yang, G.Y., and B. J. Hoskins, 1996: Propagation of Rossby waves of nonzero frequency. *J. Atmos. Sci.*, **53**, 2365-2378.

Yu, J. -Y., and D. L. Hartmann, 1993: Zonal flow vacillation and eddy forcing in a simple GCM of the atmosphere. *J. Atmos. Sci.*, **50**, 3244-3259.

Appendix A

Estimation of τ

Let Z and M be the Fourier transform of z and m, respectively. If equation 4.4 holds then the ratio of the cross spectrum to the z power spectrum (the transfer function from Z to M) is given by:

$$\frac{ZM^*}{ZZ^*} = \frac{1}{\tau} + i\omega, \tag{A.1}$$

where * denotes the complex conjugate. The observed real and imaginary part of the transfer function is plotted in Figure 3a. Like (A1) the imaginary part is linear in frequency and the real part is nearly constant for very low frequencies (at higher frequencies the imaginary part dominates so that the noise in the real part at higher frequencies is not important). We fit the observed transfer function to:

$$\frac{ZM^*}{ZZ^*} = \alpha + i\beta\omega. \tag{A.2}$$

Since the modeled feedback is proportional to z, the changes in Z and M caused by the feedback are significant at very low frequencies only. Therefore, in order to best estimate the change due to the feedback, we fit the transfer function to $\alpha+i\beta\omega$ for low frequencies (<0.025 days^{-1}) and not the entire frequency domain. Since we are only interested in the changes in Z and M relative to observed, we can divide (A2) by β and absorb the factor β into M. Thus the value for τ is β/α (=8.9 days for the Southern Hemisphere and 7.2 days for the Northern Hemisphere).

Appendix B

Statistical Significance of Lag Correlation

To assess the statistical significance in figure 4.3, we perform a Monte Carlo simulation to test following null-Hypothesis: the cross-correlation is zero for large positive lags. To perform this test, we generate a random m data set using a moving average model (see von Storch and Zwiers 1999). The generated data set has the same auto-correlation as the real m up to lag 6 and then is exactly zero afterwards (this is the same point where the real m auto-correlation appears to be negligible). Thus the generated m has no long-term memory, which is equivalent to the absence of a feedback. We then generate a very large data set using equation 4.4 to find the corresponding z. Next, we calculate 1000 independent cross-correlations using chunks of z and m that are as long as observed data record and find the standard deviation of the sample cross-correlations at large positive lags. The standard deviation determines the 95% significance level assuming the distribution is normal.

Appendix C

Feedback Calculations

To estimate the strength of the feedback, we must find the cross covariance between $\tilde{z}$ and $\tilde{m}$ from the cross covariance of z and m using (2), (3) and (4). First we take the Fourier transform of (2), (3) and (4) and rearrange to get

$$M = (\tau^{-1} + i\omega)Z, \tag{C.1}$$

$$M = \tilde{M} + bZ, \tag{C.2}$$

$$\tilde{M} = (\tau^{-1} + i\omega)\tilde{Z}, \tag{C.3}$$

where a capital letter denotes the Fourier transform of the corresponding lower case variable. Dividing (C1) by (C3) gives

$$\frac{M}{\tilde{M}} = \frac{Z}{\tilde{Z}}. \tag{C.4}$$

Substitute (C2) into (C1) and rearranging implies $\tilde{M} = (\tau^{-1} - b + i\omega)Z \equiv (\sigma^{-1} + i\omega)Z$, where σ^{-1} is defined to be τ^{-1} - b ($1/\tau > b > 0$). Dividing this result by (C3) and rearranging gives

$$\tilde{Z} = \frac{\sigma^{-1} + i\omega}{\tau^{-1} + i\omega} \cdot Z. \tag{C.5}$$

The same relation holds between $\tilde{M}$ and M because of (C4):

$$\tilde{M} = \frac{\sigma^{-1} + i\omega}{\tau^{-1} + i\omega} \cdot M. \tag{C.6}$$

The cross covariance between $\tilde{z}$ and $\tilde{m}$ ($=c_{\tilde{z}\tilde{m}}(t)$) is the inverse Fourier transform of the cross spectrum:

$$c_{\tilde{z}\tilde{m}}(t) = \int_{-\infty}^{\infty} \tilde{z}(s)\tilde{m}(s+t)ds = \frac{1}{2\pi}\int_{-\infty}^{\infty} \tilde{Z}^*(\omega)\tilde{M}(\omega)e^{i\omega t}d\omega . \tag{C.7}$$

Substituting (C5) and (C6) into (C7) implies

$$c_{\tilde{z}\tilde{m}}(t) = \frac{1}{2\pi}\int_{-\infty}^{\infty} \frac{\sigma^{-2}+\omega^2}{\tau^{-2}+\omega^2} \cdot Z^* M e^{i\omega t}d\omega . \tag{C.8}$$

Using the relationship $\frac{1}{2\pi}\int_{-\infty}^{\infty} F^*(\omega)G(\omega)e^{i\omega t}d\omega = \int_{-\infty}^{\infty} f(s)g(s+t)ds$ from Fourier theory (this is the same as (C7) for general functions f and g) with $F^*(\omega) = \frac{\sigma^{-2}+\omega^2}{\tau^{-2}+\omega^2}$ and $G(\omega) = Z^*M$ gives

$$c_{\tilde{z}\tilde{m}}(t) = \int_{-\infty}^{\infty} \left(\delta(s) - \frac{\tau}{2}(\tau^{-2}-\sigma^{-2})\exp(-|s|/\tau)\right)c_{zm}(s+t)ds , \tag{C.9}$$

where $\delta(s)$ is the Dirac delta function and we used the fact that $c_{zm}(t)$ is the inverse Fourier transform of Z^*M. Evaluating the first part of (C9) and performing a change of variables on the second gives

$$c_{\tilde{z}\tilde{m}}(t) = c_{zm}(t) - b(1-b\tau/2)\int_{-\infty}^{\infty} \exp(-|t-s|/\tau)c_{zm}(s)ds , \tag{C.10}$$

where we used the fact that $\sigma^{-1} \equiv \tau^{-1} - b$. To relate the cross correlation with and without the feedback note that $c_{zm}(t) = (c_{zz}(0)c_{mm}(0))^{1/2}\hat{c}_{zm}(t)$, where $\hat{c}_{zm}(t)$ is the cross-correlation, $c_{zz}(0)$ is the total variance of z, etc. Thus (C10) becomes

$$\hat{c}_{\tilde{z}\tilde{m}}(t) = \left(\frac{c_{zz}(0)c_{mm}(0)}{c_{\tilde{z}\tilde{z}}(0)c_{\tilde{m}\tilde{m}}(0)}\right)^{1/2}\left(\hat{c}_{zm}(t) - b(1-b\tau/2)\int_{-\infty}^{\infty} \exp(-|t-s|/\tau)\hat{c}_{zm}(s)ds\right) \tag{C.11}$$

The relationship between the variance of $\tilde{z}$ and z and between the variance of $\tilde{m}$ and m is easy to find from the above results because (C5) and (C6) are the same form. Thus (C10) also holds for $c_{zz}(t)$ and $c_{mm}(t)$. For zero lag this implies

$$c_{\tilde{z}\tilde{z}}(0) = c_{zz}(0) - b(1-b\tau/2)\int_{-\infty}^{\infty} \exp(-|s|/\tau)c_{zz}(s)ds , \tag{C.12}$$

$$c_{\tilde{m}\tilde{m}}(0) = c_{mm}(0) - b(1-b\tau/2)\int_{-\infty}^{\infty} \exp(-|s|/\tau)c_{mm}(s)ds . \tag{C.13}$$

For the results in this paper, (C10) is used to find the value of b that minimizes the mean square covariance at lags greater than 7 days for $c_{\tilde{z}\tilde{m}}(t)$. Then (C12) and (C13) are used to find the ratio of total variance between the observed and 'no feedback' case. With this information, (C11) can be used to find the cross-correlation 'without the feedback'. The integrals are evaluated from -30 to 30 days with daily resolution using Simpson's rule.

The power spectra for $\tilde{z}$ and $\tilde{m}$ are easily found from the power spectra of z and m using (C5) and (C6):

$$\tilde{Z}\tilde{Z}^* = \frac{\sigma^{-2} + \omega^2}{\tau^{-2} + \omega^2} ZZ^*, \tag{C.14}$$

$$\tilde{M}\tilde{M}^* = \frac{\sigma^{-2} + \omega^2}{\tau^{-2} + \omega^2} MM^*. \tag{C.15}$$

Appendix D

Simple model parameters and solution

We repeat the simple model below:

$$\frac{dz}{dt} = m - \frac{z}{\tau}, \tag{D.1}$$

$$\frac{da}{dt} = -m + b - \frac{a}{\tau_a}, \tag{D.2}$$

$$m = r_m - c_1 z + c_2 a, \tag{D.3}$$

$$b = r_b + c_3 z. \tag{D.4}$$

The auto-correlation of the noise forcing (r_m and r_b) is one at lag zero and 0.5 at lag = ± 1 day and zero elsewhere. Hence the noise as a small but finite memory. The two noise time series are uncorrelated with each other and the amplitude of the noise is 1.0 for r_m and 0.77 for r_b. The values for the "feedback" constants c_1, c_2 and c_3 are 0.09, 0.20 and 0.14 respectively. We take τ to be the same as that in the GCM momentum budget (=11.0 days) and τ_a = 7.7 days. The system of four equations above is solved by substituting D.3 and D.4 into D.1 and D.2. This two dimensional problem is then solved in Fourier space yielding formulas for $Z(\omega)$ and $A(\omega)$ in terms of the noise forcing (capital letters denote Fourier transforms of the corresponding lower case time series). The eddy forcing is found from the zonal wind using the relation $M = (1/\tau + i\omega)Z$. The auto- and cross-covariance can be found from the power and cross spectra using the relation

$$\int_{-\infty}^{\infty} f(s)g(s+t)ds = \frac{1}{2\pi}\int_{-\infty}^{\infty} F^*(\omega)G(\omega)e^{i\omega t}d\omega, \qquad \text{(D.5)}$$

where * denotes complex conjugate.

Vita

David J. Lorenz

Department of Atmospheric Sciences
University of Washington
Phone: 206-685-9303
Fax: 206-685-9302
email: djlorenz@atmos.washington.edu

Education

1996-Present: Ph.D. Student, Department of Atmospheric Sciences, University of Washington, Seattle, WA.
1996: B.A. Physics, University of Chicago, Chicago, IL.

Employment

1996-Present: Research Assistant, Department of Atmospheric Sciences, University of Washington, Seattle, WA. Emphasis: Wave-mean flow interaction and the selection of the leading patterns of zonal-mean variability in both observations and numerical models. (Work with D. L. Hartmann)
Fall, 1998: Teaching Assistant for undergraduate level "Climate and Climate Change".
1995-1996: Research Assistant, Department of Geophysics, University of Chicago, Chicago, IL. Emphasis: Volcanology: used physical and chemical analysis of pumice and melt inclusions in volcanic phenocrysts to assess the pressure of crystallization and the amount of gas in pre-eruptive magma (Work with A. T. Anderson).

Journal Publications

2003 Lorenz, D. J., D. L. Hartmann "Eddy-zonal flow feedback in the Northern Hemisphere winter." *J. Climate*, **16**(8), 1212-1227.
2001 Lorenz, D.J., D. L. Hartmann "Eddy-zonal flow feedback in the Southern Hemisphere." *J. Atmos. Sci.*, **58**(21), 3312-3327.

Seminars Presented

GFDL-University Consortium Colloquium: Eddy-zonal flow feedback in the Southern Hemisphere and in the GFDL R30 model (1998); Dynamics seminar, UW: Eddies and the Annular Modes (2000); American Geophysical Union Winter Meeting: Zonal flow-eddy feedback and the Annular Modes (2000), American Geophysical Union Winter Meeting: Wave-mean-flow interaction and the structure of Annular Variability (2002).